INFLUENCE OF LOADING AND MATRIX STIFFNESS ON AIRWAY SMOOTH MUSCLE CONTRACTILE FUNCTION AND PHENOTYPE WITHIN A 3D MICROTISSUE CULTURE MODEL

by

Nishat Zaman

Submitted in partial fulfilment of the requirements
for the degree of Master of Applied Science

at

Dalhousie University
Halifax, Nova Scotia
December 2013

Table of Contents

List of Tables

List of Figures

Abstract

Airway remodeling characteristic of asthma involves structural changes altering the elasticity of the airway smooth muscle (ASM) microenvironment potentially leading to ASM dysfunction. This effect of matrix stiffness was investigated using a physiologically relevant 3D culture model. Characterisation of microtissue responses with regards to contractile function and gene expression were studied varying the ECM stiffness and through stimulation with epithelial cell (AEC) conditioned media. ASM microtissues were fabricated under four different loading conditions and the matrix stiffness was increased by crosslinking through non-enzymatic glycation and increasing the collagen density. Function was assessed through the use of pharmacological agents and by imaging microcantilever deflection, used to calculate force generation. Crosslinking microtissues enhanced contractile function in response to agonists; however, this effect disappeared in microtissues tethered to stiff microcantilevers suggesting a limit of contractility within this model. Remarkably, there was a differential response in ASM function where increasing the collagen density (stiffness) significantly attenuated function. Additionally, contractility was significantly enhanced when chronically stimulated with AEC media. ASM tissue in 3D culture is responsive to the microenvironment stiffness and increases contractility in the presence of a stiffer ECM. This could occur with thickening of the airway wall in asthma. Decreased contractility with increased collagen density is in agreement with previous studies where it was shown that type I collagen is pro-proliferative and attenuates the contractile phenotype. We show the models ability to quantitatively demonstrate the impact of biomechanical cues on ASM function providing provides new ways to elucidate the mechanisms of cellular remodeling.

List of Abbreviations Used

ASM	Airway smooth muscle
AEC	Airway epithelial cells
AHR	Airway hyperresponsiveness
PDMS	Polydimethyl siloxane
CSK	Cytoskeleton
NHBE	Normal human bronchial epithelial cells
ECM	Extracellular matrix
μTug	Microfabricated tissue gauge
ACh	Acetylcholine
KCl	Potassium chloride
FSK	Forskolin
Cyto D	Cytochalasin D
sm-MHC	Smooth muscle myosin heavy chain
MLCK	Myosin light chain kinase
MLCP	Myosin light chain phosphatase
SRF	Serum response factor
GAPDH	Glyceraldehyde-3-phosphate dehydrogenase
FBS	Fetal bovine serum
SD	Standard deviation
SEM	Standard error of mean
PCR	Polymerase chain reaction
AGE	Advanced glycation end products
RAGE	Receptor for advanced glycation end products

Acknowledgements

Firstly, I would like to thank my supervisor, Dr. Geoff Maksym for his guidance and support over the past 2 years. Without his seemingly boundless knowledge and supervision, I doubt that I could have reached my goals for this project. I especially want to thank him for the interest that he showed in my work, which was evident in the 3am emails, but also for my future career aspirations.

I would like to thank my supervisory committee members, Dr. Paul Gratzer and Dr. Elizabeth Cowley for their guidance, review of my progress, and feedback of my work. Both Dr. Gratzer and Dr. Cowley provided different perspectives and showed tremendous interest in my work, while providing constant encouragement.

Additionally, I would like to thank Dr. Adrian West for his continued support and supervision these past two years during his position as a post-doctorate fellow in Dr. Maksym's lab. Without his encouragement and guidance and his extensive knowledge in physiology and cell culture, I would not be here today.

I would also like to thank the members of the Maksym Lab. To Darren Cole - your support and jokes will be missed. To Rachel Wise – the first person I saw nearly every morning for the past 2 and half years in Dentistry 4125. Thank you for all your help and emotional support during this time. I am extremely grateful for this friendship and I will dearly miss the hour long procrastination periods chatting about food, life, and kickboxing.

Completion of this thesis would not have been possible without the continuous support of my family. To my brother – thanks for all the encouragement and pep talks, and my mum and dad for endless encouragement and love.

Finally, I would like to acknowledge the funding from the Lung Association of Nova Scotia (LANS) and the Canadian Institutes of Health Research (CIHR) grant funding for our laboratory and this project in particular. Their financial support has not only aided the completion of this project but also in my development as a scientist.

Chapter 1: Introduction

1.1 Thesis Overview

This thesis is organised into seven chapters beginning with an introduction consisting of a literature review, general thesis hypothesis and the four thesis aims. Chapter two outlines the common methodology for parts of the thesis aims. Chapter three outlines the characterisation of the microfabricated tissue gauge model, and Chapters four, five and six each focus on the individual aims including the rationale, methods, results and discussion. Chapter seven contains conclusions derived from this thesis with a summary of significant findings and considerations for future work.

1.2 Asthma and Airway Remodeling

Asthma is a chronic obstructive disease of the airways affecting about 3 million Canadians and about 300 million people worldwide (15). The cost of treating asthma is continuously increasing, making it a major burden on the health and economic system (68). Asthma was traditionally regarded as a reversible disease and therapies were primarily targeted at the associated symptoms. However, it was discovered that there is considerable heterogeneity among asthmatics, and that a majority of patients show decreased airway function with time, while some demonstrate irreversible airway obstruction (34). A better understanding of the underlying causes of asthma would provide improved treatment targets in order to help reduce the societal and more importantly the personal burdens of this chronic disease.

Characteristic features of asthma include airway inflammation, airway obstruction, increased airway resistance, structural changes to the airway wall, decline in lung

function, and airway hyperresponsiveness (AHR) (30). AHR is the main clinical feature of asthma and is commonly defined as an obstructive response of the airway. This is caused by excessive narrowing of the airway in response to various external triggers which can be pharmacological, chemical or physical (19, 54, 86). In response to such a stimulus, asthmatic ASM cells exhibit both increased isotonic shortening and shortening velocity (86). The excessive airway narrowing manifests as shortness of breath, chest tightness, coughing, wheezing and airway obstruction, and this is generally attributed to ASM dysfunction (5).

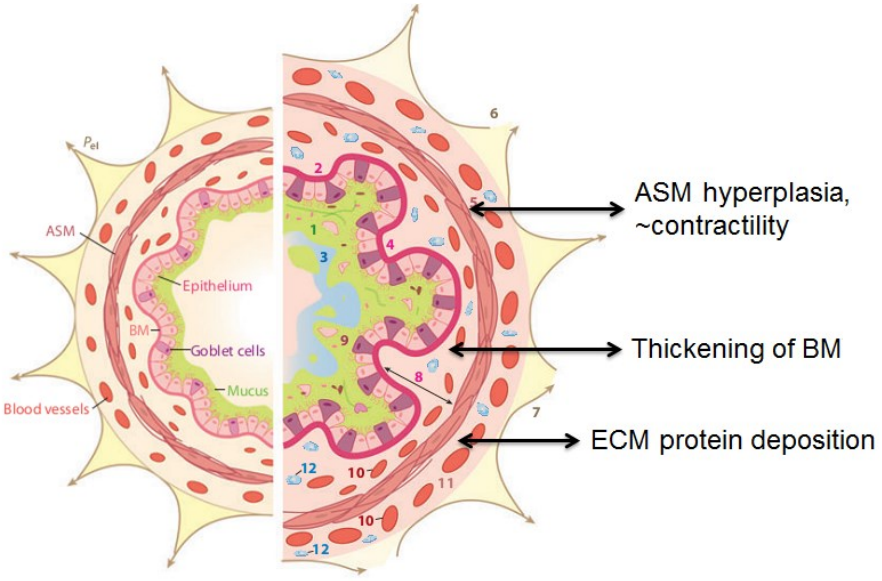

Figure 1-1. Schematic of a normal healthy airway (left) and an asthmatic airway (right) demonstrating some of the key features of remodeling in asthma (17).

Inflammation was originally thought to be the major contributor to asthma pathology. Cells would recognise specific antigens and initiate inflammatory processes involving the recruitment of eosinophils (immune cells) which damage the epithelial cells, mast cells, fibroblasts, and T cells, all of which release cytokines, which are small peptides such as interleukins involved in the healing process, and which modulate

inflammation (34). However, based on pathological studies of asthmatic airways, it is evident that the inflammatory process itself is not the fundamental cause of asthmatic airway dysfunction and does not directly account for the change in the structure of the airways. Additionally, patients that have been treated with antibodies against inflammatory mediators show a decrease in inflammation without any change in hyperresponsive (143). This led to the hypothesis that intrinsic changes in ASM function and phenotype may drive AHR, however the exact mechanisms are still debated.

More recently, it has been established that asthma is in fact characterised more closely by airway remodeling (5, 34). This process involves architectural changes to the airway defined by increased ASM (hyperplasia and hypertrophy) (33, 101), infiltration of inflammatory cells (11), thickening of the basement membrane and airway wall (101), altered extracellular matrix (ECM) composition (7, 31), and damage of the epithelial tissue (60). Most prominent features of airway remodeling in asthma are shown in Figure 1-1 modified from a paper by Bossè et al. (17). The pathogenesis of asthma is still not distinct as it is multifactorial and includes interactions between neural pathways, inflammatory cells and mediators, and components of the airway wall such as the ASM and epithelial cells (25). The principal stimulus for airway remodeling is still unknown as there is a lack of tissues available for study from patients with remodeled airways, and animal models poorly reproduce the characteristics of the disease, therefore making it difficult to determine the mechanisms of chronic responses. It has been suggested that the process of airway remodeling may occur prior to presentation of clinical symptoms (10). Indeed this has led to the hypothesis that an alteration in the architecture of the airway

may be the primary cause of ASM dysfunction through changes in the mechanical environment, which leads to excessive bronchoconstriction in asthmatic patients.

1.2.1 Airway Epithelium

One of the characteristic features of asthmatic airway remodeling is the pathological change in the airway epithelial cells (AEC) (60, 62). Traditionally, it was believed that the principal role of epithelial cells was to provide a physical barrier against the external environment thereby preventing exposure of the internal airway components to noxious inhaled substances (107). However, it has been established that epithelial cells play a major role in a variety of airway functions (107, 121, 139); for example epithelial cells are responsible for fluid balance in the airway, clearance of inhaled agents, recruitment and activation of inflammatory cells, and the release of inflammatory mediators that are responsible for regulating ASM response to contractile stimuli. Some of the released mediators include relaxing factors such arachidonic acid, nitric oxide, endothelin-1, as well as growth factors and interleukins including TGFβ, TNFα, IL-1, IL-6, IL-8 (71). The epithelium has been shown to modulate ASM tone through the secretion of these derived relaxing factors which decrease contractile response to a number of agonists, suggesting that the epithelium may be involved in inhibitory effects on smooth muscle responses (13).

The long term communication between ASM cells and epithelial cells has been studied extensively along with the AECs potential role in regulating ASM phenotype (60, 61, 77). One of the main mechanisms of AECs ability to modulate AHR is linked to airway inflammation. Epithelium denudation has not only been reported in severe and fatal asthma, but also in mild asthma (19, 77, 97). Since the epithelium is the first point of

contact of inhaled external substances, denudation of this layer can cause these external substances to easily injure the cells either directly through cytotoxicity or indirectly by involving inflammatory cells (62). Once injured, these cells initiate a wound healing process involving inflammatory cells which results in the release of various cytokines and growth factors which have been shown to acutely lead to cell constriction, and chronically may contribute to the overall remodeling of airways, namely the hyperplasia of ASM cells and the deposition of ECM proteins (59, 139).

Manual removal of the epithelium of canine bronchial rings and tracheal strips led to increased responsiveness of the bronchial rings to ACh and histamine (3). Through the use of *ex vivo* lung slice models a different study showed through laser ablation of single epithelial cells that there is an acute increase in airway contraction through calcium dependant smooth muscle shortening (142). This data was consistent with the idea that the injured epithelial cell leads to the release of soluble mediators which lead to enhanced contractility of ASM.

Preliminary results from our laboratory have shown that co-culturing primary human ASM and AEC can cause ASM baseline tension and contractility to decrease with an associated decrease in levels of contractile proteins including myosin light chain kinase (MLCK) and smooth muscle myosin heavy chain (sm-MHC). This suggests that epithelial cells may play a role in regulating ASM contractile phenotype and the study of these two cell types together may help in understanding the dysfunction of ASM in asthma. Another study investigating the role of epithelial cells in stimulating ASM hyperplasia (88) used a co-culture model of primary normal bronchial epithelial cells (NHBE) and primary normal human airway smooth muscle cells (HASM) to demonstrate

that injured epithelial cells release various cytokines and matrix metalloproteinases (MMPs), which are a family of proteases involved in the breakdown of extracellular matrix proteins, that enhance the ASM proliferation and hyperplasia evident in asthma.

A majority of *in vitro* studies of ASM and AEC interactions have involved culturing cells on traditional 2D substrates and culture systems which are not representative of the complex 3D structure *in vivo*. As the geometry of cultured cells has been shown to be a complex regulator of cellular function (46), the interaction between AECs and ASM cells within a 3D environment would be more relevant. The importance of an appropriate culture model and structurally physiological environment is discussed further in section 1.6.

1.3 Cellular Mechanics

The microenvironment stiffness of an adhesive cell, and consequently the stiffness of the substrate on which these cells are cultured *in vitro,* can regulate various cellular processes and thus have a major effect on cell function (36, 102). Cells have the ability to sense the external environment and interact with it accordingly (outside-in and inside-out signalling respectively). This interaction between the external environment and the internal cellular environment occurs through various proteins that physically bind to the substrate including integrins, focal adhesions, and the cellular cytoskeleton (CSK). Integrins are transmembrane glycoproteins that act as the mechanical linkage between the ECM and the cellular CSK (4, 114). These proteins allow for bidirectional communication between the ECM and the CSK through the cellular membrane, thus permitting dynamic reciprocity. Upon mechanical perturbation, integrins form into focal adhesions which are macromolecular assemblies that adapt mechanically. It is via

integrins and focal adhesions that the cellular CSK is bound to the ECM and permits the transmission of information throughout the cell. Information about the extracellular mechanical environment is transmitted via the presence of integrins and this process involves adherent cells exerting a force and pulling on the substrate through the actin-myosin CSK, probing the mechanical properties of the environment, and reacting through reorganisation of their cytoskeletal morphology (133).

The CSK is a major part of the contractile apparatus of cells and is composed of fibrillar proteins consisting of actin filaments, intermediate filaments, and microtubules. Actin is present intracellularly in two forms; globular actin which is the monomer (g-actin) and as fibrillar actin which is the polymer (63). The contractile apparatus of cells is composed not only of actin filaments but also of thick filaments called myosin. Myosin is one the motor proteins of cells and is made up of two light chains and two heavy chains. The heavy chains form the globular myosin head that interacts with the actin filaments. The CSK is the cellular scaffolding and provides the cell shape and support in addition to housing the contractile apparatus.

Outside-in signalling is based on cells sensing external signals via these macromolecular complexes bound to the ECM and the CSK, leading to downstream signaling pathways that control cellular responses. These responses can be acute responses due to changes in actin polymerisation, or chronic changes due to alterations in gene and eventually protein expression. Thus, the translation of physical signals from the environment into chemical signals is defined by mechanotransduction. Other than the translation of mechanical stimuli through macromolecular complexes via the CSK and ECM, there are a number of other mechanisms of mechanotransduction for example

through stimulation of mechanically activated ion channels. These channels are activated by conformational changes of the membrane leading to an influx of ions and formation of a charge gradient. This communication of mechanical stimuli into biochemical information has been shown to regulate cell signaling pathways and gene expression directing cellular differentiation, morphology, and regulation of contractile protein activation, thereby altering contractile properties (83).

Smooth muscle contraction is regulated by phosphorylation of the regulatory myosin light chain (rMLC) by MLCK which is regulated by association with the calcium binding protein calmodulin. Smooth muscle tension is generated through binding of actin and smooth muscle myosin to form cross bridges. An increase in calcium concentration within the cytosol of the muscle cell (sarcoplasm) due to a contractile stimulus, promotes binding of calcium to calmodulin activating MLCK which phosphorylates the rMLC (50, 66). In the presence of calcium, the cyclic interaction between the actin and myosin filaments continues with the hydrolysis of ATP to ADP, leading to tension development through muscle shortening (28). Relaxation of smooth muscle occurs through dephosphorylation of the rMLC by activation of MLCP (67). Therefore, upregulation of MLCP expression would coincide with a reduction in smooth muscle contraction, while upregulation of MLCK expression would promote contraction. There are two isoforms of smooth muscle myosin heavy chain (SM1 and SM2) and they are formed by alternative gene splicing, and differ in a 7-amino acid insert (81). The presence of this insert is generally found in phasic muscle while the absence of this insert is found in tonic or "slow" muscle. Upregulation of expression of these isoforms of sm-MHC can promote contraction. It has been shown that the presence of this smooth muscle insert in the

myosin heavy chain evident in asthmatics leads to rapid smooth muscle shortening which affects the cycling rate of actin-myosin cross bridges where the faster cycling rate would in turn contribute to the active force generated. However, further discussion on this topic is beyond the scope of this thesis. In summary, the function of smooth muscle myosin is mainly regulated by the rMLC activity and the balance of MLCK and MLCP.

As mentioned above, ASM tone is regulated by the level of intracellular calcium and contraction is initiated by calcium mediated changes in the thick myosin filaments. Pharmacological agents can be used as bronchoconstrictors (contractile agonists) which result in the release of calcium from intracellular stores into the cytosol through activation of calcium channels. Potassium chloride is a common contractile agonist used to assess muscle function as it depolarises the cell membrane causing calcium to be released through voltage-gated calcium channels in the sarcoplasmic reticulum through the activation of the ryanodine receptors. Acetylcholine is another contractile agonist that binds to the muscarinic receptors on the muscle membrane activating the IP3 pathway initiating the release of calcium ions from internal stores.

Additionally, pharmacological agents such as forskolin and cytochalasin D can reduce force via different mechanisms. Forskolin reduces force generation of ASM cells through the activation of adenylate cyclase which increases the quantity of intracellular cyclic adenosine monophosphate (cAMP) (12, 58). Cyclic AMP reduces force or relaxes ASM cells through the activation of protein kinase A (PKA) which phosphorylates potassium channels causing cellular hyperpolarisation leading to decreased MLCK activity and decreased intracellular calcium (12). By contrast, cytochalasin D disrupts the

CSK by binding to globular actin preventing actin polymerisation which decreases tension with the loss of cellular structure.

1.4 Airway Smooth Muscle Phenotype

The epithelium lines the inner wall of the airway while the ASM circumferentially surrounds the airway medial layer and is primarily responsible for controlling airway calibre. It is generally agreed that the ASM is the main component of the airway responsible for excessive airway narrowing, AHR, and bronchoconstriction (5). However, whether this phenomenon is caused by fundamental changes in the ASM structure or contractility, or changes in the mechanical microenvironment set by the non-contractile elements of the airway wall and the lung parenchyma, is still not clearly established (70).

After differentiation smooth muscle cells manifest a range of phenotypes, but the two most significant are the synthetic (proliferative) phenotype and the contractile phenotype (23). Different phenotypic states are characterised by the expression of a variety of different contractile, structural, and receptor proteins that are modulated by gene expression (52). The proliferative phenotype is characterised by high mitogenic activity and expression of various genes encoding proteins associated with synthesis. For example, proliferative smooth muscle cells demonstrate reduced expression of smooth muscle α-actin, γ-actin, MHC, calponin, caldesmon, phospholamban, desmin, and vinculin. In tissue culture, the synthetic phenotype can be induced by culturing cells in serum-rich environment (56). The contractile phenotype is characterised by a loss of synthetic organelles of cells in culture alongside the expression of numerous smooth muscle specific genes encoding contractile proteins and regulatory proteins that are

responsible for muscle activation. In tissue culture, the contractile phenotype can be induced by culturing cells to confluence and when cultured within a serum-deprived environment (87).

In normal healthy airways the smooth muscle layer is composed of differentiated ASM cells in a non-proliferative state which express large amounts of contractile proteins such as smooth muscle α-actin and smooth muscle myosin heavy chain (sm-MHC) (58). ASM cells can undergo phenotypic modulation and return to a proliferative state due to changes in their environment, or with the addition of a mitogen which triggers kinases involved in mitosis and cell division, which leads to the loss of contractility due to decreased expression of contractile proteins and an increased amount of biosynthetic organelles and synthetic capabilities (52, 58, 115). Moreover, it has been hypothesised that ASM cells may switch to a contractile phenotype through the amplified abundance of contractile and regulatory proteins which may lead to the airway obstruction and AHR evident in asthma (137). The ability of ASM cells to undergo phenotypic modulation from contractile back to proliferative is hypothesised to allow them to repair injured airways thereby potentially contributing to the airway remodeling evident in asthmatics (57).

A shift in the contractile phenotype of ASM cells has previously been demonstrated (86) using ASM cells isolated through bronchial biopsies from healthy and asthmatic patients. This study showed increased shortening velocity and shortening capacity of asthmatic ASM cells as well as enhanced expression of the contractile protein MLCK but no difference in sm-MHC expression. Another study by Woodruff et al. (72), showed increased ASM contractility and expression of MLCK in sensitized asthmatic canine

smooth muscle strips, consistent with a contractile phenotype. Interestingly, ASM hyperplasia is a prominent feature of asthmatic airway remodeling which is surprising since it is generally accepted that proliferation and contraction are two opposing phenotypic states. This suggests that there may be both phenotypic changes in ASM in addition to structural changes, where both of these states have been associated with dysfunction (104).

1.4.1 Markers of ASM Phenotype

In recent years there has been much progress in the advancement of knowledge in identifying phenotype specific protein markers and transcription factors that regulate smooth muscle specific gene expression. As described in section 1.3, smooth muscle contraction and relaxation occurs through the interaction between actin filaments and myosin through MLCK and MLCP activity. These genes have been studied previously in the literature with regards to transcriptional regulation. Halayko et al. (51) demonstrated, using primary cultures of canine tracheal smooth muscle cells, that the contractile phenotype was characterized by an increase in smooth muscle myosin heavy chain (sm-MHC), smooth muscle α-actin, desmin, β-tropomyosin, calponin, *h*-caldesmon and myosin light chain kinase (MLCK), while the synthetic phenotype was characterized by increased non-muscle myosin heavy chain (nm-MHC), vimentin, *l*-caldesmon, protein kinase C, and CD44.There are only a few smooth muscle contractile genes that have been studied with respect to transcriptional regulation. Among those genes already mentioned, another important marker of smooth muscle contractile phenotype is transgelin, more commonly known as SM22α. This is a calponin-related protein involved in actin remodeling and its expression has been shown to be upregulated in asthmatic ASM cells.

Transcriptional regulation of smooth muscle cell differentiation is dependent on a number of transcription factors; however, research has predominantly focused on the serum response factor (SRF) (55, 75). SRF is a widely expressed nuclear protein important for cell proliferation and differentiation (103). SRF consists of a DNA-binding region called the MADS box which interacts with the serum response element known as the CArG box which is found upstream of all SRF-regulated muscle genes (75, 103). SRF is found in the regulatory region of a number of smooth muscle specific genes including sm-MHC, α-actin, and SM22α. SRF requires cofactors for activation, the most important of which is myocardin, as it is expressed solely in smooth muscle (130). It is regarded as the master regulator of smooth muscle differentiation and induces smooth muscle marker genes (130, 131).

1.5 Substrate Stiffness

Various studies have demonstrated that ASM is regulated by ECM signalling pathways, but ASM cells are also involved in the airway remodeling process themselves thereby creating a feedback loop discussed further in section 1.5.1 (6, 57). However, these studies have produced contradictory results which may be due to methodological differences such as the application of different culture models each of which possess advantages and limitations. For example, different studies investigating allergen sensitivity have exposed animals to allergens through aerosols as opposed to administration through injection, where each method has a different effect on the immunological response. Another methodological difference is the study of mild, severe and fatal asthmatics without appreciation of the difference between these asthmatic phenotypes, as well as the difference in sample sizes, failure to measure certain metrics

when assessing function such as stress and muscle shortening. Moreover, the major underlying issue is that a majority of these previous studies have been conducted using traditional culture models for which the substrate (material) stiffness is orders of magnitude larger than what would be considered physiological stiffness.

Cells respond the stiffness of their microenvironment, and in asthma the elasticity of the airway may be altered due to remodeling. It has previously been shown that substrate stiffness is a potent regulator of various cellular processes (35, 36, 48). The effect of substrate stiffness on cellular characteristics has been studied previously using traditional culture models. With the use of polyacrylamide hydrogels, Pelham and Wang (102) showed that the elastic modulus of the substrate on which cells were cultured could be adjusted in 2D models. Independent of any changes in the ECM proteins, the stiffness of the substrate was altered through a wide range of stiffness. This study demonstrated that substrate stiffness affects cellular organisation, as cells cultured on soft substrates are highly disorganised with poor stress fibre alignment, while cells cultured on stiffer substrates show good alignment. It has also been well characterised in various studies in 2D cultures that an increase in substrate stiffness leads to an acute increase in cellular traction forces and baseline cell stiffness, cell spreading, and cell migration (6, 35). Indeed, substrate stiffness has been shown to enhance contractile phenotype and function chronically (6, 36, 73, 134). Engler et al. (36) showed that mesenchymal stem cells cultured on gels with varying stiffnesses representing the physiological environment of brain, muscle, and bone cells, differentiated into neurons, myoblasts, and osteoblasts respective of the environment. The cells also expressed gene markers of differentiation of each the three cell types.

Previous studies from our laboratory have shown that ASM cells are also affected by substrate stiffness. It has been shown by our collaborators that ASM cells become more proliferative when cultured on stiff substrates (89). These cells also express increased amounts of the contractile protein smooth muscle myosin heavy chain (sm-MHC), while expression of the regulatory proteins myosin light chain kinase (MLCK) and myosin light chain phosphatase (MLCP) controlling myosin phosphorylation are decreased (134). This suggests that a stiff environment would cause ASM cells to become more contractile and be less proliferative.

1.5.1 Asthmatic Biomechanical Environment

Asthmatic airway remodeling involves structural changes to the airway including airway thickening, which may alter the overall mechanical environment of the muscle tissue, but also lead to the changes in ASM cell regulation by ECM components. Thickening of the airway wall would potentially alter how ASM cells transduce the change in mechanical load into airway calibre (21, 65). There is substantial evidence of thickening of components of the airway assessed through high-resolution computed tomography (CT) in patients with severe asthma compared to healthy or mild asthma (8, 128).There are various causes of thickening of the airway wall and basement membrane evident with airway remodeling. It has been suggested that increased ECM deposition of collagenous and non-collagenous components in the sub-epithelial section beneath the basement membrane is the major cause of the airway wall thickening associated with asthma (34). The changes in ECM deposition include increased deposition of collagens I, III, and V, fibronectin, tenascin, hyaluron, laminin, versican, and decreased levels of collagen IV, elastin, and decorin (29, 76, 78, 111, 136). Araujo et al., (7) also

demonstrated that airway remodeling is associated with changes in various ECM components including elastic fibres, matrix metalloproteinases (MMPs) and tissue inhibitors of metalloproteinases (TIMPs) which are responsible for MMP activity inhibition.

It is known that the ECM regulates various cellular processes including proliferation, migration, survival and secretion (100). ASM cells exposed to serum obtained from asthmatic cells have been shown to secrete more ECM proteins including collagen and perlecan compared with non-asthmatic controls, which in and of itself can modulate ASM secretion and proliferation demonstrating that ASM cells themselves are part of the airway remodeling process resulting in a positive feedback loop (64, 65). Changes in the airway mechanical environment could cause phenotypic modulation of ASM cells from a proliferative state to a more contractile state through various ECM signalling pathways. Furthermore, reducing the load imposed on the ASM by the ECM stiffness through collagenase degradation of *ex vivo* ASM strips and lung slices increases the contractility of ASM, most likely through the ability of the cells to shorten more easily (20, 69). As the ECM is composed of various structural proteins, an alteration in the composition of ECM proteins may alter the mechanical environment and the properties of the ASM cells, and therefore could alter the communication of forces between ASM cells and the neighbouring tissue.

In summary, it has been shown that changes in the biomechanical environment such as the ECM protein composition can modulate ASM contractility, contractile protein expression, and proliferation. More simply, this suggests that a stiff substrate would cause ASM cells to be less proliferative and become more contractile. Therefore, this

major change in the structure of the airways through an increase in the ECM components and connective tissue will lead to a stiffer substrate for ASM cells thereby potentially altering their response. This could be a mechanism for the ASM dysfunction leading to AHR in asthma. There are other mechanical factors to take into consideration when assessing the effect of the mechanical environment on ASM including physiological strain due to breathing. However, this is beyond the scope of this thesis. As the mechanical properties of the ASM microenvironment have an immense effect on the function of these cells, studies based on traditional culture models may not provide accurate indications of ASM phenotype; therefore, a culture model with appropriate substrate stiffness is of great importance for the study of cell function (36, 102, 106).

1.6 Smooth Muscle Cell Models

This intrinsic relationship between the internal mechanical environment and ASM cell function is evident in a number of studies, but it is difficult to study properly due to the lack of appropriate *in vitro* models of asthma. Remodeling in the airway wall potentially alters ASM contractility, but the impact of individual loads imposed by various components of the airway is unclear due to the low availability of human asthmatic tissue mentioned above (86). Due to the paucity of viable human asthmatic tissue, the use of alternative techniques is needed for the analysis of ASM contractility. Various models and systems are currently in use including animal models, *ex vivo* airway segments, thin cut lung slices, ASM strips, *in vitro* cultures, and tissue engineered systems. Clearly, targets for drug therapies should be assessed in human asthmatics. However, this is not feasible due to understandable ethical and logistical limitations.

Since it is not possible to conduct drug discoveries in human asthmatic subjects, there is a need for alternative systems to model the processes of this pathology.

1.6.1 *Ex Vivo* Studies

Ex vivo airway segments are retrieved from animals by incision, filled with solution, and used to test ASM contractility indirectly by the measure of increase in hydrostatic pressure in response to stimulation (108). The pathophysiological state of *ex vivo* airway segments is greatly dependant on the animal they are obtained from, but the main advantage of these models is the ability to perform invasive procedures. However, the application of these models has demonstrated the significance of the epithelium and ASM interaction, as the changes in the epithelial tissue (damage) can alter ASM contractility. The main disadvantage of *ex vivo* segments is that they can only be used in testing acute responses preventing research on long term chronic changes in ASM phenotype.

Thin cut lung slices are another *ex vivo* model suitable for acute measurements. They are fabricated by sectioning a single lung lobe using a microtome producing slices as thin as 140μm. These lung slices are cross-sections of the airway and therefore, are anatomically intact with all the different cell types and ECM components, which is one of the main advantages that allow for the study of *ex vivo* ASM contraction in the context of the whole airway (90, 109). Lung slices combine the main features of the mechanical environment such as the load opposing ASM contraction by the parenchyma. Preservation of the mechanical environment in lung slices is a major advantage over *ex vivo* airway segments and other models as it also allows for manipulation of the mechanical components. However, the main disadvantages of lung slices are the loss of

geometry, the loss of a diffusion barrier due to thin slices, and complexity in the system due to the presence of various cell types and ECM components. Although *ex vivo* models are generally structurally relevant to an intact lung, the main issue is the intricacy of the system which prevents direct measurement of ASM contractility, and the lack of control over biochemical factors.

1.6.2 *In Vitro* Studies

In vitro cell and tissue cultures are widely used in respiratory and vascular research to study the molecular biology of cells. *In vitro* studies include 2D culture plates (i.e. Petri dishes and Transwell culture supports) as well as 3D tissue engineered constructs. These models provide a highly controllable environment both physically and biochemically but fail to recapitulate the mechanical and structural environment of native tissue. *In vivo*, cells exist within a 3D environment consisting of an ECM scaffold made of collagens and other structural proteins that are intertwined with proteoglycans, mechanical stimuli, and soluble factors from neighbouring cells, in comparison to cells on a single surface, as is the case in 2D culture systems (9).

1.6.2.1 3D Cell Culture

2D culture models generally involve the use of plastic Petri dishes for which the stiffness magnitudes are greater (gigapascal range) than physiological stiffness. While the substrate stiffness of some 2D models can be tailored using hydrogels, the 2D construct and the geometry does not provide a load opposing ASM contraction which again creates a physiologically irrelevant environment compared to the *in vivo* environment, where ASM cells constrict against an outward load of the airway wall.

Review articles and studies (114, 133) have demonstrated the importance of a 3D environment and the advantages include: 1) the 3D geometrical environment provides physiological cues and facilitates biological responses essential for mechanotransduction, which occurs through ECM and integrin interactions; 2) the dynamic nature of the 3D environment not only affects mechanotransduction but also alters cell-to-cell communication, concentration of ligands, and extracellular gradients; 3) the 3D ECM itself has an effect on the cell microenvironment through its own signalling proteins, ability to bind secreted proteins, and its ability to alter cytokine and growth factor diffusion. Thus, it can be seen that replicating a 3D environment is thought to be crucial and research is now striving to validate 2D findings in a more physiological setting to develop more robust drug targets and "organotypic" models (9).

Recently, there have been a number of efforts to establish 3D tissue engineered *in vitro* models. These models have been designed to create a more physiologically relevant environment compared to 2D *in vitro* culture models (46). Within 3D tissue models the cells are dispersed evenly within a protein gel with a tunable stiffness to match *in vivo* conditions. These models also retain the necessary control over mechanical and environmental factors to study cellular and biochemical responses. However, many 3D models of ASM tissue still possess a number of shortcomings.

Common 3D models include bulk gels and tissue engineered ring constructs made of smooth muscle cells embedded within a collagen matrix (22, 85, 92). For bulk gel contraction assays ASM contraction is measured based on the magnitude of gel shrinkage (82). The downside of this model is that the cells within the matrix show disorganised morphology, and there is no auxotonic load opposing ASM contraction which is

unrepresentative of the physiological mechanical environment (82, 98). Muscle contraction can be studied under isometric (constant length), isotonic (constant force) or auxotonic conditions where muscle shortening is a function of increasing load (84). *In vivo,* ASM cells constrict against an auxotonic load, the magnitude of which is a function of muscle shortening. ASM cells are attached to other compliant structures and components (connective tissue), therefore, shortening of the ASM cells will cause stretching of these other structures which in turn imposes an increasing load on the ASM cells (84). The physiological relevance of the auxotonic load opposing contraction of cells is equivalent to the blood pressure against smooth muscle in vasculature or in context of airways, the load opposing contraction is equivalent to the airway parenchymal tethering which is the outward recoil exerted by attachments to the airway wall (1, 79).

Choe et al. (26) developed a 3D model of the airway wall consisting of epithelial cells and fibroblasts to investigate the process of remodeling due to mechanical strain and inflammatory mediators. This model did not include ASM cells despite the fact that ASM cells do contribute to the process of airway remodeling and are considered partly responsible for airway narrowing in asthma (30).

Another recent development involved fabrication of tissue engineered bronchioles used to monitor cell to cell signalling and ECM interactions (95). These bronchioles consist of multiple cell types including ASM cells, epithelial cells and fibroblasts embedded within a collagen matrix and maintained in a bioreactor simulating the effect of breathing (95). The benefit of these engineered bronchioles is the presence and interaction of multiple cell types providing a physiological environment. The ASM cells within this construct expressed the key protein markers of contractile phenotype

demonstrating the relevance of the system although contractile function was not assessed. The disadvantages of these engineered bronchioles are the duration (~21 days) and the complexity of fabrication, rendering them inappropriate for high throughput experimentation.

1.7 Application of Microfabricated Tissue Gauges (μTuGs)

Based on the limitations of current *ex vivo* and *in vitro* culture models, a device capable of studying the effects of substrate stiffness on micron-scale 3D cell cultures is desirable. Most of the 3D models outlined in the previous section are in the centimeter scale, which deters investigations into the rapid dynamics of cellular contractility due to diffusion limited concentration gradients (83).

Legant et al. (83) developed the μTug model which employs the use of polydimethyl siloxane (PDMS) to form substrates composed of an array of wells, each well housing two flexible microcantilevers about 600μm apart around which a microtissue assembles. Cells compact a gel matrix to form a tissue encompassing the microcantilevers to form a 3D tissue closely resembling human tissue where the cells are aligned with the axis of tension and possess a baseline contractile tone. The contractile force within the microtissues deflects the flexible microcantilevers, and the magnitude of deflection is observed via optical microscopy which is then used to calculate the force generated by the tissue. The flexible microcantilevers provide a baseline load (prestress) against tissue contraction which is representative of the *in vivo* environment and allows for repeated contractility measurements. The tissue gauge is easily fabricated within a laboratory setting and the rapid turnover provides a major benefit over other 3D culture models. The model can also be manipulated easily to alter the mechanical properties and

has shown great potential for the assessment of contractile function. Legant et al. (83) used the model to measure forces from microscale constructs of fibroblasts embedded within a 3D collagen matrix. The study demonstrated matrix remodeling and force generation by fibroblasts and showed that both the microcantilever stiffness and the ECM stiffness influenced fibroblast tissue remodelling through a change in contractility and matrix protein deposition.

More recently, Boudou et al. (18) fabricated cardiac microtissues with the μTug model and demonstrated that with increased microcantilever stiffness (increased load opposing contraction) the cardiomyocytes generated more tension in addition to greater mechanical stress. It was concluded that the presence of an elastic microcantilever enhanced the development of the sarcoplasmic reticulum, enhancing cell tension, which led to compaction of the ECM gel and enhanced cellular organisation (18).

I recently helped develop a μTuG model of human ASM cells and 3T3 fibroblasts within a collagen type I ECM (135). The study assessed ASM morphology and contractility compared to *ex vivo* and *in vitro* models. The ASM microtissues generated a baseline tone against microcantilever stiffness and contracted to various drugs. In comparison to alternative culture models, this study (135) indicated that the ASM microtissue characteristics were representative of physiological ASM characteristics with respect to ASM contractility. Therefore, it can be seen that this model can be used to directly assess ASM function. Additionally, the features of the model allow for direct manipulation of the biomechanical environment.

1.8 Tissue Engineered Scaffolds

Collagen matrices are commonly used for tissue engineering applications as collagen is a natural protein present *in vivo*. However, for various applications, reconstituted collagen gels are not sufficiently strong to recapitulate the *in vivo* environments. For this reason a number of studies have looked into enhancing the stiffness and strength of collagen matrices and scaffolds (43, 113, 120, 132, 140). Common collagen crosslinking methods include ultraviolet radiation (119), dehydrothermal treatment, glutaraldehyde treatment (132), non-enzymatic glycation (38, 43), enzymatic crosslinking by transglutaminase and lysyl oxidase (45, 116).

Generally, crosslinking agents use bifunctional reagents that contain two reactive groups which form covalent cross bridges between a pair of amino acid side chains on adjacent proteins molecules (132). There are a number of amino acid side chain groups that can be targeted by crosslinking agents including carboxyl, amine, sulfhydryl and carbonyl groups. The amine and carboxyl groups which are located on the N-terminus and C-terminus respectively of each polypeptide chain and in the side chain of the lysine residue are primarily targeted for crosslinking as they are spatially convenient.

The two commonly used crosslinking agents for collagen are aldehydes and carbodiimides. Aldehyde crosslinking methods (i.e. gluteraldehyde and formaldehyde) provide sufficient crosslinking but they result in the release of unused aldehyde and by-products which are cytotoxic. Carbodiimides [i.e. N-(3-dimethylaminopropyl)-N-ethylcarbodiimide hydrochloride (EDC)] crosslink proteins through the formation of amide bonds which are formed between the carboxyl group and the primary amine group of proteins (120). As they do not get incorporated into the final reaction, they are

generally not cytotoxic. Carbodiimides are generally enhanced with N-hydroxysuccinimide (NHS) which results in the formation of ester bonds. These are less cytotoxic to cells compared to aldehydes, however, the major drawback is the loss of structural integrity of the crosslink (141).

Other crosslinking agents include transglutaminases which are enzymes that crosslink lysine residues (45). Crosslinking enzymatically with transglutaminases is advantageous for enhancing matrix integrity and incorporating other molecules into the matrix, however, it is expensive for use in altering the mechanical properties of matrices. Lysyl Oxidase (LOX) is an enzyme present *in vivo* and is used for crosslinking collagen proteins (116). LOX is a copper-dependant amine oxidase enzyme which catalyses the formation of aldehydes from lysine residues which then react with other aldehyde residues resulting in crosslinks between polypeptide chains.

The main issue with most conventional chemical and physical collagen crosslinking methods is their potential cytotoxicity. Among the various processes, non-enzymatic glycation has been shown to be non-toxic in the presence of cells as it involves d-ribose which is a naturally occurring monosaccharide. Glycation involves the non-enzymatic crosslinking of amine groups of collagen by reducing sugars such as d-ribose or glucose (41, 113, 126). Glycation also occurs naturally within the body with age due to the accumulation of advanced glycation end (AGE) products which lead to increased stiffness and resistance to degradation of the matrix (96, 126).

A previous study by Girton et al. (43) assessed the mechanical properties of a tubular collagen construct embedded with aortic smooth muscle cells. The tubular construct was submerged in media supplemented with ribose or glucose (15mM and 30

mM respectively) and the mechanical properties were measured using a biomechanical testing system. This study (43) demonstrated with 30mM d-ribose there was no effect on cell viability. They showed that stiffening of the matrix occurred faster and to a greater extent with 30mM d-ribose supplemented media resulting in a threefold increase in the Young's modulus over a period of 5 days compared to the control group. More recently, Reinhart-King et al. (91) showed considerable stiffening of collagen matrices with varying concentrations of ribose and glucose with no cytotoxic effects.

1.9 General Hypothesis

Previously in our laboratory, it has been shown using tailored 2D hydrogels that substrate stiffness regulates contractile phenotype and function (134). The change in the biomechanical environment of ASM cells due to asthmatic airway remodelling may contribute to AHR. However, the molecular mechanisms responsible for this change in ASM cell contractility are complex and involve a great deal of signalling pathways and feedback regulation. Therefore, it is challenging to study the effects of remodelling from a mechanistic perspective. For this reason, aiming to assess changes in the functional and phenotypic cellular response is more relevant to asthma. To elucidate the dynamics of this enhanced contractility, there is a need to study this effect on ASM cells within a physiological setting. This is because in a 2D configuration, cells can probe the substrate stiffness, but this monolayer of cells results in an apical-basal polarity which is unrepresentative of the *in vivo* environment rendering this model limited as certain physiological cues are missing. In a 3D configuration respective of the *in vivo* environment, we can decipher multiple interactions between the cell and surrounding

environment and assess whether it is the ECM density, the crosslinking or the loading on ASM cells that affects their contractile function and phenotype.

The governing hypothesis of my thesis is that the biomechanical characteristic of asthma is a key regulator of airway smooth muscle function and phenotype. Therefore, I hypothesise that matrix and substrate stiffness can chronically contribute to increased ASM cell contractility through a positive phenotypic change. The basic approach I adopted to test this hypothesis was to manipulate the biomechanical environment of 3D ASM microtissues to simulate the increased stiffness of the ASM microenvironment associated with asthmatic airway remodeling. This hypothesis is addressed by the following set of specific thesis aims.

1.10 Thesis Aims

The focus of my research was to manipulate the biomechanical environment in which the 3D ASM microtissues were fabricated using a 3D μTug model (83) to simulate asthmatic conditions. The four specific aims of my thesis are as follows:

Aim 1

Optimise the 3D microtissue fabrication protocol to increase survivability of ASM microtissues. The objective was to increase the longevity of viable microtissues within a single substrate of 113 microtissues to a minimum of 80% survival at three days post tissue fabrication.

Aim 2

Manipulate the mechanical environment by altering the stiffness of the microcantilevers of μTuG substrates to form both compliant and stiff cantilevers to

reflect the change in airway stiffness due to remodeling. This will alter the ability of the ASM microtissue to shorten during culture.

Aim 3

Manipulate the ECM of 3D ASM microtissues to form ECM gels with varying stiffnesses to detect phenotypic changes in ASM cells evident in asthmatics due to airway remodeling using two approaches; matrix crosslinking and matrix density.

Aim 4

Fabricate ASM microtissues using conditioned AEC media to monitor the effect on ASM structure and function.

Chapter 2: Common Methodology

2.1 Cell Culture

The cell culture for all experiments was conducted using human airway smooth muscle cells from a single donor (donor 12) immortalised by stable transfection with human telomerase reverse transcriptase [previously characterised in (44)] obtained as a generous gift from Dr. William Gerthoffer (University of South Alabama), and WI-38 human lung fibroblasts purchased commercially (American Type Culture Collection®, CCL-75™, Vancouver, BC). Cells were seeded into T-75 flasks (Costar, Cambridge, MA) and maintained in feeder media consisting of DMEM/F12 (Invitrogen #11330, Burlington, ON) with 10% FBS (Invitrogen #12483, Burlington, ON) and 1% penicillin-streptomycin (Invitrogen #15140, Burlington, ON). Normal Human Bronchial Epithelial (NHBE) cells purchased commercially (Lonza© # CC2540, Walkersville, MD) were cultured according to the Lonza© NHBE cell protocol and PneumaCult™-ALI protocol. All cell cultures were kept in a 37°C humidified incubator with 5% CO2 until 90% confluent.

2.2 Microtissue Fabrication

Microtissues were manufactured in microfabricated tissue gauges (μTugs) with microcantilevers of varying compliance. The μTugs were initially sterilised with 100% ethanol and ultraviolet (UV) irradiation for 20 minutes. The ethanol was aspirated and substrates were allowed to air dry under UV irradiation. The substrates were treated with 0.2% Pluronic F-127 (Invitrogen #P6866, Burlington, ON) to prevent unwarranted adherence of cells to the sides of the wells. The F-127 solution was added to the substrate

slowly to prevent penetration into individual wells for one and a half minutes to reduce cell adhesion across the tops of multiple wells. The F-127 solution was then pipetted into each well and the treatment was left to stand in the wells for 4 minutes. The solution was aspirated and the substrates rinsed with PBS, and air dried.

A collagen and media mixture was prepared from concentrated solutions to obtain a final concentration of 1x DMEM/F12 (Invitrogen #12400, Burlington, ON), 14.3 mM $NaHCO_3$, 15 mM d-ribose (Sigma-Aldrich #R9629, Oakville, ON), 1% FBS (Invitrogen #12483, Burlington, ON), 2.5 mg/mL collagen I (BD Biosciences #354326, Mississauga, ON) plus 1M NaOH to achieve a final pH of 7.0-7.4. To prevent premature polymerisation of the collagen mixture, all solutions and substrates were kept on ice up until the point of incubation. This collagen-media mixture was used for all control experiments. The cold collagen-media mixture was pipetted into the wells and the substrate was degassed for 10 min to remove any remaining air bubbles from individual wells. ASM and WI-38 cells trypsinised and pelleted (750,000 cells; 80% ASM plus 20% WI-38 fibroblasts) were re-suspended in the collagen-media mixture and added to the substrates before centrifuging for 90 seconds at 300x relative centrifugal force (RCF) in an IEC Centra MP4R with swinging bucket rotor 224. Excess collagen and cells were aspirated and removed with a cell scraper before incubating at 37°C for 15 minutes to allow for collagen polymerisation. An additional 750,000 cells (80% ASM plus 20% WI-38 fibroblasts) suspended in feeder media were added to the substrate and then centrifuged for 45 seconds at 300x RCF before incubating at 37°C for 10 minutes to allow for cell attachment. Excess cells were gently washed from the surface of the substrate using PBS, leaving a layer of cells on top of the polymerised collagen.

Microtissues were manufactured in 10% serum feeder media for approximately 6 hours to allow for initial cell/collagen compaction and then switched to 1% serum feeder media (please see 4.3.1). The media was changed after 24 hours and subsequently every 48 hours, and all microtissues were used for experimentation at day 3-4 (Figure 2-1).

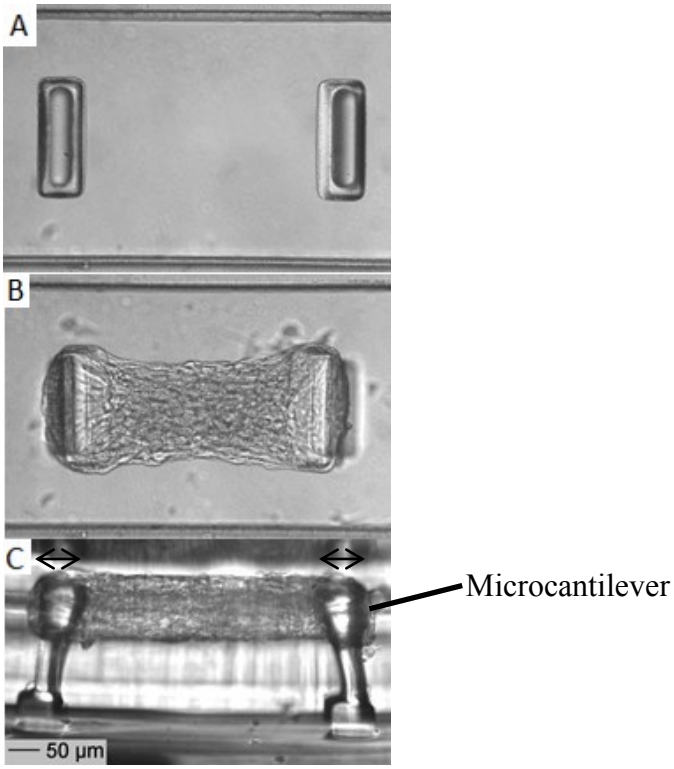

Figure 2-1. Representative brightfield images of ASM/WI-38 microtissues in individual wells. A) top-down view of a single microtissue well, B) top–down view of a single ASM/WI-38 microtissue, C) Side view image of AS/WI-38 microtissue. Arrow indicates bi-directional movement of flexible PDMS microcantilevers.

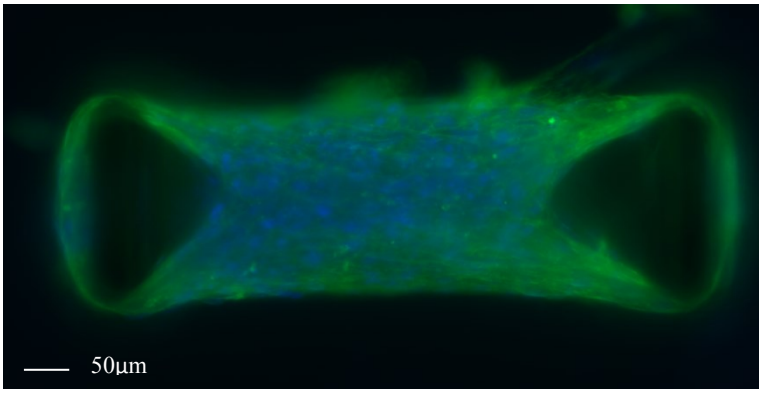

Figure 2-2. A representative composite epifluorescent image of phalloidin f-actin stain (green) and DAPI nuclei stain (blue).

2.3 Histology

Imaging of live and fixed microtissues was performed on a Leica microscope using a 20x lens. Microtissue fixation involved rinsing the tissues with cytoskeleton buffer (CB), fixing them with 4% paraformaldehyde in CB for 20 min then permeabilising them to breakdown the cell membrane and allow the stains to penetrate the cell with 0.3% triton X-100 and 4% paraformaldehyde in CB for 10 min. Microtissues were washed with CB and stored in storage buffer (CB-TBS) at 4°C prior to staining. Microtissue cell nuclei were stained with 0.4 μg/mL of DAPI (Invitrogen D1306, Burlington, ON) in PBS for 30 minutes, while actin filaments were stained with 1U phalloidin-AF488 (Invitrogen A12379, Burlington, ON) for 30 minutes. Images of microtissues stained with DAPI and phalloidin were superimposed using ImageJ software.

2.4 Contractile Function

2.4.1 3D Drug Testing

ASM/WI-38 microtissues were serum deprived for two and a half hours prior to tension measurement experiments by exchanging the feeder media with IT media consisting of DMEM/F12 (Invitrogen #11330, Burlington, ON) with 5.8 µg/mL insulin (Sigma-Aldrich # I1882, Oakville, ON) and 1.0 µg/mL transferrin (Sigma-Aldrich # T4382, Oakville, ON). A range of contractile and relaxant agonists were used to assess contractile function of microtissues 3 or 4 days post fabrication depending on tissue health. Eight stable microtissues from each substrate were selected based on their qualitative appearance and initial images were captured for baseline tension. The drugs used included 80 mM KCl (Sigma-Aldrich, Oakville, ON), 100 µM acetylcholine (Sigma-Aldrich # A6625, Oakville, ON), 100 µM forskolin (Sigma-Aldrich # F6886, Oakville, ON), and 10µM cytochalasin D (Sigma-Aldrich # C8273, Oakville, ON).

The maximal drug doses of each of the pharmacological agents were based on previous work from our laboratory looking at ASM contractile function and related studies (135). The drugs were prepared in IT media and added to the microtissues at 10 minute intervals in an order of contracting and relaxing as follows; ACh, KCl, FSK, cyto D. Before administration of subsequent drugs, the previous drug/media solution was rinsed out of the µTug substrate with warm IT media. Images of all eight microtissues were captured 10 minutes post administration of each drug. Once the images were captured after the final drug treatment, the microtissues were disrupted by sonication and pipetting, and the eight wells were imaged again to determine the unloaded cantilever distances for measurement of tissue tension. Substrates were recycled by treatment with

collagenase (Sigma-Aldrich # C0130, Oakville, ON) in IT media plus 5mM $CaCl_2$, and with TrypLE™ Express (Gibco®) to remove ECM proteins. Substrates were rinsed with PBS, distilled water and ethanol and air dried for storage.

Image processing for calculation of microtissue tension was conducted using ImageJ 1.44. Force generation was calculated based on the deflection of the microcantilevers which was optically measured. The (X,Y) centroid of the tops of both microcantilevers in each image (unloaded, baseline, and drug-treated) was determined by manually tracing around the top of the microcantilevers. Figure 2-3 is a representative brightfield image of an ASM/WI-38 microtissue to demonstrate the region of interest which is represented by the blue lines. The centroid of both of the microcantilevers in each image was measured using ImageJ and the pixel and consequently micron distance between the regions was calculated based on a conversion factor. Microcantilever deflection for the baseline and drug-treated images was calculated by subtracting the distances from the unloaded cantilever distance. Microtissue tension was calculated based on the spring constant k of the microcantilevers in that particular substrate. The deflections were considered linear up to 30 μm per cantilever with a maximum practical measurement limit of 45μm per cantilever (18).

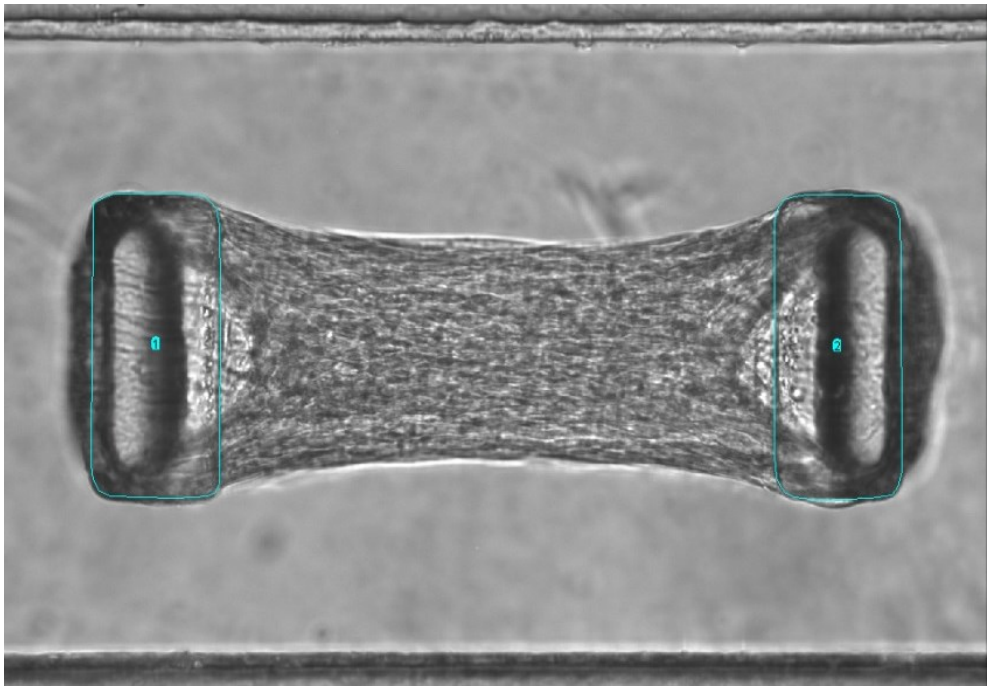

Figure 2-3. A brightfield image of a single microtissue with the region of interest highlighted. The tops of the microcantilevers outlined in blue were manually traced in ImageJ as the region of interest. The (X,Y) centroid of this region in each image (unloaded, baseline, and drug-treated) was traced and measured in ImageJ.

2.4.2 2D Drug Testing

Cell stiffness of ASM cells plated in 2D collagen coated Petri dishes was performed by optical magnetic twisting cytometry (OMTC). Plastic Petri dishes were coated with 0.1mg/mL liquid type I collagen in PBS for about 1 hour at room temperature and then rinsed with PBS. ASM cells were seeded into Petri dishes at a density of 20000 cells per cm^2 and incubated in 10% serum feeder media for 3 days. Cells were serum deprived for 24 hours prior to experimentation by replacing the feeder media with IT media.

OMTC employs the use of about 4.5μm ferromagnetic beads which are coated with an RGD peptide (RGD-199) which binds to integrin molecules on the ASM cells. ASM

cells were washed with IT media and 30μL of the bead solution was added to the centre of the dish, and incubated at 37°C for 20 minutes. Excess beads were removed by washing with IT media, and the dishes were incubated for another 20 minutes. The Petri dishes were placed on the microscope, magnetised twice, and twisted in an oscillating magnetic field with a coil current that applied 91.8 Pa specific torque to the beads to collect baseline stiffness of the cells (37). To assess cellular contractility, an isotonic KCl solution (80mM) made up in IT media, was added to each dish, gently mixed, and then incubated for 3 minutes. An isotonic mixture was used to prevent cells from swelling due to salt-imbalance. The cells were magnetised once again and the post-drug stiffness data were collected. Cytoskeletal stiffness (G', Pa/nm) was calculated based on the bead displacement and applied torque using a custom Matlab code, and the median value was used to determine the percent contractility from baseline.

2.5 Reverse Transcription and Quantitative Polymerase Chain Reactions

The biochemical analysis of the microtissues involved gene expression studies which included RNA quantification, reverse transcription, and real time quantitative polymerase chain reaction (qPCR) of microtissues cultured under various conditions. Gene expression analysis was conducted for key smooth muscle specific contractile and regulatory proteins, transcription factors and reference gene controls. Target genes included myosin heavy chain (MHC), myosin light chain kinase (MYLK), myosin light chain phosphatase (MYPT1), alpha-actin (ACTA1), transgelin (SM22α), vimentin, serum-response factor (SRF), and myocardin (MYOCD). The relative gene expression of

three endogenous reference genes was also measured which included GAPDH, UBC, and YWHAZ. These were used as the housekeeping control genes which are expressed in all cells at a steady state level. The most stable reference gene was selected using Bestkeeper and NormFinder (105).

All gene expression experiments were conducted using Qiagen Sample and Assay Technology kits. The Qiagen RNeasy Mini Kit was used for purification and isolation of RNA from microtissues. Microtissues were cultured under various conditions and RNA was isolated and purified from each substrate 2-3 days post fabrication depending on the health of the microtissues. Excess cells and artifacts on the top of the PDMS were gently removed using a cell scraper and the substrates were rinsed with PBS. Unhealthy microtissues were manually removed by pipetting into individuals wells. RNA isolation involved preparation of the lysate and the use of ethanol to promote selective binding of total RNA to the RNeasy membrane. The RNA was separated from the other components by binding to the RNeasy membrane of specially designed RNeasy Mini spin columns and centrifuging the column multiple times. As total RNA binds to the membrane, contaminants were washed off using RNase-free water. Quantification and purity of total RNA was performed with spectrophotometry. RNA purity was assessed based on the absorbance of ultraviolet light at a wavelength of 260nm and 280nm. Generally, the ratio of these two absorbance values is used to assess purity and lies between 1.6-1.8 for samples diluted in RNase free water.

Prior to qPCR, cDNA synthesis was conducted using the Qiagen QuantiTect Reverse Transcription Kit. RNA samples were reverse transcribed using approximately 0.6µg of total RNA per microtissue substrate. Initially samples were incubated at 42°C

for 2 minutes in gDNA Wipeout Buffer to remove genomic DNA contaminants. The RNA samples were prepared for reverse transcription by mixing with Quantiscript Reverse Transcriptase, Quantiscript RT Buffer, and RT Primer Mix. The mRNA was reverse transcribed to double stranded cDNA using an oligo dT primer which is random, short, single stranded nucleic acid fragments called oligomers. These primers hybridise to the poly-A tail and initiate reverse transcription from the beginning of the mRNA (3'-end) (74). The sample was incubated at 42°C for 30 minutes and at 95°C for 3 minutes.

Table 2-1. Measurement of RNA purity and quantity. A range of RNA dilutions were quantified through spectrophotometry in RNase free water. A dilution of 1/10 was used for further analysis due to the appropriate concentration and purity of RNA.

RNA Dilution (µL)	Ratio of Absorbance ($A_{260:280}$)	Concentration of RNA (µg/µL)
1/70	1.615	0.059
4/70	1.795	0.221
8/70	1.847	0.440
16/70	1.884	0.907

To allow for accurate primer annealing and high sensitivity of the reaction, primers were designed using commercial software tools including Primer-BLAST® (GenBank®, National Center for Biotechnology Information). Good primer design is most importantly dependant on primer length, melting temperature, annealing temperature, guanine-cytosine nitrogenous base content, and secondary structures. Proper primer design prevents the formation of self-complementary regions which can fold into hair pins and other structures, and also prevents the formation of primer-dimers through complementarity between primers. Primers were chosen to span exon/exon junctions, with a guanine-cytosine (GC) content of about 50-60%, melting temperature of 50-60°C, and no secondary structures. A qPCR standard curve was used to assess the efficiency of

primers as well as their dynamic range (80). A standard curve was generated for each primer set by forming serial dilutions. A five-fold dilution across 5 orders of magnitude was performed and amplified through qPCR.

Table 2-2. Primer sets tested in qpCR gene expression analysis . Each primer was selected using Primer-BLAST to span exon-exon junctions to prevent amplification of genomic DNA. Primer specificity was assessed by melting curve analysis.

Gene common name/code	Gene code	Forward/ Reverse primer sequence	Accession no. (Amplicon location)
Smooth muscle myosin heavy chain	MYH11	5'-CTGGAAGGCATTCGCATCTG-3' 5'-CCAGGATCTCGTAGCGTTGG-3'	NM_002474.2
Myosin light chain kinase	MYLK	5'-CTGCTGCCTGACCACGAATA-3' 5'-CATCCTTCGGCTCTTCAGGT-3'	NM_053025.3
Myosin light chain phosphatase	MYPT1	5'-AGTTAATCGGCAAGGGGTTGA-3' 5'-CCTCCAGATTTTGCATGCCG-3'	NM_002480.2
α-actin	ACTA1	5'-TAAGACGGGAATCCTGTGAAGC-3' 5'-TACAGAGCCCAGAGCCATTG-3'	NM_001141945
SM22α	TAGLN	ATCATAGTGCAGTGTGGCCC CAGCTTGCTCAGAATCACGC	NM_003186
Vimentin	VIM	5'-CGAGGAGAGCAGGATTTCTC-3' 5'-AGTGGGTATCAACCAGAGGG-3'	NM_003380
Serum response factor	SRF	5'-AGCTCCACCAGATGGCTGTGATAG-3' 5'-ACTCTTGGTGCTGTGGGCGGT-3'	NM_003131.2
Myocardin	MYOCD	5'-ACTCGAAGTGAAGACCCCCA-3' 5'-AGCAAGATCCTGGTTTGTCCC-3'	NM_001146312.1
Glyceraldehdye 3-phosphate dehydrogenase	GAPDH	5'-CTGCTGATGCCCCCATGTTCGT-3' 5'-TGGTGCAGGAGGCATTGCTGATG-3'	NM_002046.4
Phospholipase A2	YWHAZ	5'-CGCTGGTGATGACAAGAAAGGGAT-3' 5'-GGGCCAGACCCAGTCTGATAGGA-3'	NM_003406.3
Ubiquitin C	UBC	5'-ATAAGGACGCGCCGGGTGTG-3' 5'-GCATTGTCAAGTGACGATCACAGCG-3'	NM_021009.5

Amplification was then conducted according to the protocol outlined by the Qiagen QuantiTect SYBR Green PCR Kit. Samples of 25ng of total RNA of the cDNA were

prepared for qPCR by mixing with 1x Quantitect SYBR Green PCR master mix, forward and reverse primers, and RNase free-water. Samples were amplified in duplicate using the stratagene Mx3000P thermal cycler with 0.3µM of each of the primers of interest for each of the target genes. Thermal cycling conditions involved an initial 15 minute incubation at 95°C for Taq activation, followed by 45 cycles of denaturing at 95°C for 15 s, annealing of primers at 56°C for 30 s, and extension of the primers at 72°C for 49 s. Data was acquired at the end of the extension cycle and the melting curves were generated by incubation of samples at 95°C to denature followed by incubation at 65°C. The melting curve outlines the melting point of products which is dependent on the length and base composition; therefore, all PCR products for a particular primer should in essence have the same melting temperature.

The crossing thresholds were determined using the Stratagene MxPro v3.2 software and the LinRegPCR Software. There are two strategies that can be used to quantify mRNA with real time RT-qPCR. The expression of target genes can be measured by absolute or relative quantitative RT-qPCR. For the purposes of this thesis, relative gene expression was applied and was calculated based on the efficiency-corrected ΔΔCt method. Amplification efficiency strongly affects PCR kinetics and is dependent on PCR reaction components therefore, efficiency correction was necessary since the relationship between the target gene and a housekeeping gene was assessed independently. The final relative expression data was normalised such that the sample with the highest expression was assigned a mean expression of 1. All samples from each condition were run at the same time for each primer set. The crossing point cycle for each gene was around 19-25 cycles, while the crossing point for the endogeneous reference gene GAPDH was 19

cycles (Appendix C: qPCR Reference Gene Selection). Biological replicates were amplified in duplicate and a negative control (no cDNA) was run concurrently to ensure there was no RNA or DNA contamination.

For statistical analysis of gene expression data, One-way ANOVA with Tukey post-hoc comparisons was used to detect significant differences in gene expression between the two treatment groups (soft compared to stiff environment). All statistical tests were performed with the GraphPad 4.0 software package. The data is reported as mean±SEM with $p<0.05$ considered statistically significant.

Chapter 3: PDMS Microcantilever Characterisation

3.1 Rationale

The purpose of Aim 2 of this thesis was to assess the effects of increased loading on ASM contractile function and phenotype as assessed in Chapter 4:. ASM loading was manipulated by controlling the stiffness of the PDMS microcantilever stiffness. For this reason, there was a need to characterise the mechanical properties of the PDMS microcantilevers manufactured in the μTug substrates prior to fabricating microtissues.

3.2 Methods

3.2.1 μTug Fabrication

The μTug substrates were manufactured using a prepolymer of Sylgard 184 polydimethlyl siloxane (PDMS, Dow-Corning, Stoney Creek, Ontario). The PDMS stamps were obtained from our collaborator Dr. Christopher Chen and were made using a silicon photo resist and photolithography techniques as described previously (83). The stamps were fabricated as an inverse of the μTug substrate. The stamps were prepared for silanisation by removing dust and debris using isopropyl alcohol (IPA). Stamps were degassed in IPA for 5 min, dried using N_2 gas and placed onto a glass slide pattern side up. The PDMS stamps were plasma cleaned to establish a hydrophilic surface using the SPI Plasma-Prep™ II Plasma Etcher at one quarter power for 30-45 seconds. The stamps were placed into a desiccator in a fume hood and silanised to prevent sticking during PDMS casting using Trichloro(1H,1H,2H,2H-perfluorooctyl)silane (Sigma-Aldrich # 448931, Oakville, ON). A few drops of silane were added to a glass slide and placed into

the desiccator alongside the stamps. The desiccator was placed under vacuum for 24 hours.

On the second day, Petri dishes with PDMS were prepared by mixing a 1:18, 1:10, and 1:4 ratio of initiator (curing agent): monomer in a plastic beaker and then degassed to remove all air bubbles. Approximately 1.0g of the degassed PDMS mixture was added to Petri dishes to completely cover the bottom with <1mm of liquid PDMS. The Petri dishes were placed on a hotplate set at 60°C for 20 minutes to initiate polymerisation of the thin layer of PDMS and to prevent the stamp from sinking to the bottom of the dish when inverted. Meanwhile, the silanised stamps were prepared by pipetting a small amount of the degassed liquid PDMS onto the stamps to cover the entire pattern. The stamps were then degassed under high vacuum to remove any air bubbles and to allow the liquid PDMS to penetrate into the stamp pattern. The Petri dishes were periodically checked during the 20 minutes of curing to prevent over-hardening of the PDMS. With the pattern face down, the stamps were then inverted onto the Petri dishes gently to avoid trapping bubbles. The stamps were centered in each dish and the dish which was filled with liquid PDMS until it was level with the stamp. Substrates were cured in an oven at 60°C for 5 minutes, re-centered in the dish, and then left to cure for 24 hours or longer based on the stiffness of the substrate being manufactured (see section 3.2.2).

A scalpel was used to remove the stamp from the dish on the third day of manufacturing. Cuts were made along the edge at the interface between the stamp and the substrate for each dish. An ethanol-triton solution (0.75%) was pipetted around the sides of the stamp into the crevice along the interface to reduce surface tension. Before peeling

the stamps, the dishes were positioned so that the microcantilevers were oriented vertically to prevent tearing. Using a pair of tweezers, the stamps were slowly peeled out of the dishes. Stamps and dishes were rinsed in IPA and dried with N_2 gas for storage and re-use.

3.2.2 PDMS Modulus

The microcantilever stiffness was altered by fabricating 3D μTuGs with different ratios of PDMS monomer to curing agent. μTuGs with four different microcantilever stiffnesses were manufactured to provide a range of discrete modulus values. The Young's modulus of the PDMS was measured with a uniaxial tensile testing system equipped with a 10 N load cell. PDMS strips were fabricated and 4 strips each from 5 independent preparations were measured using imaging techniques, preloaded to 0.5 N and then stretched at a strain rate of 1%/second. The Young's modulus was calculated via a linear fit of the stress vs. strain curves over the region of 10-20% strain. These measurements of the Young's modulus were then used to numerically estimate microcantilever spring constants.

3.2.3 Microcantilever Stiffness

To confirm the numerical estimations, the spring constants of microcantilevers were experimentally measured *in situ* from 2 deflections of 4 microcantilevers of each of the 4 samples using a glass micropipette tip and a force transducer (406A, Aurora Scientific, Aurora, ON). The deflection of the microcantilevers was captured by a firewire camera (MC-F433C, 1st Vision, Andover, MA) with a resolution of 640x480. The camera was firmly fixed above the μTuG to one of the two arms of the

micromanipulator (MLW-3 three axis water hydraulic, Narishige, Tokyo, Japan). A 40x microscope objective was used in front of the camera to magnify the image. Measuring the pixel distance between lines on an image of a haemocytometer taken with this setup gave a sensitivity of 1.04μm/pixel. All the measurements were done on a vibration isolation table to prevent any deflection artifacts. The camera feed was acquired on a NI LabVIEW program along with the voltage readings from the force transducer. The deflection of the microcantilevers and the associated force readings were used to calculate the spring constant.

3.2.3.1 Beam Deflection

The spring constants of the microcantilevers were manually measured to confirm the theoretical estimates. The height at which the load is applied (height of micropipette) to the microcantilever (point of deflection) greatly influences the spring constant measurement based on linear beam bending assumptions. This is because the spring constant k of the cantilever is based on material properties, the distance below the tip of cantilever where the load is applied (a), and the length of the beam (L). Based on the equation below for linear beam bending, it can be seen that slight differences in the height at which the load is applied can have a significant impact on the measured spring constant k where the height at which the load is applied is the theoretical centre of a microtissue encompassing the microcantilevers. To determine the effect of bending the microcantilevers at different distances below the tip of the microcantilever, force vs. displacement curves were generated for two different μTug substrates.

$$k = \frac{6EI}{a^2(3L - a)} \qquad (1)$$

3.2.3.2 Timoshenko Beam Bending

According to Timoshenko beam bending theory (129), the differential equations regarding the deflection of cantilever beams can be used to determine the stiffness of the PDMS microcantilevers. The following differential equations were solved based on boundary conditions for cantilever beams with a fixed end and intermediate loading where M is the bending moment of the beam, V is the transverse shear force, ϕ is the rotation about the y-axis, ω is the transverse deflection of the centroidal axis of the beam, K is the shear correction coefficient, G is the shear modulus, A is the cross-sectional area, E is the Young's modulus, and I is the second moment of area.

$$M = -EI \frac{d\varphi}{dx} \qquad (2)$$

$$V = -GAK\left(\varphi - \frac{d\omega}{dx}\right) \qquad (3)$$

$$q = EI \frac{d^3\varphi}{dx^3} \qquad (4)$$

3.3 Results

3.3.1 PDMS Modulus

Multiple PDMS strips were fabricated and the Young's modulus was measured with a uniaxial tensile testing system (Tissue Mechanics Laboratory, Dalhousie

University). Four discrete moduli values covering a wide range were obtained as can be seen in Table 3-1. The data is represented as mean±SEM (standard error of mean) where the standard deviation was based on the optical measurement of the dimension of the PDMS strips.

Table 3-1. List of the four PDMS samples and the four different ratios of monomer to curing agent used to fabricate substrates. Young's modulus measured using uniaxial tensile testing system to provide four discrete moduli values. Mean moduli values represented as mean±SEM.

PDMS ratio of crosslinker : monomer	**Young's Modulus (MPa)**
1:18@ 60°C, 24 hrs	0.55±0.02
1:10@ 60°C, 24 hrs	1.47±0.05
1:10 @ 60°C, 24 hrs and 110°C, 48 hrs	2.27±0.08
1:4 @ 60°C, 24 hrs and 110°C, 48 hrs	3.51±0.18

Stress vs. strain curves generated from the data demonstrated a linear relationship between force and displacement, and minimal hysteresis between the loading and unloading of each of the samples, as can be seen in the stress vs. strain curve shown in Figure 3-1 for a PDMS sample with a Young's modulus of 3.51MPa (PDMS ratio of 1:4).

The equation for intermediate loading of a cantilever beam was used to estimate the spring constant values of the microcantilevers based on the measured Young's moduli according to linear beam bending assumptions with and without shear deformation (Table 3-2).

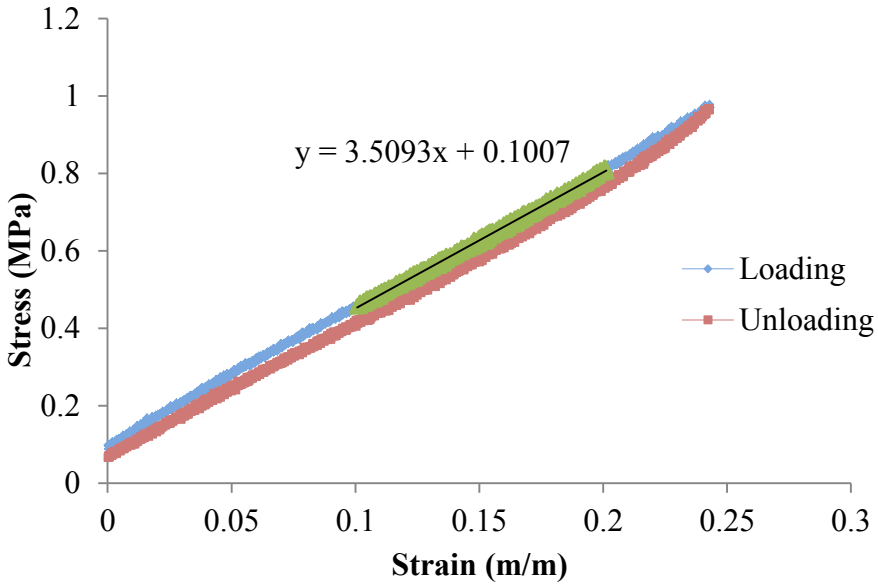

Figure 3-1. Representative stress versus strain curve for a single PDMS strip with a curing agent to monomer ratio of 1:4. Line of best fit to loading and unloading curves as indicated where the slope of the curve=3.5093 provides the Young's Modulus E. Green points represent linear region between 10-20% strain where E was calculated.

3.3.2 Microcantilever Stiffness

To confirm the theoretical spring constant estimations, the spring constants of the microcantilevers as manufactured in the µTugs was also manually measured for each of the four µTug substrates using a force transducer and glass micropipette. All force displacement plots were linear for deformations spanning the range of those exerted by microtissues (max 50µm). However, the experimental measurements of the microcantilever spring constants for 3 of the PDMS samples were lower than the theoretical estimates (Table 3-2). Since the theoretical values did not match the measured spring constant values, two theories were postulated to explain the possible cause of the underestimation of the manually measured spring constant values.

Table 3-2. Characterisation of microcantilever mechanics. Spring constants measured using micropipette and force transducer system, and estimated spring constants calculated based on equations for Euler-Bernoulli linear beam bending. Data presented as mean±SD. Standard deviation in estimated spring constant values is due to measurements of microcantilever dimension.

µTug Sample #	**Measured Spring Constant (µN/µm)**	**Euler-Bernoulli: Estimated Spring Constant (µN/µm)**
1	0.22±0.14	0.21±0.01
2	0.32±0.12	0.57±0.04
3	0.68±0.29	0.88±0.05
4	1.01±0.26	1.36±0.08

3.3.2.1 Beam Deflection

Spring constant measurements from sequential deflections of individual cantilevers demonstrated high variability as can be seen with the large standard deviations for the measured values in Table 3-2. This large variation may have been due to the position of the micropipette during manual bending of the microcantilever since it is challenging to determine the accurate distance below the tip of the microcantilever where the load should be applied to deflect it.

To quantify the effect of deflecting the microcantilevers at different distances below the tip, the spring constants for 2 µTug substrates were measured at varying heights below the tip. Side view images of individual microtissue wells with and without microtissues were captured to measure the height of the centre of the microtissue as well as the cantilever dimensions optically using a 20x objective (Figure 3-2). The distance below the tip of the cantilever is shown in Figure 3-2 as the difference between the red and green lines. The pixel distance between lines on an image of a haemocytometer was used

to calculate a calibration factor for conversion from pixels to microns as described in 3.2.3.

The data showed that as the indenter was positioned closer to the base of the microcantilever, the spring constant measured increased correspondingly (Figure 3-3). However, at a height of approximately 30μm below the top of the microcantilever the measured spring constant was within 5% of the estimated theoretical spring constant value.

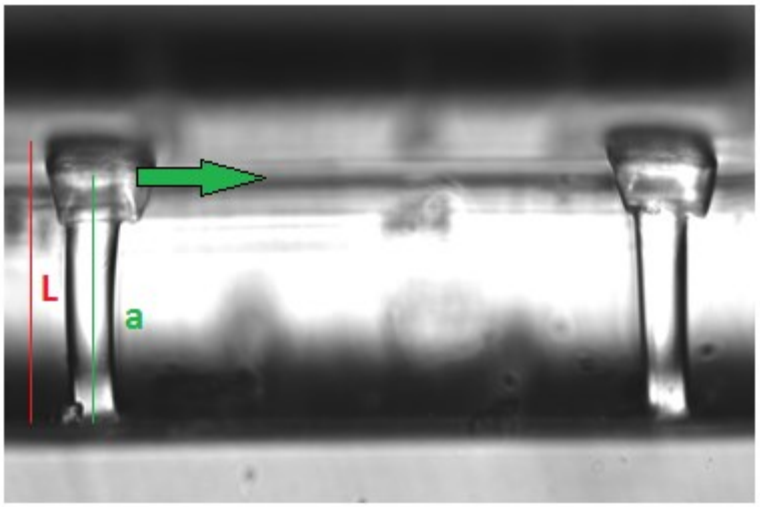

Figure 3-2. Side view image of a single microtissue well with a pair of microcantilevers used to measure the dimensions. (L) Length of the microcantilever, (a) the distance from the fixed end of the cantilever to the point where the load is applied (centre of microtissue). The distance below the tip of the microcantilever is the difference between the red and green lines.

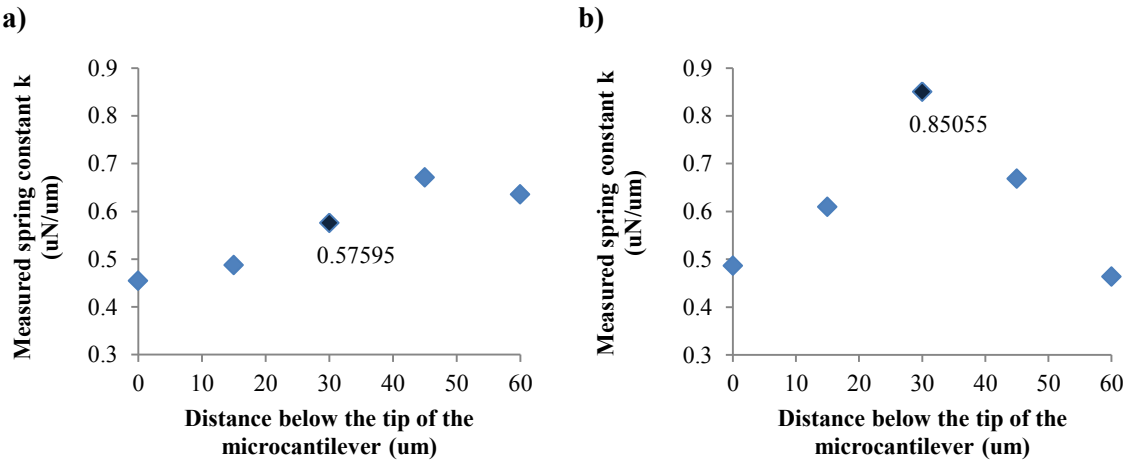

Figure 3-3. Microcantilever stiffness (spring constant) when deflected at different distances below the tip. Micropipette (force transducer head) was placed at different distances below the tip of the microcantilever in increments of 15µm to obtain a force vs. displacement curve to calculate the spring constant of compliant microcantilevers with **a)** PDMS ratio of 1:10 baked at 60°C for 24 hours and **b)** stiff microcantilevers with a PDMS ratio of 1:10 baked at 60°C for 24 hours and then 110°C for 48 hours. Graph demonstrates the variation in the spring constant k with increasing the distance below the tip of the microcantilever at which point the load is applied to bend the cantilever. Dark blue dot demonstrates matching between estimated/theoretical and measured spring constant k.

3.3.2.2 Timoshenko Beam Bending

As stated in the previous section, the measured spring constant values for each of the four PDMS µTug microcantilevers were much lower than the estimated values based on Euler-Bernoulli linear beam bending assumptions (Table 3-2). Looking at equation (1) this underestimation could be explained by variation in the distance below the tip of microcantilevers where the micropipette tip is placed during the deflection experiments as discussed above. However, another possible explanation for the disparity between the measured and the Euler-Bernoulli theoretical spring constant values may be the effect of shear deformation on microcantilever bending.

Euler-Bernoulli beam bending theory is based on linear beam bending without any effect of shear. It assumes that the planar cross-section of the beam perpendicular to

the axis of the beam remains perpendicular to the axis after deformation negating all transverse shear strain. On the other hand, Timoshenko beam bending theory (129) is linear beam bending (extension of Euler-Bernoulli) which takes into account shear deformation. Timoshenko beam bending may be applicable in this circumstance as it is generally used to describe linear beam bending of short and thick beams where the effect of shear strain cannot be negated as the plane section remains plane but not perpendicular to the axis of the beam post deformation. The differential equations for Timoshenko beam bending for a cantilever beam with intermediate loading (loading below the tip of the cantilever) were solved and the spring constants were calculated for each of the four PDMS samples (Table 3-3). The resulting spring constants were lower than the spring constants estimated based on the PDMS Young's moduli under linear Euler-Bernoulli bending assumptions as seen in Table 3-2.

Table 3-3. Theoretical spring constants based on Timoshenko beam bending accounting for shear deformation for each of the four PDMS samples . Data is shown as mean±SD, where the standard deviation is due to the measurement of the dimensions of the cantilevers.

µTug Sample #	**Timoshenko: Estimated Spring Constant (µN/µm)**
1	0.18±0.01
2	0.48±0.03
3	0.75±0.05
4	1.16±0.07

3.4 Discussion

The main finding of this chapter was that the mechanical properties of the microcantilevers in this PDMS µTug model can be manipulated to possess a wide range of stiffnesses by controlling the ratio of monomer to curing agent and the heat treatment.

Additionally, the bending and deflection of these microcantilevers was characterised more appropriately under Timoshenko bending assumptions.

One of the key features of this model is the ability to manipulate the mechanical properties. The ability to alter the mechanical properties of the PDMS μTug substrates permits assessment of the effect of increased loading on ASM contraction. For this, PDMS strips were manufactured and the Young's modulus was measured which was used to estimate the range of spring constants for four different samples. The microcantilever spring constants were also manually measured to confirm these estimates. However, the results showed that the measured spring constants were all about 15% less than the estimated values. Previously, the characteristics of this model were established by Chen et al. (83), however, their findings demonstrated correlation between measured and theoretical spring constant values. Two possible theories that could explain the underestimation of the measured spring constant values in this thesis include: 1) the distance below the tip of the microcantilever where the load was applied by the micropipette during the bending experiments; 2) the effect of shear deformation during cantilever bending.

As outlined, one of the possible reasons of underestimation of the measured spring constants may have been because of inaccurate estimation of the placement of the micropipette during deflection. To test this hypothesis, the microcantilevers were deflected by placing the micropipette at various distances below the tip and the results showed that as the distance below the tip (where the cantilever was deflected) increased, the effective spring constant increased. Therefore, during manual measurement of the spring constant values, the height of the micropipette may have been overestimated and

positioned higher than expected. The experimental measurements of the microcantilever spring constant were conducted using an inverted microscope and camera set up as described in section 3.2.3. This set up prevented accurate estimation of the placement of the micropipette tip and consequently the point at which the load was applied to deflect the cantilever, since the microcantilever was visualised from a top down perspective. This demonstrates a possible reason for the low measured spring constant values using the micropipette and force transducer system for each of the samples in comparison to the theoretical spring constants.

Another possible reason for the difference between the measured and theoretical spring constants may be the occurrence of shear deformation. The original study describing this 3D model by Chen et al. (83), demonstrated the bending of these microcantilevers as linear under the assumption of no shear deformation. This assumption may have been valid for that study since the dimensions of the microcantilevers were different. For this study the microcantilevers were thicker and wider compared to those used in that study making it probable that shear deformation could be occurring since, shear deformation is an issue for beams that are short and thick with a low slender ratio (32). Therefore, the effect of shear deformation on microcantilever bending provides an explanation for the disparity between the measured and the Euler-Bernoulli theoretical spring constant values. Based on the dimensions of the microcantilevers, in addition to linear beam deformation, taking shear deformation into consideration would effectively lower the spring constants or apparent stiffness of the microcantilevers, which was seen in the results.

In summary, accounting for shear deformation, the effective spring constant of the PDMS was decreased by about 10-15%, bringing the measured spring constant data closer to the predictions from theory. Taking into consideration the underestimation of the manually measured spring constants, and the large variation due to methodological issues, the theoretical Timoshenko spring constants were applied hereafter in this thesis.

Chapter 4: Mechanical Loading of Microtissues

4.1 Rationale

A number of 3D culture models that have been used to assess ASM function employ free-floating matrix gels as discussed in section 1.6.2.1. However, it has been shown that encapsulating free-floating gels or constraining them in some form alters the expression of various proteins (24, 47); for instance, fibroblasts embedded within free-floating gels display low actin stress fibers, and low focal adhesion formation, but display an organised structure and augmented contractile gene expression once cultured onto a constrained scaffold (47). For a 3D culture model of ASM cells, the tissues must be constrained to provide a load opposing ASM contraction as this mimics physiological conditions. *In vivo*, the force generated by ASM cells is in mechanical equilibrium with the passive reaction forces acting on the airway wall i.e. the cells are naturally constricting against an outward load (16). This outward elastic load is from a number of components of the airway wall, as well as the parenchymal tethering (40). The smooth muscle is linked to connective tissue in the small airways, and to connective tissue linked to cartilage in the larger airways, which together with the elastic component of the muscle provides an auxotonic load on the contractile apparatus. (84). Therefore, to better mimic the *in vivo* environment, ASM cells need to be constrained in some manner. Additionally, constraining the ASM/WI-38 microtissues allows control over the boundary stiffness imposed on the microtissues as opposed to the bulk stiffness of the ECM.

The importance of the microcantilevers present in the 3D μTug model is demonstrated by two previous studies involving fibroblast and cardiac microtissues

respectively (18, 83). These studies demonstrated that boundary stiffness (loading) and bulk modulus of the ECM initiate diverse responses in contractile function and mechanical stress (18, 83). In relation to the pathology, asthma leads to changes in the structure of the airways which may alter the load on ASM cell contraction potentially enhancing contractile capabilities (16). On the other hand, airway inflammation may decouple the airway and parenchyma altering the balance of forces between ASM constriction and parenchymal tethering (outward load). Combined with a change in ASM contractile function, this can potentially lead to AHR in asthma. For these reasons, studying the effects of an altered load opposing contraction of ASM/WI-38 microtissues is essential in simulating the change in the mechanical environment due to airway remodeling.

Prior to experimenting on ASM/WI-38 microtissues, the protocol used to fabricate these tissues required optimisation. The μTug is engineered in such a manner as to allow the microtissue to anchor to the substrate. As the well surface of the μTugs is rendered non-adhesive to cells (see section 2.2), the contractile action of the cells causes the cell and collagen mixture to compact around the microcantilevers within hours. This initial contraction of ASM cells allows the formation of dog-bone shape microtissues anchored between the two microcantilevers that are prevented from slipping off the microcantilever heads. Even with the anchoring of the cell/collagen construct to the microcantilever head, microtissues slip off, rendering them unusable for function studies. The previous ASM/WI-38 microtissue fabrication protocol (135) had some practical limitations. The survival rate of the microtissues was only 50% which is largely thought to be due to the way the tissue compacts around the microcantilevers. Other microtissue failure modes

involved cells not forming a healthy tissue and sticking to the sides of the wells as opposed to the tops of the microcantilevers, tissues growing on a single microcantilever, and finally tissues spreading across multiple wells (Figure 4-1). The main focus of this study is to assess the chronic effect of changes in the mechanical environment on ASM/WI-38 microtissue function and phenotype. For this reason, improving the survivability and longevity of microtissues was necessary.

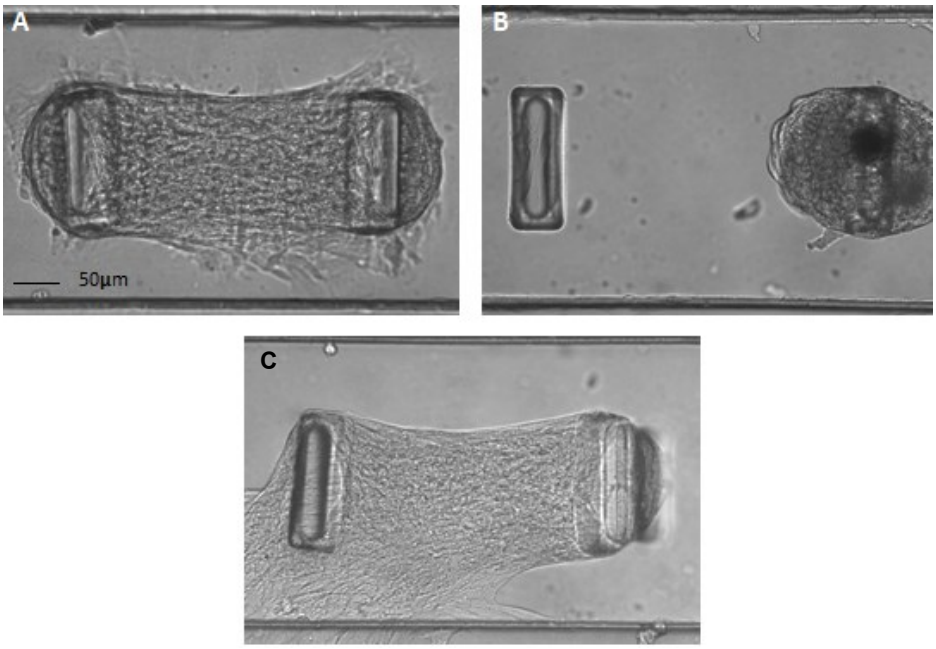

Figure 4-1. An array of ASM/WI-38 microtissues that did not form healthy tissues (failure modes) . A) Cells adhering to the bottom of the µTug well, B) Cells not fully forming a tissue and aggregating on a single microcantilever, C) Microtissue growing across two adjacent well.

4.2 Methods

4.2.1 Optimisation of Microtissue Fabrication

Two approaches were investigated to enhance survivability and longevity of ASM/WI-38 microtissues. Survivability (record of healthy tissues) was assessed by qualitative verification of healthy microtissues as well as counting positive number of microtissues over a period of 7-10 days. All statistical analyses were completed using two-way ANOVAs with Bonferroni post-hoc comparison tests to assess differences between groups and within individual groups. For all statistical comparisons, $p<0.05$ was taken to be significant.

4.2.1.1 Fibrin

To promote the integrity of the 3D matrix and the ASM/WI-38 microtissue, the first approach of aim 1 was to add another matrix protein such as fibrin. This would provide additional structural support to the ECM and the microtissue, as it is not degraded by the matrix metalloproteinases (MMPs) responsible for the breakdown of collagen (2, 27, 112). ASM/WI-38 microtissues were fabricated according to standard protocol outlined in section 2.2; however, in addition to the 2.5mg/ml collagen, 0.5mg/ml fibrinogen was added to the collagen/media mixture which was subsequently pipetted into the μTug substrate. After the initial polymerisation step, the microtissues were exposed to thrombin (1 NIH units) to allow for fibrinogen polymerisation to fibrin (27). The final steps in the fabrication process were carried out and finally the tissues were incubated in 10% serum feeder media. Microtissue survivability was monitored over a period of 7-10 days (record of healthy tissues).

4.2.1.2 Serum

The second approach to promote survivability of microtissues was to alter the serum concentration of the feeder media. Serum concentration of feeder media is a critical factor in the survivability and state of cells (87). As per the previous microtissue fabrication protocol (135), tissues were cultured in 10% serum feeder media. However, lower serum concentration subdues growth rates which would prevent ASM cells from releasing their anchoring early on and slipping off the microcantilevers. Therefore, microtissues were fabricated according to the protocol outlined in section 2.2 and cultured in 10% serum feeder media for 6 hours to allow for initial compaction of the gel matrix and then switched to 1% serum feeder media or 5% serum feeder media (data not shown).

4.2.2 Mechanical Loading

The load opposing ASM contraction was increased by altering the ratio of PDMS monomer to curing agent and the heating treatment as described above in Methods 3.2.1. ASM/WI-38 microtissues were fabricated accordingly and contractile function and phenotype was assessed 3-4 days post tissue fabrication as described above in Chapter 2:

4.3 Results

4.3.1 Optimisation of Microtissue Fabrication Protocol

The first approach of adding fibrin to the matrix enhanced survivability of the ASM/WI-38 microtissues considerably compared to the control group (74.8% at day 3, $p<0.05$) (Figure 4-2). In addition, fabricating ASM/WI-38 microtissues in low serum (1% serum) media also increased survivability significantly (71% at day 3, $p<0.05$). Increased

survivability was observed at days 2 and 3 post tissue fabrication. However, there was no significant difference in the effect on survivability between the two approaches; adding fibrin to the matrix or culturing tissues under low serum conditions.

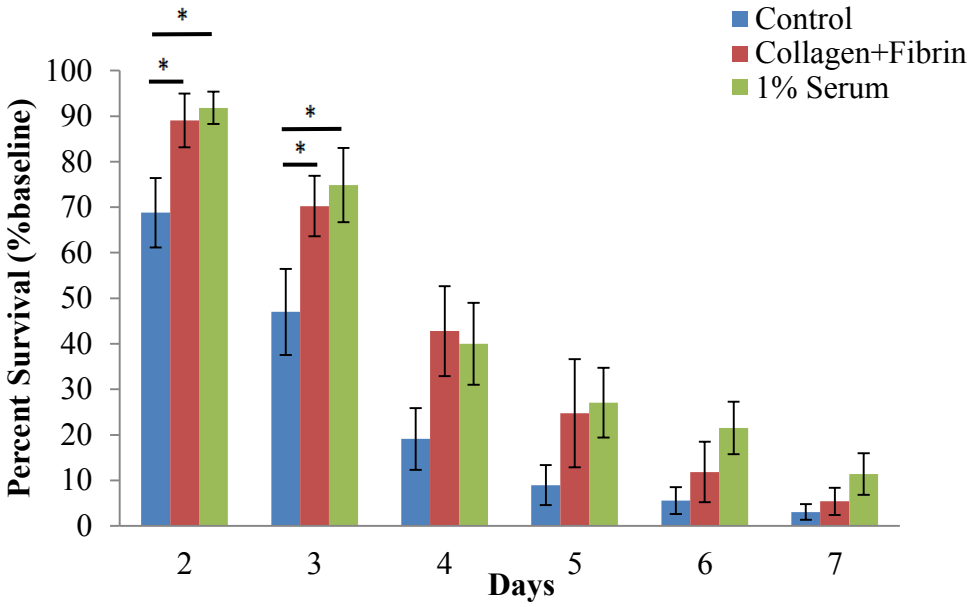

Figure 4-2: Survivability of the ASM/WI-38 microtissues fabricated under different conditions - optimisation of collagen gel matrix. Blue: control group - collagen gel with 10% serum feeder. Red: collagen+fibrin group with 10% serum feeder. Green: collagen gel with 1% serum feeder. Survivability increased with the addition of fibrin to the gel matrix as well as fabrication of ASM/WI-38 microtissues with 1% serum media. Two-way ANOVA with Bonferroni post hoc comparison, $p<0.05$ considered significant.

4.3.2 Microtissue Contractile Function

Aim 2 of this thesis was to assess the effect of increased loading on ASM function and phenotype addressed in the following sections. The contractile function of ASM/WI-38 microtissues was measured using 2 contractile drugs ACh and KCl, a relaxant drug FSK, and a cytoskeletal disruptor cyto D (Figure 4-3). With a higher load (k=1.16 μN/μm) opposing the microtissues, ASM contractility was increased significantly

(22.72±1.82μN, $p<0.01$). Contractile function experiments for microtissues fabricated in μTugs with the two lowest spring constants of k=0.18μN/μm and k=0.48 μN/μm were not conducted. This is because the high baseline tone caused microtissues to deflect microcantilevers past their linear range and pull off the microcantilevers preventing further analysis of contractility.

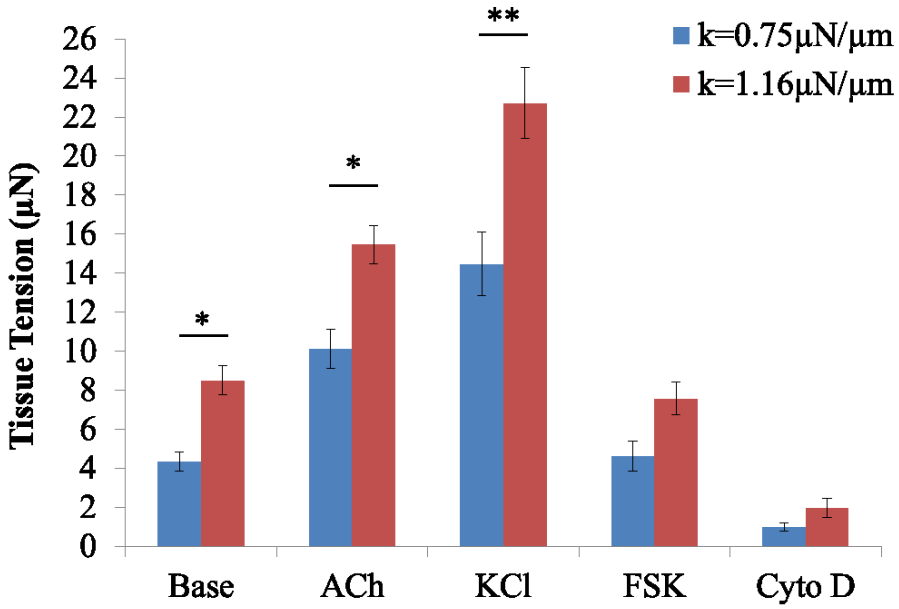

Figure 4-3. Contractile function of ASM/WI-38 microtissues varying mechanical loading (n=24). Microtissues generated significantly more tension when fabricated in μTugs with stiff microcantilevers (constriction against a larger load) at baseline, and contracted with ACh and KCl. * $p<0.05$, ** $p<0.01$. Statistical analyses completed using two-way ANOVA with Bonferroni post hoc test. Base: baseline, ACh: acetylcholine 100 μM, KCl: 80 mM, FSK: forskolin 100 μM, Cyto D: cytochalasin D 10 μM.

4.3.3 Gene Expression - qPCR

To assess whether gene expression was altered with increasing microcantilever stiffness, qPCR gene expression data was obtained for microtissues fabricated in each of the four μTugs with the different microcantilever stiffnesses. The genes were all expressed relative to a calibration sample which was the microtissues fabricated in the

μTugs with k=0.75μN/μm and normalised to the reference gene GAPDH (Appendix C: qPCR Reference Gene Selection). Relative gene expression data was shown such that the sample with the maximum gene expression was assigned a unit of 1 for each gene of interest. Although contractile function was enhanced by increasing the load opposing smooth muscle contraction as demonstrated in Figure 4-3, there was no significant difference in gene expression of the various regulatory and contractile proteins (Figure 4-4).

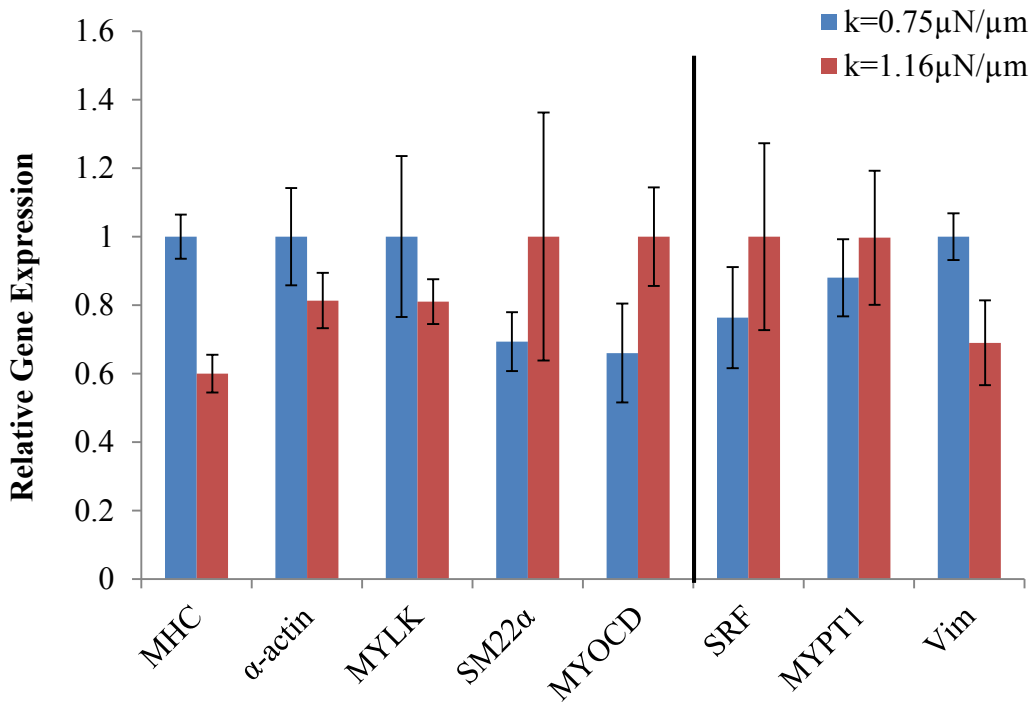

Figure 4-4. Comparison of relative gene expression for 8 genes from ASM microtissues fabricated in μTugs with two different microcantilever stiffnesses (n=3). Line separates genes promoting contraction (left) and those opposing contraction (right). Efficiency corrected method of quantification against a stable reference gene GAPDH. $p<0.05$ was considered significant.

4.4 Discussion

4.4.1 Microtissue Fabrication Optimisation

The main finding from this portion of the thesis was that fabricating microtissues in low serum media increased their survivability to 71% at day 3 compared to 50% at day 3 as per the previous protocol (Figure 4-2).

Lower serum in the media of the ASM/WI-38 microtissues may have decreased ASM cell proliferation rate thereby enhancing the integrity of the microtissue. These results could possibly be understood because smooth muscle cell proliferation involves cells breaking their linkage with the neighbouring cells and the ECM, dividing through mitosis, and then reattaching to the environment. Therefore, if the proliferation rate was decreased with lower serum, this would result in fewer cells going through the growth cycle simultaneously, thereby, keeping the microtissue structure intact over a longer period of time. Based on these results, I continued fabricating the ASM/WI-38 microtissues in low serum feeder as opposed to adding fibrin to the gel matrix, since both approaches produced the same effect on survivability. Moreover, the addition of fibrin may in turn alter the stiffness of the collagen gel matrix thereby potentially affecting the other experiments involved in my thesis, since fibrin has previously been used to enhance the strength and stiffness of collagen matrices (27).

4.4.2 Effect of Mechanical Loading

The main finding of this portion of the thesis was that increased load on ASM/WI-38 microtissues substantially increased contractile function; however, functional changes did not match gene expression changes.

Airway remodeling in asthma involves structural changes to the airways caused by increased deposition of various matrix proteins combined with inflammation, thickening of airway compartments, and an altered balance of forces. The purpose of aim 3 addressed in the following chapter, was to manipulate the bulk properties of the ECM of ASM microtissues in combination with altering the load opposing contraction to simulate the overall changes evident in asthmatics. However, the main purpose of aim 2 addressed in this chapter was to explore the effect of increased load by altering the post stiffness. Thus together these chapters explore the effect of load and matrix stiffness separately. It is difficult to assess these variables and how they are altered *in vivo* in asthma, although both variables may be altered. The stiffness of the ECM is likely increased but the load may either be unaffected, or may actually be reduced relatively. While both variables may be altered, these experiments were not meant to directly represent a pathophysiological equivalent, which is difficult since asthma is multifactorial and there is much debate over the mechanical implications of airway remodeling on smooth muscle. Indeed, increasing the microcantilever stiffness in this 3D culture model may be more akin to the impact of stiffening of the parenchyma increasing the load against the ASM in other pulmonary pathologies such as pulmonary fibrosis. This 3D model of airway remodeling thus is meant to simplify the mechanical environment to

understand their independent influence and separate these biomechanical factors that may be involved in modulating cell function.

Nevertheless, in relation to the pathology, it has been shown that airway remodeling in asthma alters the structure of the airway and components surrounding the ASM layer thereby potentially increasing the stiffness of the ASM microenvironment and load opposing ASM contraction (93). In this thesis, the contractile function results showed that increased loading on ASM microtissues enhanced contractility suggesting that if true *in vivo*, a stiffer airway itself can lead to enhanced ASM contractile function. This increase in ASM tension generation could lead to increased airway narrowing. However, since the airway is stiffer, this response may actually act to help maintain normal contractility since greater force is required to obtain similar narrowing in a stiffer airway.

It was hypothesised that increased loading on ASM cells would enhance contractile function through a phenotypic change. Although function was enhanced with increased loading on ASM microtissues, there was no significant difference in the abundance of mRNA for the genes of interest. The purpose of this study was to assess the chronic effect of increased loading on ASM function and phenotype. For this reason function was assessed 3 days post tissue fabrication and correspondingly, RNA was extracted from microtissues 2-3 days post tissue fabrication to assess the long term change in mRNA levels. However, this may have prevented accurate representation of the phenotypic state of the cells as mRNA and protein levels do not necessarily correlate (49). Changes in mRNA abundance occur much sooner than protein changes, therefore, the level of mRNA in steady state might have been low at that specific time of RNA extraction but

the protein translated was accumulated over time. In a vascular study assessing the effect of a different mechanical stimulus compared to this thesis, oscillatory mechanical strain, on smooth muscle myosin expression, it was shown using immunoblotting that sm-MHC isoform protein expression was significantly enhanced with chronic mechanical strain over a period of 72 hours (110). Accordingly, mRNA levels of sm-MHC were directionally the same with a significant increase, but this did not occur over the same course of time. The mRNA levels for sm-MHC was increased maximally by 12 hours and then returned to control levels (steady state) after 36 hours. This suggests that changes in protein expression following mechanical stimulation were most likely due to changes in mRNA abundance, but the levels were transient due to regulation at the level of protein modification (110). Consequently, it may be difficult to correlate the abundance of contractile genes using qPCR to phenotypic changes when assessing one specific time point.

Another factor that may cause the lack of correlation between gene expression and function may be the large variation in gene expression for each sample. This could largely be due to a relatively low number of samples measured with qPCR in this study. Generally, a sample size of n=3 or more is used when assessing gene expression with qPCR. The measurement of more biological replicates (larger sample size) would decrease the variability between the samples with the same stimulus. The lack of finding significance was also possibly limited by the statistical power in this study. Post hoc statistical power calculations were performed using G*Power© (version 3.1.5). As a standard for adequacy a statistical power of 0.8 was used (80% probability that the test will detect a significant difference) (Appendix A: Statistical Power Analysis). With a

sample size of n=3 for each treatment group, 8 genes, and >20% standard deviation which is approximately the average standard deviation seen in this data, a difference would have to be greater than 90%. Alternatively, if the differences shown in Figure 4-4 were true, then this would require a sample size of greater than or equal to 6 for this difference to achieve significance.

Previously using this model Boudou et al. (18) demonstrated how contractile work by the microtissues against elastic boundaries (microcantilevers) such as auxotonic loads improves tissue development and sarcoplasmic reticulum development which results in higher tension. Increased tissue development leads to a highly compact ECM and increased cell alignment thereby enhancing cellular tension. This may also explain the increased contractile function reported here. Without any change in mRNA or protein, restructuring of the cytoskeleton and contractile filaments could have increased the contractility by increasing the number of cross bridges between actin and myosin, an increase in the ratio of f-actin to g-actin, as well as concentration of force along the centre of the tissue (117).

Other possibilities exist such as increased activation in the contractile signalling pathway. For example, another mechanism for the enhanced contractile function could be the activation of integrin associated proteins such as focal adhesion kinases, which have been identified to play a role in regulation of cell contractility (122). Altered phosphorylation of these membrane associated proteins in intact smooth muscle has been shown to be responsible for improved organisation of contractile elements or enhanced contractile function and calcium regulation.

In summary, the purpose of investigating smooth muscle gene expression was to detect whether there were any differences that would indicate a phenotypic change in ASM to explain the changes in contractility. There were no significant differences detected in gene expression, either because the changes were too small to detect at that time point with chronic treatment, or due to alternate mechanisms such as cellular organisation, or contractile signalling activation.

Chapter 5: Extracellular Matrix Manipulation

The third aim of this thesis was to manipulate the ECM of the ASM/WI-38 microtissues applying two approaches; increasing the collagen crosslink concentration through non-enzymatic glycation and altering the collagen density by increasing the collagen concentration.

5.1 Rationale

One principal drawback of nearly all current culture models used to study ASM interactions with the ECM, including the process of airway remodeling is an inability to manipulate the biomechanical environment whilst providing a physiological setting (138). The limitations of various current e*x vivo* and *in vitro* culture methods were discussed earlier in section 1.6.

As discussed above in section 1.4, airway remodeling leads to various changes in the ASM microenvironment. A number of studies have demonstrated a variation in the profile of ECM proteins within asthmatic airways (100, 106). Some of the most prominent changes in the ECM of asthmatic airways are an increase in type I collagen, fibronectin, tenascin, hyaluron, and laminin, and a decrease in type IV collagen and elastin (7). Changes in the ECM profile in the airways can also lead to ASM hyperplasia further influencing AHR (65). Therefore, these changes may alter the local stiffness of the ASM microenvironment, potentially affecting cytoskeletal organisation and contractile phenotype. The effect of substrate stiffness has been studied previously in other cell types including fibroblasts, cardiac myocytes, and stem cells, where it has been shown that stiffness modulates function and phenotype (18, 83, 123). Additionally, it has

been shown that ASM cells grown in the presence of Type I collagen modulate their phenotype to a more proliferative state but this was in 2D *in vitro* studies where cells were cultured on very stiff substrates (7). It is not known if this effect is maintained when ASM cells are grown in a more physiologically relevant 3D culture model. For these reasons, altering the stiffness of the ECM of ASM microtissues was attempted in an effort to simulate part of the airway remodeling process.

The strength and structure of collagen matrices and scaffolds have been manipulated using different approaches for several different applications as discussed in Chapter 1 section 1.8 (38, 43, 91, 94). In this thesis, two different methods were applied to simulate the change in stiffness of the ASM microenvironment. The first approach was to increase matrix stiffness through collagen crosslinking and the second approach was to increase matrix stiffness by increasing collagen density. All methods, including these two approaches, are limited in assessing the effects of matrix mechanics on cell function because changes to matrix stiffness also cause other changes in material properties (Figure 5-1). For example, while increasing collagen density increases the matrix stiffness, it also increases the availability of ECM binding sites (cell adhesive sites) to the ASM, which may alter phenotype. Crosslinking the collagen matrix does not alter the number of ECM binding sites, but does introduce a new substance which may alter phenotype as well (125).

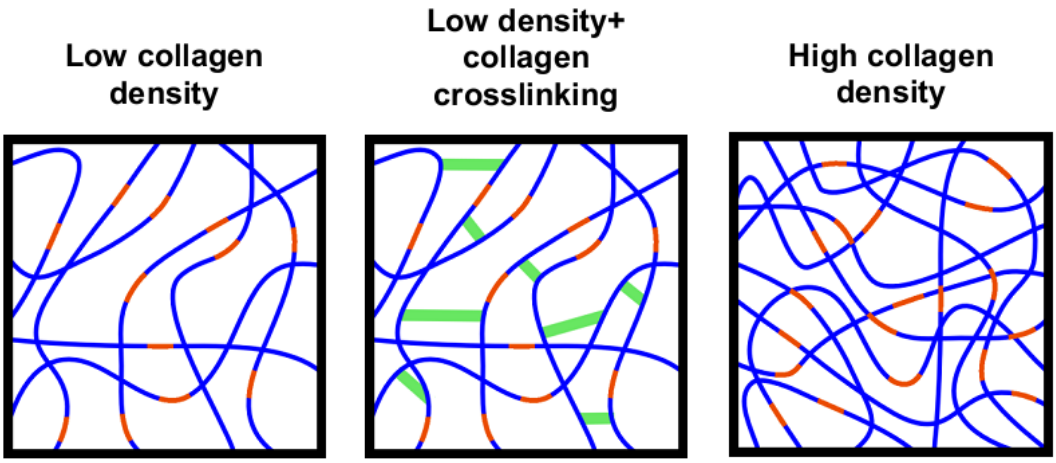

Figure 5-1. Structural feature of collagen matrices at the nano-scale to demonstrate the two main approaches used to modulate matrix stiffness: increasing crosslinking (middle) and increasing density (right). Blue lines: collagen fibres, orange: cell adhesive site, green: crosslink.

5.2 Approach 1: Collagen Crosslinking

In order to alter the ECM stiffness I applied two approaches. The first approach was to increase the crosslinking concentration of the collagen gel through non-enzymatic glycation of the matrix (43). As described previously in section 1.8, non-enzymatic glycation is a popular/advantageous method used to crosslink collagen gels due to its low cytotoxicity and ability to alter stiffness by orders of magnitude. Microtissues were fabricated accordingly (see section 2.2) and incubated with feeder media for 6 hours to allow for initial compaction of the gel matrix. The media was then switched to 30mM d-ribose supplemented 1% serum feeder media. Contractile function of the microtissues was assessed by the method described in section 2.4.1 and contractile phenotype was assessed through gene expression studies to examine markers of contractile proteins (see section **Error! Reference source not found.**). To assess whether there was a biochemical side effect of d-ribose sugar on ASM contractile function, anti-RAGE

antibody was used to inhibit the interaction of AGE products with the receptor for AGE (RAGE). Collagen fibrils are crosslinked by ribose sugar through a reaction between the sugar and the amino groups on the collagen molecules. This reaction is a non-enzymatic covalent modification of proteins (Maillard reaction) that results in the formation of reversible Schiff bases which are converted to covalently bonded Amadori complexes (43). These complexes then undergo chemical rearrangements to form advanced glycation end (AGE) products such as pentosidine which crosslink collagen fibrils. AGE products can affect cell function through interaction with the receptor for AGE (RAGE) which is a pattern recognition receptor that binds to various ligands, most importantly AGE products. RAGE activation has been shown to increase cell proliferation and initiate a number of inflammatory pathways (14). To test the effect of AGE products on ASM function, microtissues were stiffened with d-ribose and then treated with a polyclonal anti-RAGE antibody (Santa Cruz Biotechnology Inc, Dallas, Texas, sc-8230). The anti-RAGE antibody was added to microtissues at a concentration of 10 μg/ml in standard media supplemented with d-ribose as described previously (91).

The Young's modulus of collagen gels stiffened using non-enzymatic crosslinking with d-ribose was measured by microindentation. Bulk collagen gels with a thickness of ~3mm were fabricated under the same conditions as for ASM/WI-38 microtissues. Gels were indented 150μm using a force transducer, micropipette and micromanipulator system and a stress vs. strain curve was generated based on depth of indentation and force measurements. The Young's modulus was calculated based on the geometry of the indenter (micropipette) and the depth of indentation as per the Oliver-Pharr nonlinear curve fit method (99).

As described in the results, all statistical tests were performed with the GraphPad 4.0 software package. The data is reported as mean±SEM with $p<0.05$ considered statistically significant.

5.2.1 Results

5.2.1.1 Gel Microindentation

The Young's modulus (stiffness) of bulk collagen gels (n=12) crosslinked by non-enzymatic glycation was measured using microindentation techniques. Collagen gels that were crosslinked non-enzymatically with d-ribose were significantly stiffer (896.5±50.4Pa, p=0.0251) compared to the control group (615±56.2 Pa) verifying the effect of d-ribose on collagen gel mechanical properties (Figure 5-2).

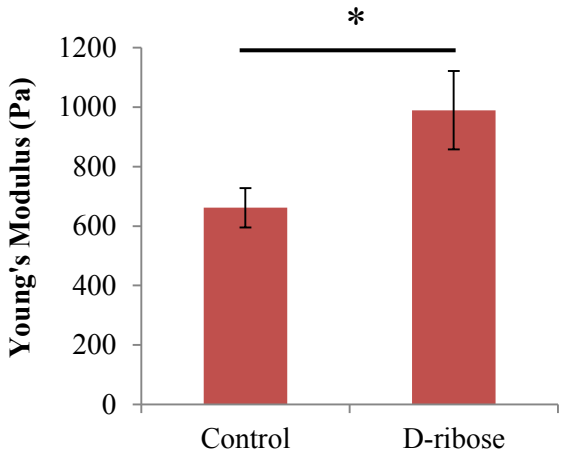

Figure 5-2. Young's modulus of bulk collagen gels (n=12) stiffened through non-enzymatic glycation. D-ribose crosslinked collagen gels were significantly stiffer compared to the control group (one tailed t-test, $p<0.05$)

5.2.1.2 3D Microtissue Contractile Function

Initially ASM/WI-38 microtissues were manufactured in μTugs with soft microcantilevers (k=0.48μN/μm) and I found that growing the cells in the stiffened matrix via d-ribose crosslinking significantly enhanced the contractile function ($p<0.05$) of these microtissues (Figure 5-3a). However, the deflection of these compliant cantilevers was excessive and exceeded the point where cantilever bending responses were linear. ASM/WI-38 microtissues were then fabricated in μTugs with stiffer microcantilevers that thus increased the load on the microtissues (k=0.75μN/μm). Stiffening the matrix with d-ribose significantly enhanced contractile function of the microtissues in response to both ACh and KCl (20.65±1.65 μN, $p<0.01$) (Figure 5-3b). However, when microtissues were fabricated in μTugs with even stiffer microcantilevers (k=1.16μN/μm), the increased load opposing ASM contraction combined with the stiffened ECM had no significant effect on force generation (Figure 5-4).

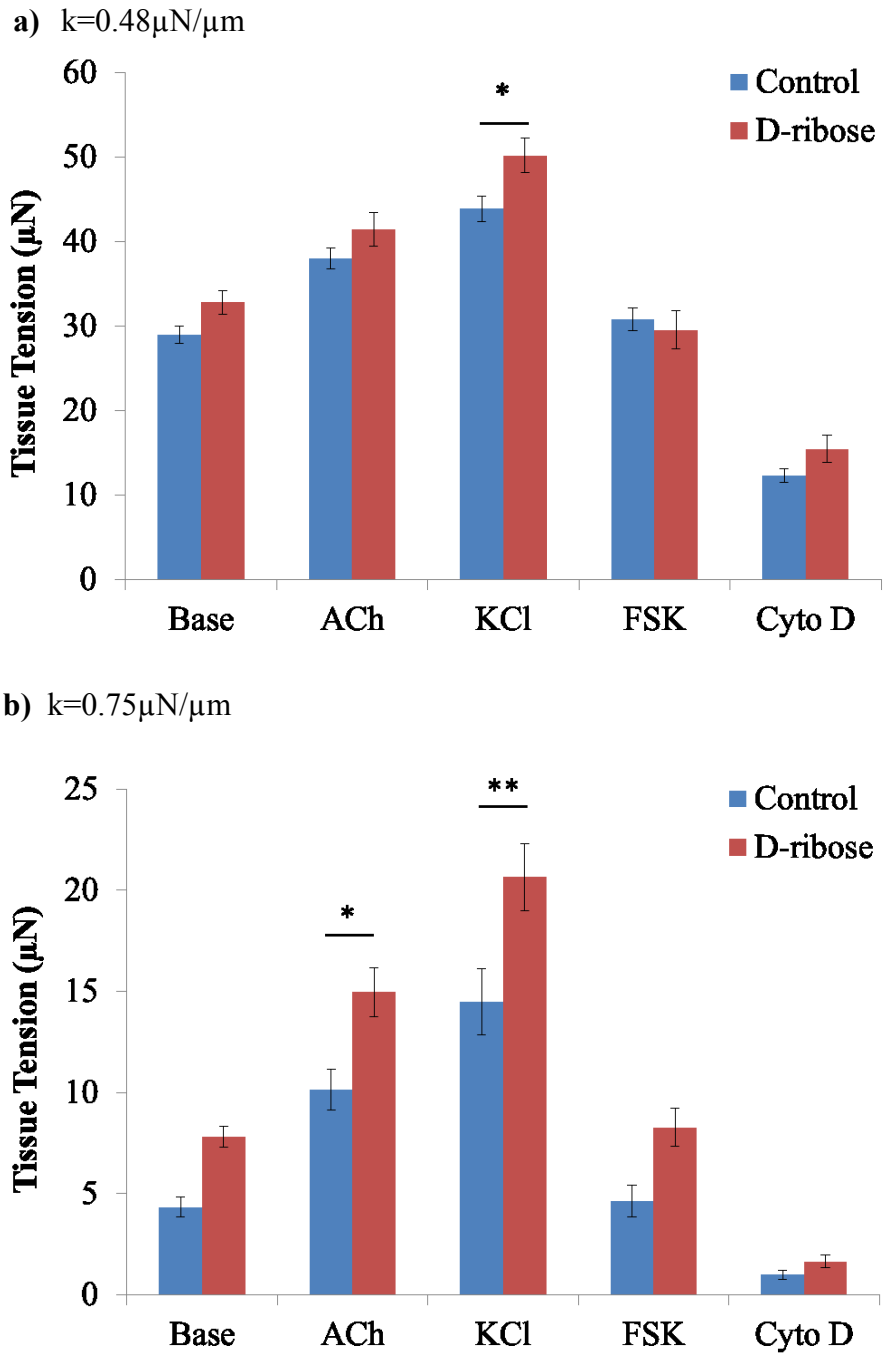

Figure 5-3. Effect of collagen crosslinking on the contractile function of ASM/WI-38 microtissues tethered to microcantilevers with different spring constants. a) Stiffening ECM with d-ribose enhanced ASM/WI-38 microtissue contractile function to ACh and KCl ($p<0.01$, $n=24$) in µTugs with microcantilever spring constant k=0.48µN/µm (compliant microcantilevers). b) Stiffening ECM with d-ribose enhanced ASM/WI-38 microtissue tension generation ($p<0.01$, $n=24$) in µTugs with a microcantilever spring constant k=0.75µN/µm (semi-compliant microcantilevers). Statistical analyses completed using two-way ANOVA with Bonferroni post hoc test. Base: baseline, ACh: acetylcholine 100 µM, KCl: 80 mM, FSK: forskolin 100 µM, Cyto D: cytochalasin D 10 µM.

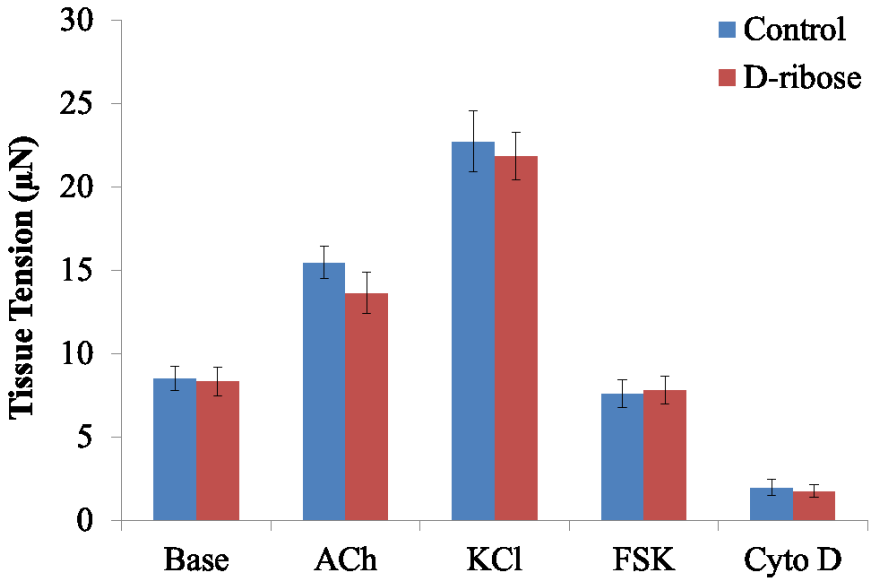

Figure 5-4. Effect of collagen crosslinking on the contractile function of ASM/WI-38 microtissues tethered to microcantilevers with a spring constant k=1.16µN/µm.ASM/WI-38 microtissue contractile Stiffening ECM with d-ribose had no effect on ASM/WI-38 microtissue tension generation (n=24). Statistical analyses completed using two-way ANOVA with Bonferroni post hoc test. Base: baseline, ACh: acetylcholine 100 µM, KCl: 80 mM, FSK: forskolin 100 µM, Cyto D: cytochalasin D 10 µM.

To examine if there was a biochemical side effect of AGE products on ASM/WI-38 microtissue contractility, the interaction between AGE products and the receptor for AGE products RAGE was inhibited using anti-RAGE antibody. Contractile function of microtissues crosslinked with d-ribose alone and with d-ribose inhibited with anti-RAGE antibody was measured and the data showed no significant difference between the groups (Figure 5-5).

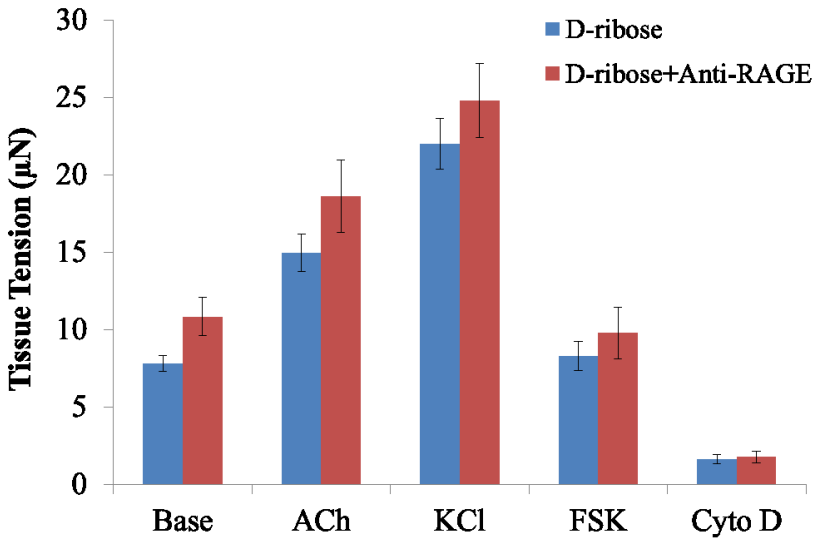

Figure 5-5. Effect of AGE products on ASM/WI-38 microtissue contractility (n=16). Anti-RAGE antibody was used to block the interaction between AGE products and RAGE. There was no significant difference in contractility between microtissues crosslinked with d-ribose and microtissues crosslinked with d-ribose and inhibited with anti-RAGE antibody. Statistical analyses completed using two-way ANOVA with Bonferroni post hoc test. Base: baseline, ACh: acetylcholine 100 µM, KCl: 80 mM, FSK: forskolin 100 µM, Cyto D: cytochalasin D 10 µM.

5.2.1.3 2D ASM Contractility

To further confirm there was no biochemical side effect of AGE/RAGE interaction, ASM cells were cultured in conventional 2D Petri dishes. The cells were incubated with d-ribose supplemented media for the same period of time as for ASM/WI-38 microtissues and function was assessed using optical magnetic twisting cytometry (OMTC) as described in section 2.4.2.

a)

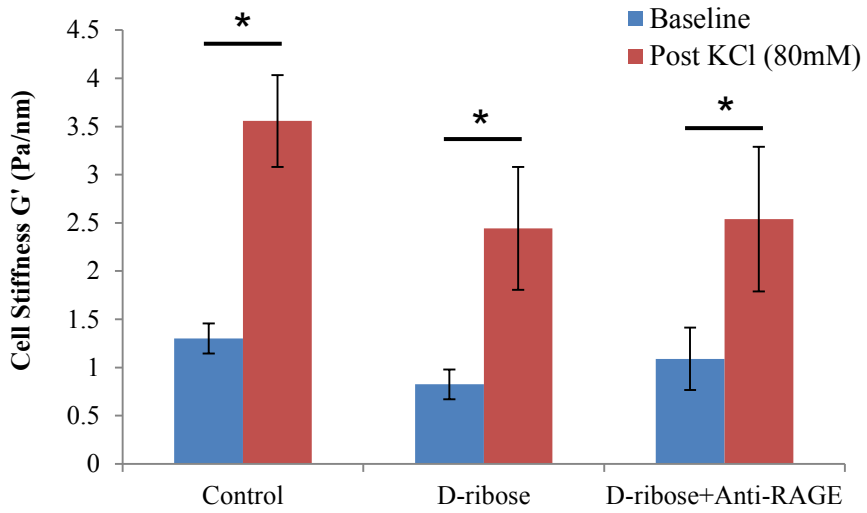

b)

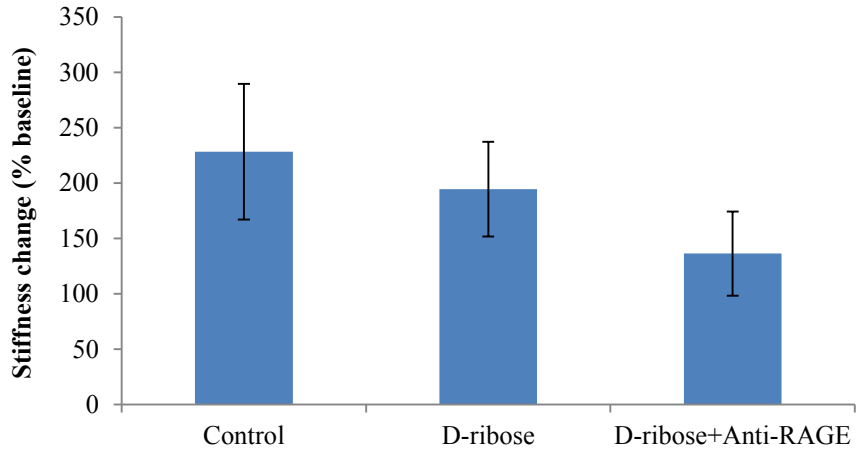

Figure 5-6. Cell stiffness and percent contractility of ASM cells in 2D mono-culture (n=16). **a)** ASM cells cultured on collagen coated plastic dishes, with d-ribose, and with d-ribose and anti-RAGE antibody demonstrated no significant difference in baseline and post KCl stiffness between treatments but demonstrated significant intragroup difference between baseline and post KCl stiffness. **b)** Contractility of ASM cells as a percentage of baseline stiffness was also not affected by the treatments. Statistical analyses completed using two-way ANOVA with Bonferroni post hoc test. $p<0.05$ was considered significant.

In 2D, ASM cells that were cultured on a stiffer ECM and those on a stiffer ECM inhibited with anti-RAGE antibody showed no significant difference in baseline or contracted cell stiffness. This result was similar to that observed with the 3D microtissues

(Figure 5-6a). However, when d-ribose supplemented media was added to 2D ASM cells to crosslink the collagen matrix and increase the stiffness, there was no significant difference in contractility between cells cultured on collagen coated Petri dishes without d-ribose and cells cultured on the stiffer crosslinked collagen coated Petri dishes (Figure 5-6b). This result was unexpected since in the 3D microtissues stiffening the matrix through crosslinking significantly enhanced contractility.

5.2.1.4 Gene Expression

Gene expression of several regulatory and contractile proteins was assessed alongside the contractile function experiments for microtissues fabricated in each of the four μTugs with the different microcantilever stiffnesses. The genes were all expressed relative to a calibration sample, which was obtained from microtissues fabricated in the μTugs with k=0.18μN/μm and normalised to the reference gene GAPDH. As in Chapter 4.3.3 relative gene expression data was shown such that the sample with the maximum gene expression was assigned an arbitrary unit of 1 for each gene of interest. As opposed to the contractile function data, mRNA abundance of the genes of interest was, for the most part not significantly different between the crosslinked and control groups across the four μTugs stiffnesses. The graphs are shown in order of increasing microcantilever stiffness k (load) for uncrosslinked microtissues (blue bar) and those crosslinked with d-ribose (red bar). Genes involved in promoting contraction are shown on the left hand side and those opposing contraction on the right hand side of Figure 5-7. Biological replicates were amplified in duplicate and aliquots of cDNA were used as template for qPCR reactions containing primers for sm-MHC, MYLK (MLCK), MYPT1 (MLCP), α-actin, SM22α, vimentin, SRF, and myocardin. Statistical analysis involved a one-way ANOVA

with Bonferroni post-hoc comparisons. Increasing loading on microtissues through microcantilever stiffness and increased bulk matrix stiffness through crosslinking with d-ribose, had no significant impact on mRNA transcript levels (Figure 5-7).

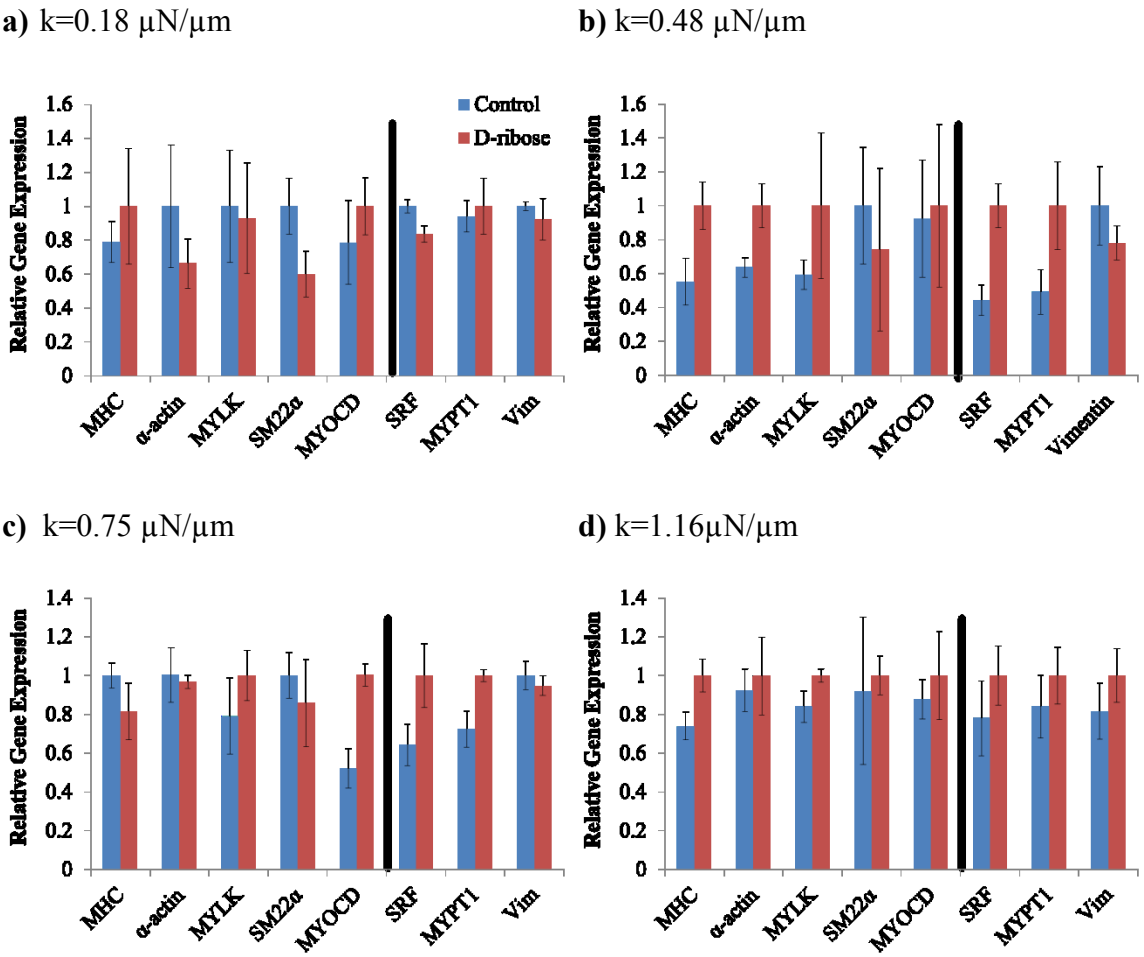

Figure 5-7. Gene expression analysis of ASM/WI-38 microtissues stiffened through crosslinking with d-ribose. In clockwise manner graphs are shown in order of increasing microcantilever stiffness k (loading) for uncrosslinked microtissues (control, blue bar) and those crosslinked with d-ribose (red bar). Black line separates genes involved in promoting contraction (left) and those opposing contraction (right). Efficiency corrected method of quantification against a stable reference gene GAPDH was performed. Statistical analysis: one-way ANOVA with Bonferroni post-hoc comparisons where $p<0.05$ was considered significant.

5.2.2 Discussion

The principal findings of this portion of my thesis are that: stiffening the ECM of ASM/WI-38 microtissues through non-enzymatic glycation significantly increased contractile function, but had no impact on gene expression of key contractile markers. Additionally, crosslinking collagen matrices in 2D culture models had no effect on ASM function.

Crosslinking collagen matrices with a sugar such as d-ribose leads to the production of AGE products, which can affect cellular function through interaction with the receptor RAGE. ASM/WI-38 microtissues were fabricated with d-ribose supplemented media and media with anti-RAGE antibody to prevent interaction between AGE and its receptor. The data show no significant difference in contractile function. This suggests that the contractility response seen with increasing ECM stiffness was most likely a stiffness effect regulating cell function rather than a side effect of d-ribose sugar. Additionally, the effect of non-enzymatic glycation was assessed in 2D with ASM cells cultured on a thin layer of collagen. Stiffening the collagen matrix in 2D through crosslinking had no significant effect on ASM contractility as opposed to what was seen in 3D. This disparate effect of substrate stiffness between the two model types (3D vs. 2D) was most likely due to the difference in structure and range of stiffness. In 2D, with a monolayer of cells and thin layer of collagen, the cells most likely sense the stiffness of the rigid plastic substrate underneath. Therefore, in 2D with an already stiff environment, crosslinking the thin layer of collagen does not elicit a response in contractility. However, with the less stiff but 3D collagen gels, the stiffness range was low enough such that the increase in stiffness caused by crosslinking with d-ribose had an effect on ASM

contractility. Therefore, these data strongly suggest that the enhanced contractility response seen in 3D ASM/WI-38 microtissues with a stiffened ECM was most likely solely due to a stiffness effect.

Non-enzymatic glycation is one of many methods that are used to crosslink natural protein matrices. One of the main limitations of this approach to crosslinking collagen matrices could be that the crosslinking might alter fibre architecture sufficiently enough to affect cellular function. However, it was previously shown that at concentrations of d-ribose between 0-100mM, there is no effect on collagen fibre diameter or length (91). This suggests that fibre architecture may not be substantially altered, allowing this method of crosslinking to be feasible for assessing the effect of matrix stiffness on ASM function.

The contractile function data demonstrated that with increased matrix stiffness there was a significant increase in ASM/WI-38 contractile function. However, the enhanced contractile function was only evident when the load opposing ASM contraction was small enough to allow the tissue to shorten. When the posts were very stiff, the contractility was not affected by crosslinking/stiffening of the matrix. One possible explanation for this could be that there was a difference in contractility but, the difference may have been too small to detect. This is a methodological limitation; the deflection of the microcantilevers was below the sensitivity range and below the range measurable through optical tracking of the microcantilevers. Based on the standard deviation of microtissues tension when stimulated with KCl between the two groups it is difficult to conclude whether there was no change in function.

While I was not able to detect the difference in contractility between crosslinked and uncrosslinked ASM/WI-38 microtissues fabricated with increased load opposing contraction, this finding may still be true. It may be that there is an upper limit of contractile function with increased loading and matrix stiffness, demonstrating a maximum *in vitro* contractile function. As the matrix stiffness and/or loading on the microtissues is increased, the cells reach a maximum shortening capacity, and any increase in matrix stiffness or microcantilever stiffness (load) has no further effect on contractility.

Another possibility that could limit the response to matrix stiffness is that the matrix in this study was composed of collagen with relatively high serum, which would tend to drive the tissue to a proliferative phenotype. Furthermore, other matrix proteins that are present *in vivo* may be important and possibly affect this limit. For example, laminin, a basement membrane protein found *in vivo* that is important for modulation of cell differentiation and proliferation, is known to promote a more contractile phenotype (124).

Although contractile function of the microtissues was enhanced within a stiffer crosslinked matrix, there is the possibility of viscoelastic responses in the collagen gel ECM which might be the cause of the lower microtissue tension in the uncrosslinked matrix. Collagen gels are viscoelastic materials as they consist of a collagen network as well as interstitial fluid. Viscoelastic materials such as collagen can undergo stress relaxation or creep effects over time due to the hierarchical structure of collagen. Crosslinking a collagen matrix forms links between collagen fibrils bringing them closer together thereby essentially dispersing the interstitial fluid making the gel more rigid.

This in turn prevents inter fibril slippage. Accordingly, an uncrosslinked matrix may undergo collagen fibril slippage over time due to the viscoelastic nature of the matrix. This would lead to decreased baseline tension within the microtissue matrix and thereby the decreased force generation in the crosslinked group as seen in the results. However, this may not be the case in this study where the active tension within the tissue is being continuously generated by the airway smooth muscle cells over the course of 3 days. This can be seen in the magnitude of tissue tension after ablation of the cytoskeletal tension through administration of cyto D. This tension would be the passive tension of the collagen matrix, which was around 1-3μN which was significantly lower than the baseline cytoskeletal tension generated as seen in the results. Additionally, images were captured of microtissue formation and collagen compaction (data not shown) at 6, 12, 24 and 72 hours post tissue fabrication, and there was no evidence of viscoelastic responses over that time period as baseline tension increased accordingly up to 72hrs. To determine if there was a viscoelastic response of the collagen matrix, microtissues would need to be imaged during initial compaction of the gel matrix and over the course of 3 days at short intervals.

In healthy individuals dynamic stretching of the airway due to tidal breathing has a potent dilating effect that limits the magnitude of airway narrowing after inhalation of a bronchoconstrictor. Conversely, the effect of a large stretch to dilate the airways is absent in asthmatics and some have shown that stretch may actually augment hyperresponsiveness. Thus stretching the ASM may be an important mechanism that acts to limit ASM contractility in healthy airways. If true, any increase in ECM stiffness would be a mechanism to explain the lack of dilatory effect observed in asthma, simply

because of an increase in airway stiffness, but also possibly because the stiffer airway leads to increased ASM contractility. Other explanations have been suggested including a change in bridge dynamics between actin and myosin, plastic reorganisation of the CSK in ASM, and an increase in the shortening velocity (39). In this thesis, it was shown that ASM contractile function was enhanced in response to stiffening of the matrix which may then contribute to hyperresponsiveness associated with asthma.

Cells sense the mechanical properties of their microenvironment through the presence of membrane spanning proteins called integrins which form complexes with other proteins to form focal adhesions that bind to ECM proteins (4). The interaction of the focal adhesions with the ECM allows the cell to sense the elasticity of the environment which initiates reorganisation of the cytoskeleton (114). This reorganisation initiates transcription pathways. Therefore, to probe whether changes in contractility were possibly due to alteration in gene expression real time reverse transcription quantitative PCR (qPCR) was used to assess the quantity of common markers of smooth muscle contractile phenotype. While it was hypothesised that the enhanced contractile function of the ASM microtissues might be due to a change in ASM phenotype, we were unable to find a substantial shift in gene expression. Only in the case where matrix stiffness was increased but load opposing contraction (microcantilever stiffness) was limited was there enhanced expression of sm-MHC, α-actin, and SRF.

However, there are several limitations of these findings. Principally, the number of samples was low, so that any significant change would have to be large. Furthermore, only one time point was tested at 2-3 days post tissue fabrication. One of the main focuses of this study was to assess the chronic effect of substrate stiffness on ASM

function and phenotype. Because of this, smooth muscle function was assessed 3 days post tissue fabrication. To keep the experimental protocols consistent, RNA was collected for gene expression analysis 2-3 days post tissue fabrication. Thus, there may have been no significant differences in the gene expression because changes in gene expression occurred at earlier time points. It is established that there is a discrepancy between mRNA transcript level and protein concentration, such that the quantity of mRNA does not necessarily provide information as to whether it will be translated into a functional protein (49, 127). This suggests that even though the quantity of mRNA assessed in this study was not significantly impacted by the mechanical stimuli, it may not dictate what is occurring at the level of the proteins in question.

Another explanation for the discrepancy between function and gene expression is that the enhanced contractile function was due to changes in post-translational modification of the proteins of interest. There are several steps in the gene expression process that may be modulated, including DNA-RNA transcription, RNA splicing, translation, and post-translational modification of the protein. Genetic information from DNA is transcribed into messenger RNA (mRNA) which carries the information required for encoding proteins. At this point, ribosomes and transfer RNAs are involved in the translation of mRNAs into structure-less proteins. These proteins then undergo post-translation modifications to improve their functional diversity. This may involve the addition of functional groups or proteins or the cleavage of regulatory subunits such as protein phosphorylation, glycosylation, and methylation, all of which affect cell biology and functional properties. Alternatively, western blot analysis of the proteins of interest would allow for identification of post-translational modifications of proteins from

changes in the size of the protein expressed. However, for the purposes of this study western blot analysis was not undertaken since this method of analysis is semi-quantitative and requires large quantities of cellular lysate.

Enhanced contractile function as seen in the results of this chapter may also be caused by an increase in overall cell number. A larger quantity of ASM cells, with the same capacity of shortening, would lead to greater tension generation. However, this likely was not the case as cell density was kept constant and nuclei were quantified with nuclei staining (data not shown). There was no apparent difference found in cell numbers between the stiffened crosslinked microtissues and the control group ($n \approx 325$).

There are a number of studies that perceive remodeling and stiffening of the airway as a protective response in asthma (93). The idea is that stiffening of the airway hinders contractility of the smooth muscle and prevents airway narrowing. Studies have shown through collagenase degradation that ASM contractility was increased (20). However, these studies assessed the acute response in ASM contractility to collagenase degradation, where a decreased load would allow the muscle to shorten must faster, while the experiments in this thesis were addressing the effect on contractile function of ASM from chronic stiffening.

Finding no significant changes in mRNA levels (gene expression) does not eliminate the possibility that there was a change in contractile proteins, leading to the phenotypic change observed by the enhancement of contractility. However, it is also possible that the enhanced contractility may have been due to other factors that do not require a change in the phenotypic state of the ASM cells. The enhanced contractile function and shortening capacity of the ASM microtissues may have been due to

improved structural integrity of the microtissue. Crosslinking the matrix provides strength and rigidity to the matrix, thereby improving cell anchorage to the substrate through stable adhesions and potentially enhancing force transmission (4). Also, it was previously shown that the enhanced matrix stiffness of cardiac smooth muscle microtissues improves contractile function (18). Indeed it may have been that the ASM cells or cytoskeletal apparatus became better aligned because of the increased structural integrity of the matrix thereby augmenting the contractile function of the tissue. This change in cytoskeletal organisation was qualitatively assessed in Appendix B: Cellular Organisation. In the two brightfield images of microtissues with and without d-ribose respectively as seen in Appendix B, the cells within a stiffened crosslinked environment are more organised and the cytoskeletal fibres are aligned with the force vector, whereas with the uncrosslinked microtissues, the cells are configured in a disoriented manner. Therefore, there may be increased activation of the contractile apparatus through increased cytoskeletal organisation, without any change in expression of the common regulatory proteins such as MLCK and MLCP.

5.3 Approach 2: Collagen Density

The second approach to alter the ECM stiffness of ASM/WI-38 microtissues was to vary the concentration of collagen from 1.5mg/ml to 3.0mg/ml. Contractile function of the microtissues was assessed using an array of drugs and tracking the deflection of the microcantilevers during contraction and subsequent relaxation (see section 2.4.1). Contractile phenotype was assessed through gene expression studies for markers of contractile proteins (see section **Error! Reference source not found.**). The Young's modulus of collagen gels that were stiffened by increasing the density of collagen was

measured by microindentation (described in section 5.2). All statistical tests as described in the results were performed with the GraphPad 4.0 software package. The data is reported as mean±SEM with $p<0.05$ considered statistically significant.

5.3.1 Results

5.3.1.1 Gel Microindentation

To determine the effect of stiffening the collagen gel matrix by increasing the collagen density, microindentation of bulk collagen gels was performed to measure the Young's modulus. Collagen gels that were fabricated with double the concentration of collagen (3.0mg/ml) were significantly stiffer (679.3±36.73μN) in comparison to the control group (401.0±30.52 μN) with half the concentration of collagen (1.5mg/ml) (Figure 5-8). This shows that the stiffness of the matrix gels was effectively increased by increasing collagen density.

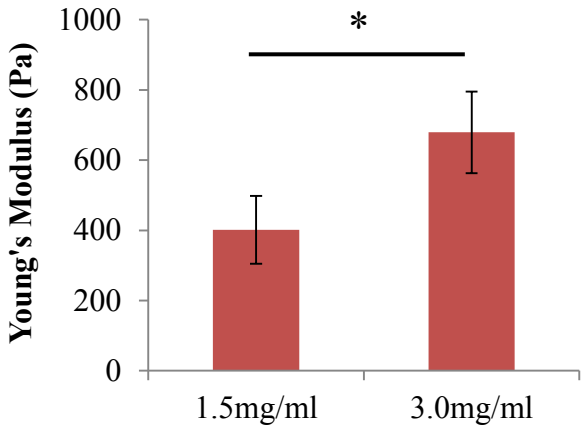

Figure 5-8. Young's modulus of bulk collagen gels (n=12) that were stiffened by varying the collagen density from 1.5mg/mL to 3.0mg/mL. Bulk collagen gels with 3.0mg/mL collagen were significantly stiffer compared to bulk collagen gels with half the concentration of collagen (one tailed t-test, * $p<0.05$).

5.3.1.2 Contractile Function

Initially ASM/WI-38 microtissues were manufactured in μTugs with soft microcantilevers (k=0.48μN/μm) and increasing collagen density to stiffen the matrix had no effect on contractility (Figure 5-9). However, the excessive deflection of these compliant cantilevers exceeded the point where cantilever bending responses were linear as seen previously and discussed above in section 5.2.1.2. Therefore, ASM/WI-38 microtissues were fabricated in μTugs with stiffer microcantilevers (k=0.75μN/μm). Surprisingly, microtissue contractile function was significantly decreased in response to KCl (20.39±1.46 μN, $p<0.01$) with increased collagen density and matrix stiffness (Figure 5-10a). To also assess the effect of increasing the loading (boundary stiffness) on the ASM microtissues stiffened by increasing collagen density, microtissues were fabricated in μTugs with the stiffest microcantilevers (k=1.16μN/μm). The increased load opposing ASM contraction in addition to the stiffer ECM through increased collagen density significantly decreased contractile function in response to KCl (16.87±1.02μN, $p<0.01$) relative to the less stiff collagen gels (Figure 5-10b).

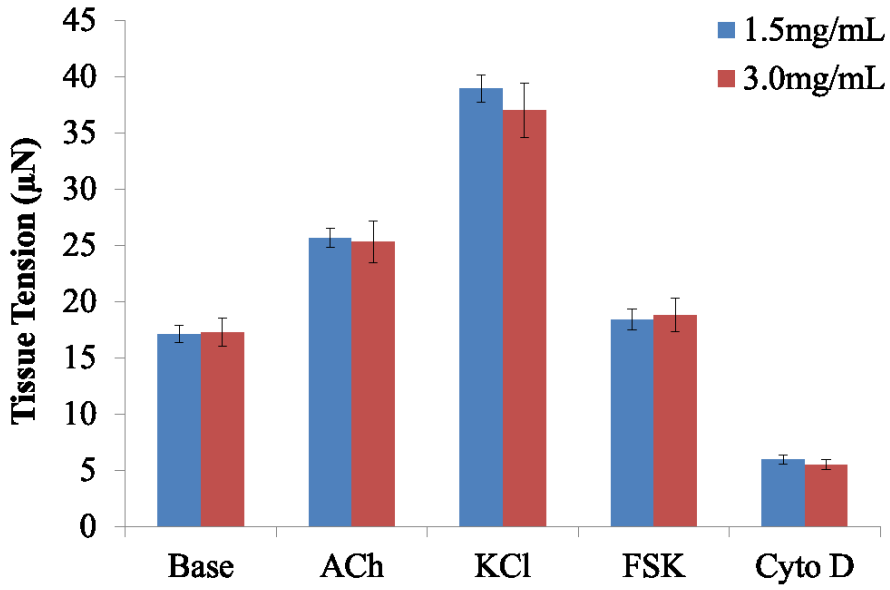

Figure 5-9. Effect of collagen density on contractile function of ASM/WI-38 microtissues tethered to microcantilevers with a spring constant of k=0.48µN/µm. Stiffening ECM by increasing the collagen density had no significant effect on ASM/WI-38 microtissue contractile function. Statistical analyses completed using two-way ANOVA with Bonferroni post hoc test. Base: baseline, ACh: acetylcholine 100 µM, KCl: 80 mM, FSK: forskolin 100 µM, Cyto D: cytochalasin D 10 µM.

a) k=0.75µN/µm

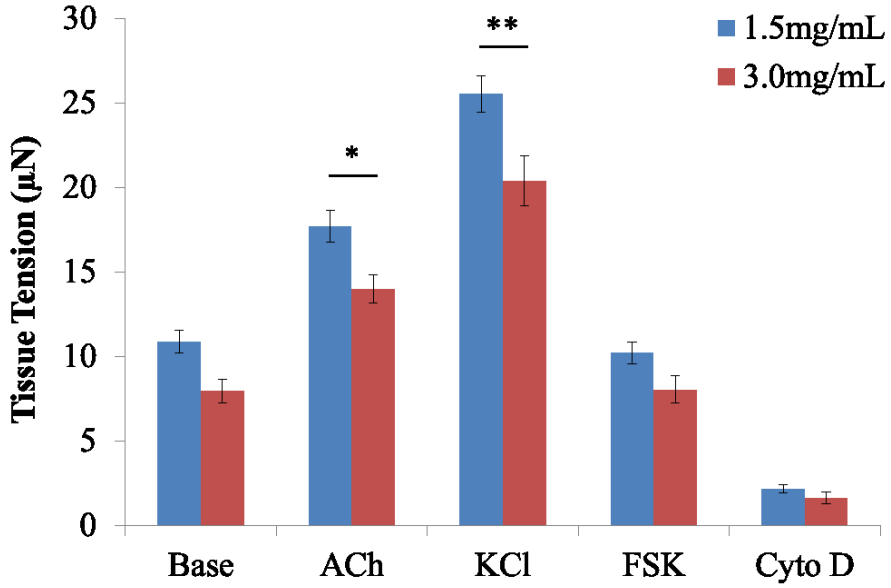

b) k=1.16µN/µm

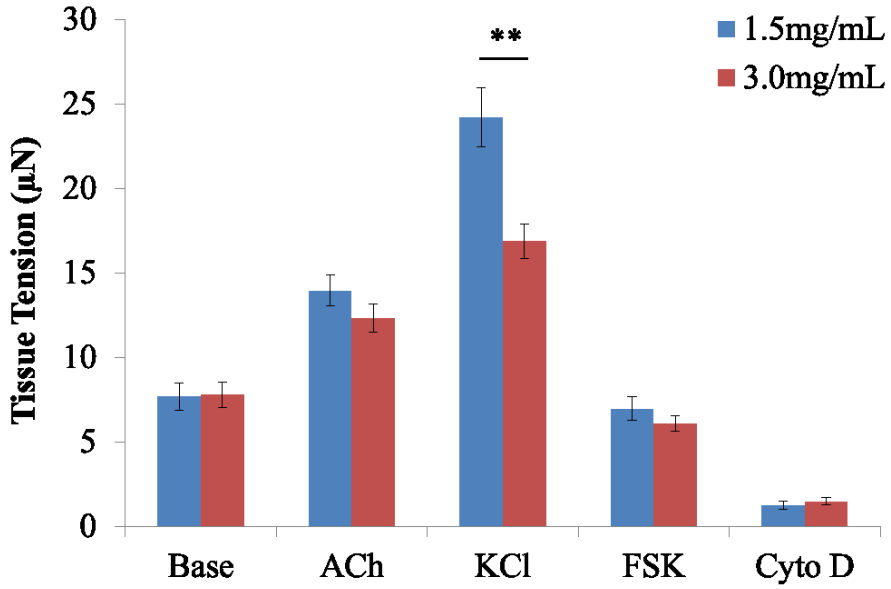

Figure 5-10. Effect of collagen density on contractile function of ASM/WI-38 microtissues tethered to microcantilevers with different stiffnesses.Stiffening ECM by increasing the collagen density significantly decreased ASM/WI-38 microtissue contractile function to **a)** ACh and KCl ($p<0.01$, $n=24$) in µTugs with microcantilever spring constant k=0.75µN/µm (compliant microcantilevers), and to **b)** KCl ($p<0.01$, $n=24$) in µTugs with a microcantilever spring constant k=1.16µN/µm (stiff microcantilevers). Statistical analyses completed using two-way ANOVA with Bonferroni post hoc test. Base: baseline, ACh: acetylcholine 100 µM, KCl: 80 mM, FSK: forskolin 100 µM, Cyto D: cytochalasin D 10 µM.

5.3.1.3 Gene Expression

Once again, gene expression of several regulatory and contractile proteins was assessed alongside the contractile function experiments for microtissues fabricated in each of the four μTugs with the different microcantilever stiffnesses. The genes were all expressed relative to a calibration sample and normalised to the reference gene GAPDH. As in Chapter 4.3.3 relative gene expression data was shown such that the sample with the maximum gene expression was assigned an arbitrary unit of 1 for each gene of interest. The graphs are shown in order of increasing microcantilever stiffness k (load) for low collagen density microtissues (1.5mg/mL, blue bar) and high collagen density microtissues (3.0mg/mL, red bar). Genes involved in promoting contraction are shown on the left hand side and those opposing contraction on the right hand side of Figure 5-11. Aliquots of cDNA were used as template for real-time PCR reactions containing primers for sm-MHC, MYLK (MLCK), MYPT1 (MLCP), α-actin, SM22α, vimentin, SRF, and myocardin. Statistical analysis involved a one-way ANOVA with Bonferroni post-hoc comparisons. As opposed to the contractile function data, mRNA abundance of the genes of interest was, for the most part, not significantly different between the high collagen density and low collagen density groups across the four μTugs stiffnesses as seen in Figure 5-11.

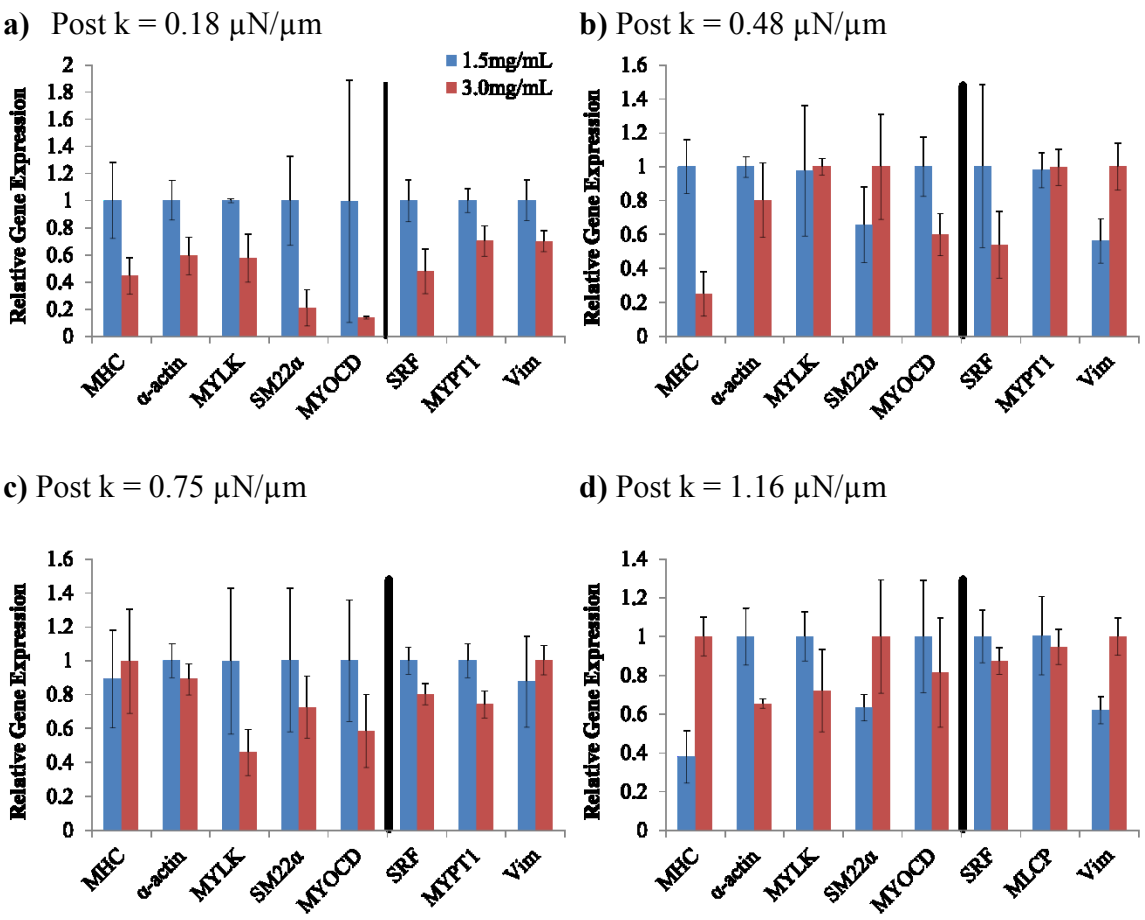

Figure 5-11.Gene expression analysis of ASM/WI-38 microtissues stiffened by increasing the collagen density. In clockwise manner graphs are shown in order of increasing microcantilever stiffness k (loading) for microtissues with 1.5mg/mL collagen (blue bar) and those 3.0mg/mL collagen (red bar). Black line separates genes involved in promoting contraction (left) and those opposing contraction (right). Efficiency corrected method of quantification against a stable reference gene GAPDH was performed. Statistical analysis: one-way ANOVA with Bonferroni post-hoc comparisons where $p<0.05$ was considered significant.

5.3.2 Discussion

The principal finding of this portion of my thesis was that stiffening the ECM of ASM/WI-38 microtissues by increasing the collagen density significantly decreased contractile function. However, functional changes did not match changes in gene expression.

It was hypothesised that a stiffer ASM microenvironment would enhance ASM contractility through a phenotypic change, which could be a potential cause of airway hyperresponsiveness. However, the findings from the contractile function experiments after altering ECM stiffness of microtissues with collagen density were unexpected. Even though the bulk stiffness of the ECM was increased with collagen density, the change in ASM tissue contractility contradicted observations using the first approach, where increasing matrix stiffness through crosslinking significantly enhanced contractility. Additionally, important markers of ASM contractile phenotype were measured using qPCR. The data obtained showed no overall significant difference in mRNA abundance for key regulatory and contractile proteins, though there may have been some interesting trends (Figure 5-11).

The differential response of the ASM/WI-38 microtissues to ECM crosslinking and ECM density may be due to a difference in the microstructure as well as the components of the ECM (65). Crosslinking the ECM enhances the rigidity of the collagen matrix without affecting matrix composition while increasing collagen density alters the bulk composition of the ECM as it alters the number of available cell adhesive sites. Furthermore, in keeping with the findings of this thesis, previous studies have demonstrated that type I collagen decreases ASM contractility while enhancing gene markers for proliferation (7, 30, 65). Perhaps there is a change in ASM phenotype within this 3D model in the presence of excess collagen towards a pro-proliferative state. This suggestion could be supported with an increase in the expression of vimentin. This gene is less characterised in the literature but is involved in actin remodeling and has been shown to preferentially increase with the proliferative state of ASM cells (51). While

there is a possible trend of increasing expression of vimentin in this study, no significant difference was detected. This may have been limited by the low sample size used for qPCR and the large variability in gene expression between samples with the same stimulus. Therefore, it is possible that the higher collagen concentration in the matrix may have prompted the ASM cells to change to a more proliferative state, thereby attenuating contractile function (58). From an ECM signalling perspective, the presence of excess collagen within this model may overwhelm the effect of the enhanced stiffness, presenting a competitive interplay between collagen signalling and matrix rigidity.

Although there was a significant difference in contractile function between the low collagen density and high collagen density groups, there was no significant difference in gene expression of key markers of ASM contractile phenotype. This difference between the function data and the gene expression data may be due to a low correlation between mRNA levels and protein, such that the mRNA is undergoing post-transcriptional regulation leading to a difference in the final protein formation, as discussed in section 5.2.2. Additionally, a 2-fold change in transcript levels is equivalent to a 1 amplification cycle difference in the crossing point for the two samples. Indeed, while there were some differences in the gene expression data, these fold changes in mRNA quantity were still quite small, and may not signify substantive changes occurring at the protein level. The biological implication of a 2-fold change at the transcript level is hard to validate also in any case due to the large variability between samples (biological replicates).

Chapter 6: Epithelial Cells and ASM microtissues

6.1 Rationale

Lung tissue is composed of several cell types including the ASM layer which lies below the basement membrane on which is attached the epithelial cell layer. Thus, the ASM is in very close proximity to the epithelial cell layer. The epithelial cell layer is essential in acting as a barrier to inhaled pathogens. Surprisingly little is known about cellular interaction between the epithelium and ASM cells but it is known that the epithelium secretes a number of soluble factors which can act to regulate various cellular processes of nearby cells including the ASM (71). There have been some reports of epithelium denudation (damage) that occurs in severe asthma which may promote AHR but the mechanicsms are unclear (77). Taken together the epithelium may play a role in regulating ASM contractile phenotype in both health and disease pathology (3, 13, 142) as discussed above (1.2.1). Thus, developing a system to study epithelial and ASM cell interaction is important for elucidating putative regulatory pathways. For the purposes of this thesis, I will conduct a preliminary investigation that explores the interaction of ASM and epithelial cells using the 3D microtissue model as a feasible model.

6.2 Methods

6.2.1 NHBE Cell Culture

Normal human bronchial epithelial (NHBE) cells were cultured according to the protocol specified by Lonza™ for Clonetics Normal Human Airway Epithelial Cell Systems and PneumaCult™ ALI. NHBE cells require two different types of media;

BEGM to expand passages on a plastic surface and ALI media to potentiate growth and differentiation on a porous surface. NHBE cells were isolated from normal donor airway epithelial tissue and were cultured in a 37°C incubator at 5% CO_2.

Initially NHBE cells at passage 2 were cultured in T75 flasks with 500mL BEGM (bronchial epithelial growth media, Lonza). Growth media was changed on the cells every two days. Once the cells reached confluence, they were seeded onto Transwell permeable filter inserts (12 mm in diameter with a pore size of 0.4um; Corning, NY) in the presence of BEGM to obtain well-differentiated mucociliary cultures. Cells were cultured in submerged conditions in the Transwell inserts in BEGM. About 1.5ml of BEGM was added to the basal chamber of each well in the Transwell plate and 450µL was added to each apical chamber (Transwell inserts). The cells were placed into air-liquid configuration after 2-4 days or until fully confluent to promote mucociliary differentiation. This involved removing the media from the insert and replacing the media in the basal chambers with PneumaCult-ALI maintenance media consisting of 1X PneumaCult-ALI base medium (Stemcell Technologies, Cat# 05001, Vancouver, B.C) 10X PneumaCult-ALI supplement (Stemcell Technologies, Cat# 05001, Vancouver, B.C), 1X PneumaCult-ALI maintenance supplement (Stemcell Technologies, Cat# 05001, Vancouver, B.C), 0.004mg/mL heparin (Stemcell Technologies, Cat# 07980, Vancouver, B.C), and 0.48µg/mL hydrocortisone. Media in the basal chamber was replaced every 2 days and the inserts were rinsed once a week with 1X phosphate buffered saline solution to remove excess mucus. The cells were kept in air liquid interface for approximately 3 weeks to be properly differentiated for use in experiments.

After the three week time point, the conditioned media was collected from the NHBE Transwell plates and used to stimulate the ASM microtissues.

6.2.2 ASM/WI-38 Microtissues with Conditioned AEC Media

To assess the effects of epithelial cell soluble factors on ASM microtissues within the 3D microtissue culture model in a simple manner, NHBE cells were cultured for 3-4 days, prior to fabricating ASM/WI-38 microtissues. The media from the ASM/WI-38 microtissues was removed and replaced with conditioned epithelial cell media 6 hours post microtissue fabrication. ASM/WI-38 microtissues were dosed with fresh AEC conditioned media every 24 hours for 3-4 days. Microtissues were also incubated with unconditioned NHBE media (AEC control). Another control group of ASM/WI-38 microtissues were incubated in fresh 1% serum media (ASM control). Changes in ASM contractile function due to the presence or absence of AEC conditioned media were quantified as previously described in Methods 2.4.1. Briefly, contractile function was assessed by optically tracking the deflection of the microcantilevers at baseline and then 10 minutes after the addition of a contractile agonist KCl (80mM). After this the KCl drug solution was removed, the substrate was rinsed with warm IT media, and a solution of Cyto D (100μM) was added to the substrate and incubated for 10 minutes at which point images were captured one again. Response of the microtissues to Cyto D was measured in an attempt to assess the passive tension generated from the ASM cytoskeleton.

As described in the results, all statistical tests were performed with the GraphPad 4.0 software package. A two-way ANOVA with Bonferroni post-tests was applied to

assess differences between groups. The data is reported as mean±SEM with $p<0.05$ considered statistically significant.

6.3 Results

Initially NHBE cells were cultured at an air-liquid configuration to allow for proper cellular differentiation. Full cell confluence is required to prevent leakage of media from the basal chamber into the apical chamber. However, the epithelial cells did not produce an effective barrier and fluid (media) leaked from the basal chamber of the insert into the apical chamber. This may have been due the media supplements in the NHBE maintenance media used to initiate NHBE differentiation. For that reason, the formation of an air-liquid interface was not possible preventing differentiation of these cells. For this reason, epithelial cells were only cultured undifferentiated, with no air-liquid interface as this was at least feasible, and ASM/WI-38 microtissues were instead stimulated with undifferentiated AEC conditioned media.

Microtissues were fabricated according to the protocol described in Methods section 2.2. Microtissues were grown in standard 10% serum media for 6 hours and then the media was replaced with AEC conditioned media. AEC conditioned media was added 6 hours post tissue fabrication to allow for initial compaction of the gel matrix. All the microtissues assessed were stable over the course of several days (Figure 6-1).

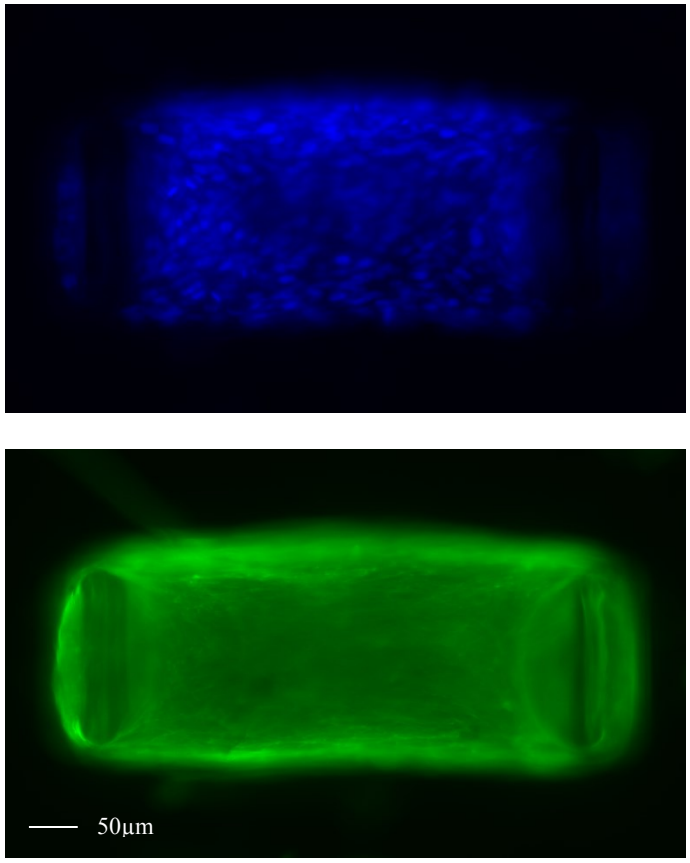

Figure 6-1. Representative epifluorescent images of a DAPI nuclei (top) and Phalloidin f-actin (bottom) stained microtissues. ASM/WI-38 microtissues were stimulated with AEC conditioned media for 3 days.

Contractile function was assessed 3 days post microtissue fabrication using 80mM KCl (80mM) and Cyto D (100μM) to investigate the chronic effect of AEC soluble factors on ASM function as described in section 2.4.1. The results of the contractile function experiments showed that in response to KCl, there was no difference in force generation between the ASM control microtissue (26.63±2.13μN) and AEC control microtissue (30.06±1.99μN) as seen in Figure 6-2. Interestingly, the AEC conditioned media significantly enhanced ASM contractility to KCl (60.83±2.48μN, $p<0.001$).

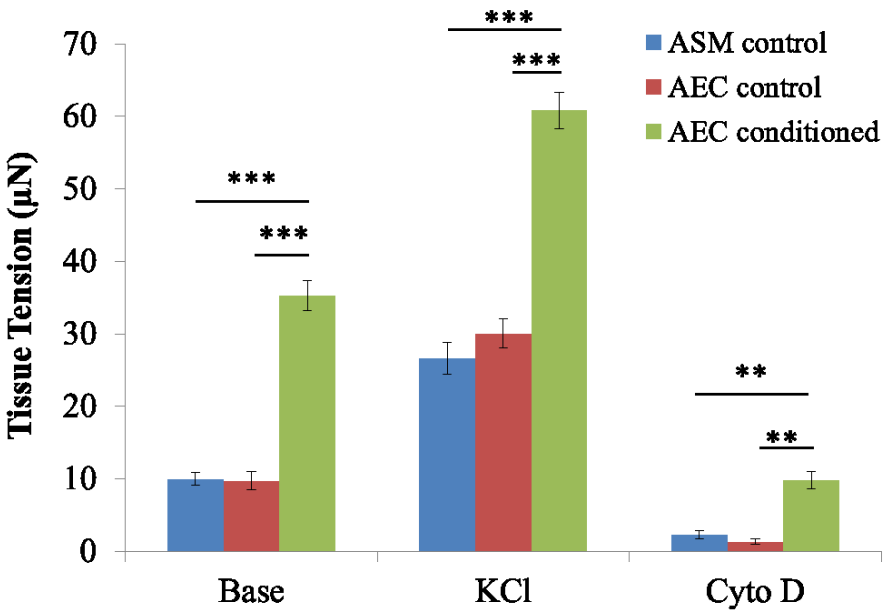

Figure 6-2. Effect of AEC conditioned media on ASM/WI-38 microtissue function. Blue: 1% serum ASM media, Red: AEC unconditioned media, Green: AEC conditioned media. AEC conditioned media significantly enhanced ASM/WI-38 contractile function at baseline and in response to KCl. Relaxation with cytochalasin D was also significantly less for the AEC conditioned media group. Statistical analysis involved a two-way ANOVA with Bonferroni post-hoc comparison and data presented as mean±SEM, n=16, $p<0.05$ considered significant. * $p<0.05$, ** $p<0.01$, *** $p<0.001$.

6.4 Discussion

The principal finding of this chapter is that there was a significant impact on ASM contractility in response to AEC conditioned media compared to either the AEC unconditioned media group (AEC control) or no change in media group (ASM control). There was no significant difference between the AEC control group which was microtissues fabricated with unconditioned AEC media and the ASM control group which was microtissues with ASM media. This suggests that supplements within the AEC media itself were not the cause of the enhanced ASM function, but rather the

soluble factors released by the AEC cells into the media which were responsible for this effect.

It was expected that fabricating ASM cells with AEC conditioned media would cause them to be less responsive to a contractile stimulus, since the presence of the epithelium would create a more physiological environment, and *in vivo*, a normal ASM has low contractility compared with asthma, where the signalling may be altered. That is, it was expected that in culture when presented with epithelial derived factors in the conditioned media, the microtissues would have less contractility. A number of previous studies (3, 13, 42, 142) have assessed ASM and AEC interaction using *ex vivo* and *in vitro* models. Using an *ex vivo* model of tracheal strips, it has been shown that the presence of an intact epithelium causes an acute relaxation effect of the tissue. However, removal of the epithelium through manual breakdown leads to an acute increase in contractility of the tissue through increased shortening capacity (13). This is contrary to what was observed in this study where ASM contractile function was enhanced in the presence of AEC soluble factors. Nevertheless, the data from that study may not be appropriate for comparison as it involves the use of organ baths where there exists a large diffusion distance which is problematic for soluble factors with a short half-life such as nitric oxide (NO). NO is an important neurotransmitter released by the epithelium through the action of an enzyme NO synthase which can account for the protective role of the epithelium against contractile agonists as it is possesses potent bronchodilatory capabilities (118). The presence of a large diffusion distance might potentially prevent mediators such as NO to reach the ASM tissue thereby portraying enhanced ASM responsiveness. The size of the organ bath used in these studies can be another issue as it

causes secreted factors such as prostaglandins to be diluted which can also affect ASM response.

Additionally, the removal of single epithelial cells using laser ablation has also been shown to induce airway contraction to 70% of the original cross section in thin cut lung slices (142). This data suggests that soluble mediators released by neighbouring epithelial cells in response to the wound can induce airway contraction. Perhaps, this is the case in the findings of this thesis chapter where ASM contraction was enhanced with the addition of undifferentiated AEC conditioned media, due to the presence of soluble mediators from epithelial cells that are in a proliferative state, however, this is speculative.

Furthermore, previous *in vitro* co-culture studies of ASM cells and AECs from our laboratory demonstrated decreased ASM cell stiffness in the presence of AECs assessed through optical magnetic twisting cytometry (OMTC). However, all the experiments in that study testing ASM cell stiffness and contractility were conducted in the presence of serum. This may have interfered with the results of the analysis since serum is used to promote cell proliferation and keep ASM cells in a proliferative state while attenuating the expression of contractile proteins.

Moreover, the increased baseline tension observed in the 3D ASM microtissues with the addition of AEC conditioned media in this thesis may actually not be a representation of pathological behaviour, but perhaps a restoration of ASM contractility that is normally lost in culture. Cells in culture produce much less force than in freshly isolated tissue, and this is true in 3D as well where the cross sectional stress of contracted 3D ASM microtissues compared to *ex vivo* ASM strips has been shown to be significantly lower (135). This is because cultured ASM cells *in vitro* possess considerably less contractile

protein content, approximately 1/20th compared with *ex vivo* tissue (51). Indeed, although serum deprivation does have some success in promoting cell culture contractile function, the failure of cultured cells to replicate *in vivo* functionality is an under recognised artifact of cultured cells. Therefore, based on the current data, it may be that the presence of some particular unidentified AEC soluble mediators within this 3D model help to restore normal function of ASM cells *in vitro* to better replicate native tissue as opposed to ASM cells alone, however, the exact mechanism remains to be answered.

Additionally, for the purposes of these studies, immortalised airway smooth muscle cells were used which were obtained from a single donor. The response in contractility seen in these studies may vary with the use of multiple donor cell lines or the use of primary human cells as there does exist high variability in phenotype between donor cells.

It should also be noted that the AEC conditioned media used to stimulate the ASM/WI-38 microtissues was from undifferentiated NHBE cells. *In vivo* epithelial cells are differentiated. Differentiated epithelial cells feature two distinct plasma membrane surfaces; a basal surface and an apical surface (53). This means they experience different basal and apical stimuli and express different proteins at each membrane surface. In addition, secretory products differ between the two interfaces of the epithelium. Key features of a fully differentiated NHBE cell is the growth of hair like structures called cilia and the production of mucus. Therefore, for proper analysis of AEC and ASM interaction, AECs should be in an air-liquid configuration to allow for cellular differentiation as any soluble factors that depend on cell polarisation are also required for any potential regulation of ASM function.

Chapter 7: Thesis Conclusions

In this thesis, I established a 3D model of airway smooth muscle microtissues to simulate the increased microenvironment stiffness associated with asthmatic airway remodeling to probe cellular contractile and phenotypic responses. Three approaches were applied to assess the chronic effect of varying the extracellular biomechanical properties on ASM response. This included altering the load opposing ASM contraction, and increasing matrix stiffness by manipulating the bulk matrix properties. This was done by crosslinking the matrix and by increasing the matrix density.

In asthma, airway remodeling leads to structural changes in the airway which can alter the local ASM microenvironment stiffness. This change in the biomechanical properties can potentially alter the contractile properties of the smooth muscle cells. Accordingly, it was hypothesised that increased matrix stiffness would enhance ASM contractility through a change in contractile phenotype which was assessed by measuring the expression of common regulatory and contractile genes.

Crosslinking the microtissue matrix and increasing the stiffness of the ASM microenvironment led to enhanced contractility which is in agreement with the hypothesis that substrate stiffness is a potent modulator of cellular function. However, function was only enhanced when microtissues were able to shorten against a compliant external load. This was in agreement with the hypothesis that ASM microenvironment stiffness would augment contractile function; however, this increase in function was not through a change in contractile phenotype evident in the gene expression data, but may have been due to improved tissue stability and cellular organisation.

Remarkably, there was a differential response in smooth muscle function where crosslinking the matrix enhanced function while increasing the collagen density attenuated function. This finding is in agreement with previous studies that have studied the effect of upregulation of type I collagen on ASM function or phenotype. It has been shown that type I collagen deposition is increased in asthma and enhances proliferative capabilities of ASM cells but attenuates the contractile phenotype. This would suggest that the bulk ECM signaling had overridden any effect of the enhanced matrix stiffness that might increase contractility. This result did not agree with the initial hypothesis that stiffness is the sole regulatory factor in ASM contractility suggesting that there are a number of other contributing factors.

It was hypothesised that stiffening of the ASM microenvironment is a potent regulator of contractility. However, stiffening of the airway in asthma and the remodeling process is thought by some to be a protective pathological response to prevent excessive airway narrowing. This idea assumes that contractility of the smooth muscle would need to increase before remodeling occurs. However, there is evidence of airway remodeling in asthma before clinical symptoms such as AHR occur (10). Based on this there are clearly two opposing effects: stiffness increasing contraction and stiffness opposing airway narrowing. Where the mechanical equilibrium lies in the lung would depend on the extent and location of airway stiffening, the magnitude of increased smooth muscle contractility, and the extent to which airway narrowing is opposed. Furthermore, it may be that only in combination with other remodeling or asthma effects that the increased contractility might actually overcome stiffness to give hyperresponsiveness since asthma is a multi-factorial disease.

The final aim was to assess the interaction between ASM and epithelial cells through the use of conditioned media. The data showed that undifferentiated AEC conditioned media enhanced ASM microtissue contractile capabilities dramatically suggesting there must be some unidentified soluble mediators released by the epithelial cells modulating contractility. In this thesis undifferentiated epithelial cells were used which are generally in a synthetic proliferative state which may have been similar to the *in vivo* state of these cells in asthmatics when injured, where they augment ASM contractility similar to what was seen in this thesis.

In summary, the model's ability to quantitatively demonstrate the impact of various biomechanical cues on smooth muscle cell function provide new ways to elucidate the mechanisms of cellular remodeling due to substrate stiffness in physiological 3D structures. Understanding how the cell responds to substrate stiffness in a physiologically representative 3D culture model will contribute to a better understanding of mechanobiology and the ability to separate and breakdown the multiple factors involved in asthma pathology.

7.1 Statement of Contributions

(1) Established a 3D culture model of airway smooth muscle microtissues to simulate the increased airway stiffness associated with asthmatic remodeling. Additionally, the mechanics of the 3D microtissue model were further characterised based on a previous study.

(2) Assessed contractile function of ASM/WI-38 microtissues under four different loading conditions and two matrix stiffnesses.

(3) Assessed in a limited study if gene expression of particular contractile phenotypic markers by mRNA quantification was altered at a single time-point in response to four different loading conditions and two matrix stiffnesses of ASM/WI-38 microtissues and found, in one case with increased matrix stiffness, that sm-MHC was increased, but all other markers did not change, within a certain sensitivity range.

(4) Demonstrated enhanced contractility of ASM/WI-38 microtissues with increased matrix stiffness with crosslinking when the microtissues were able to shorten.

(5) Demonstrated reduced contractility of ASM/WI-38 microtissues with increased collagen density most likely due to matrix signalling driving a phenotypic shift of ASM/WI-38 microtissues from a contractile to a proliferative state.

(6) Demonstrated feasibility of ASM/WI-38 microtissues fabricated with epithelial cell media maintained tissue and cell viability, and assessed contractile function of ASM/WI-38 microtissues with undifferentiated AEC conditioned media.

(7) Preliminary results showed for the first time using a 3D ASM/WI-38 microtissue culture model, enhanced contractility of ASM microtissues in the presence of AEC conditioned media.

7.2 Future Directions

7.2.1 Microtissue Contractile Phenotype

(1) As the gene expression data demonstrated large variability between samples possibly due to the low concentration of RNA, dynamic range of primers, or low sample size,

performing gene expression analysis on a larger sample size will reduce the standard error of mean and increase the power of statistical tests.

(2) The purpose of this thesis was to assess the chronic effect of substrate stiffness on 3D ASM/WI-38 microtissues. For this reason, contractile function and gene expression was assessed 3 days post tissue fabrication. The lack of correlation between the functional data and the gene expression data may most likely be due to the transient expression of mRNA over this time period. To better characterise the phenotypic state of ASM microtissues, gene expression (mRNA) should be assessed at multiple times points over the chronic treatment period of 3 days. Based on the literature, it would be recommended to assess gene expression at 12 hours, 24 hours and 3 days post tissue fabrication to provide the best representation of mRNA transcript level transiency.

(3) Since this study was focused on the chronic effects of changes in the biomechanical environment on ASM function and phenotype, protein expression should be assessed in combination with qPCR data using the qPCR data to guide which proteins to measure.

(4) As this was a preliminary investigation into the effects of changes in the stiffness of the ASM environment on contractile phenotype, all experiments were conducted using immortalised ASM cells obtained from a single donor. Due to the large variability between donors, future studies should include the use of multiple donor cell lines as well as the application of primary human airway smooth muscle cells.

7.2.2 Matrix Properties

(1) The data from this study demonstrated considerable stiffening of the collagen gels crosslinked with d-ribose. However, the magnitude of stiffening was still less than what many have suggested to be approximately the *in vivo* asthmatic airway stiffness due to remodeling (89). Future studies should assess the use of higher concentrations of d-ribose (≤100mM) over a longer period of time, which has been shown to be non-cytotoxic and does not alter collagen fibre architecture. Alternatively, the use of another crosslinking agent such as lysyl oxidase (LOX) may provide enhanced stiffening of the matrix.

(2) With increased collagen density, the microtissues became less contractile in contrast to what was seen with increasing matrix stiffness through crosslinking with d-ribose. As mentioned, this may be due to the pro-proliferative nature of type I collagen. To confirm this hypothesis, it should be possible to assess markers of smooth muscle proliferation or the application of 5-Ethynyl-2′-deoxyuridine (EdU) incorporation to probe DNA synthesis.

(3) The purpose of this thesis was to assess the chronic effect of substrate stiffness on ASM microtissue function and phenotype. However, the data obtained with regards to cell mechanics may be altered in the presence of chronic strain. In contrast to static forces and loads in equilibrium, *in vivo* ASM cells are under chronic cyclic strain due to normal tidal breathing. It has previously been shown using polyacrylamide hydrogels in 2D culture models that chronic strain blunts the effect of substrate

stiffness on cell function. Therefore, it would be interesting to see whether the combination of cyclic strain and substrate stiffness has the same effect in a more physiological 3D culture model.

(4) The pro-contractile response of smooth muscle cells seen in conventional 2D cell culture with applied cyclic stretch is also hypothesized to be due to an increase in baseline tone (37). Therefore, it would be interesting to study the 3D ASM/WI-38 microtissue functional and phenotypic response after chronic incubation with either a long-acting contractile agonist or relaxant to assess the effects of altered cellular tone, but it would be important to also develop a system that could apply chronic cyclic stretching since without stretch the tone does not have a pro-contractile effect (37).

(5) The presence of inflammatory cells as well as inflammatory mediators has been shown to initiate a pro-contractile response in smooth muscle cells seen using *ex vivo* and 2D culture models. Therefore, it would be interesting to study the 3D ASM/WI-38 contractile response under the influence of various cytokines involved in asthmatic airway inflammation or through the addition of mast cells and macrophages.

(6) Additionally, it has been shown that the ECM profile of asthmatic airways is altered (7, 31). Therefore, it would be interesting to assess the influence of other ECM proteins on ASM function for example elastin and laminin.

7.2.3 ASM and AEC Microtissue Model

(1) In this study, ASM/WI-38 microtissues were fabricated with undifferentiated AEC media, meaning the NHBE cells were in their growth phase (proliferative state) thus

making it difficult to make clear conclusions about the effects observed. Differentiated NHBE cells possess very different characteristics compared to undifferentiated cells as cellular polarity alters the profile of receptors on each surface of the cell membrane and the secretory products thereby potentially affecting regulation of ASM function. NHBE cells that are fully differentiated should also be characterised within this 3D culture model with ASM/WI-38 microtissues.

(2) A majority of the previous studies assessing ASM and AEC interactions have looked at the effect of damaged AEC cells on ASM function. Based on that, future studies should involve the assessment of injured AEC conditioned media on ASM contractility in comparison to healthy AEC conditioned media.

(3) The major pathological change in the epithelium of asthmatics is the promotion of an inflammatory phenotype. This is caused by the release of various inflammatory cytokines and growth factors responsible for epithelial repair. Based on these observations it would be interesting to assess markers of inflammatory mediators within this 3D model of ASM microtissues involving mediators such as IL-17 which has been shown to be correlated with the severity of AHR. More recently, studies have begun to explore the impact of IL-25 and IL-33 on the onset of asthma and their role in the immune response.

(4) Lastly, the fabrication of microtissues using asthmatic airway smooth muscle cells in addition to epithelial cells within this 3D model would allow for comparison of responses of healthy tissue to diseased tissue.

References

1. **Adler A, and Bates JH**. A micromechanical model of airway-parenchymal interdependence. *Annals of biomedical engineering* 28: 309-317, 2000.

2. **Ahmed TA, Dare EV, and Hincke M**. Fibrin: a versatile scaffold for tissue engineering applications. *Tissue engineering Part B, Reviews* 14: 199-215, 2008.

3. **Aizawa H, Miyazaki N, Shigematsu N, and Tomooka M**. A possible role of airway epithelium in modulating hyperresponsiveness. *British journal of pharmacology* 93: 139-145, 1988.

4. **Alenghat FJ, and Ingber DE**. Mechanotransduction: All Signals Point to Cytoskeleton, Matrix, and Integrins. *Sci STKE* 2002: pe6-, 2002.

5. **An SS, Bai TR, Bates JH, Black JL, Brown RH, Brusasco V, Chitano P, Deng L, Dowell M, Eidelman DH, Fabry B, Fairbank NJ, Ford LE, Fredberg JJ, Gerthoffer WT, Gilbert SH, Gosens R, Gunst SJ, Halayko AJ, Ingram RH, Irvin CG, James AL, Janssen LJ, King GG, Knight DA, Lauzon AM, Lakser OJ, Ludwig MS, Lutchen KR, Maksym GN, Martin JG, Mauad T, McParland BE, Mijailovich SM, Mitchell HW, Mitchell RW, Mitzner W, Murphy TM, Pare PD, Pellegrino R, Sanderson MJ, Schellenberg RR, Seow CY, Silveira PS, Smith PG, Solway J, Stephens NL, Sterk PJ, Stewart AG, Tang DD, Tepper RS, Tran T, and Wang L**. Airway smooth muscle dynamics: a common pathway of airway obstruction in asthma. *The European respiratory journal : official journal of the European Society for Clinical Respiratory Physiology* 29: 834-860, 2007.

6. **An SS, Kim J, Ahn K, Trepat X, Drake KJ, Kumar S, Ling G, Purington C, Rangasamy T, Kensler TW, Mitzner W, Fredberg JJ, and Biswal S**. Cell stiffness, contractile stress and the role of extracellular matrix. *Biochemical and biophysical research communications* 382: 697-703, 2009.

7. **Araujo BB, Dolhnikoff M, Silva LF, Elliot J, Lindeman JH, Ferreira DS, Mulder A, Gomes HA, Fernezlian SM, James A, and Mauad T**. Extracellular matrix components and regulators in the airway smooth muscle in asthma. *The European respiratory journal : official journal of the European Society for Clinical Respiratory Physiology* 32: 61-69, 2008.

8. **Awadh N, Muller NL, Park CS, Abboud RT, and FitzGerald JM**. Airway wall thickness in patients with near fatal asthma and control groups: assessment with high resolution computed tomographic scanning. *Thorax* 53: 248-253, 1998.

9. **Baker BM, and Chen CS**. Deconstructing the third dimension: how 3D culture microenvironments alter cellular cues. *J Cell Sci* 125: 3015-3024, 2012.

10. **Baldwin L, and Roche WR**. Does remodelling of the airway wall precede asthma? *Paediatric respiratory reviews* 3: 315-320, 2002.

11. **Barnes PJ**. Immunology of asthma and chronic obstructive pulmonary disease. *Nat Rev Immunol* 8: 183-192, 2008.

12. **Barnes PJ**. Pharmacology of airway smooth muscle. *American journal of respiratory and critical care medicine* 158: S123-132, 1998.

13. **Barnes PJ, Cuss FM, and Palmer JB**. The effect of airway epithelium on smooth muscle contractility in bovine trachea. *British journal of pharmacology* 86: 685-691, 1985.

14. **Basta G, Lazzerini G, Massaro M, Simoncini T, Tanganelli P, Fu C, Kislinger T, Stern DM, Schmidt AM, and De Caterina R**. Advanced glycation end products activate endothelium through signal-transduction receptor RAGE: a mechanism for amplification of inflammatory responses. *Circulation* 105: 816-822, 2002.

15. **Bateman ED, Hurd SS, Barnes PJ, Bousquet J, Drazen JM, FitzGerald M, Gibson P, Ohta K, O'Byrne P, Pedersen SE, Pizzichini E, Sullivan SD, Wenzel SE, and Zar HJ**. Global strategy for asthma management and prevention: GINA executive summary. *The European respiratory journal : official journal of the European Society for Clinical Respiratory Physiology* 31: 143-178, 2008.

16. **Bates JH, and Lauzon AM**. Parenchymal tethering, airway wall stiffness, and the dynamics of bronchoconstriction. *Journal of applied physiology* 102: 1912-1920, 2007.

17. **Bosse Y, Riesenfeld EP, Pare PD, and Irvin CG**. It's not all smooth muscle: non-smooth-muscle elements in control of resistance to airflow. *Annual review of physiology* 72: 437-462, 2010.

18. **Boudou T, Legant WR, Mu A, Borochin MA, Thavandiran N, Radisic M, Zandstra PW, Epstein JA, Margulies KB, and Chen CS**. A Microfabricated Platform to Measure and Manipulate the Mechanics of Engineered Cardiac Microtissues. *Tissue engineering Part A* 2012.

19. **Bousquet J, Jeffery PK, Busse WW, Johnson M, and Vignola AM**. Asthma. From bronchoconstriction to airways inflammation and remodeling. *American journal of respiratory and critical care medicine* 161: 1720-1745, 2000.

20. **Bramley AM, Roberts CR, and Schellenberg RR**. Collagenase increases shortening of human bronchial smooth muscle in vitro. *American journal of respiratory and critical care medicine* 152: 1513-1517, 1995.

21. **Burgess JK, Ceresa C, Johnson SR, Kanabar V, Moir LM, Nguyen TT, Oliver BG, Schuliga M, and Ward J**. Tissue and matrix influences on airway smooth muscle function. *Pulmonary pharmacology & therapeutics* 22: 379-387, 2009.

22. **Ceresa CC, Knox AJ, and Johnson SR**. Use of a three-dimensional cell culture model to study airway smooth muscle-mast cell interactions in airway remodeling. *American journal of physiology Lung cellular and molecular physiology* 296: L1059-1066, 2009.

23. **Chamley-Campbell J, Campbell GR, and Ross R**. The smooth muscle cell in culture. *Physiological reviews* 59: 1-61, 1979.

24. **Chiquet-Ehrismann R, Tannheimer M, Koch M, Brunner A, Spring J, Martin D, Baumgartner S, and Chiquet M**. Tenascin-C expression by fibroblasts is elevated in stressed collagen gels. *J Cell Biol* 127: 2093-2101, 1994.

25. **Chitano P**. Models to understand contractile function in the airways. *Pulmonary pharmacology & therapeutics* 24: 444-451, 2011.

26. **Choe MM, Sporn PH, and Swartz MA**. An in vitro airway wall model of remodeling. *American journal of physiology Lung cellular and molecular physiology* 285: L427-433, 2003.

27. **Cummings CL, Gawlitta D, Nerem RM, and Stegemann JP**. Properties of engineered vascular constructs made from collagen, fibrin, and collagen-fibrin mixtures. *Biomaterials* 25: 3699-3706, 2004.

28. **Dabrowska R, Sherry JM, Aromatorio DK, and Hartshorne DJ**. Modulator protein as a component of the myosin light chain kinase from chicken gizzard. *Biochemistry* 17: 253-258, 1978.

29. **de Kluijver J, Schrumpf JA, Evertse CE, Sont JK, Roughley PJ, Rabe KF, Hiemstra PS, Mauad T, and Sterk PJ**. Bronchial matrix and inflammation respond to inhaled steroids despite ongoing allergen exposure in asthma. *Clin Exp Allergy* 35: 1361-1369, 2005.

30. **Dekkers BG, Maarsingh H, Meurs H, and Gosens R**. Airway structural components drive airway smooth muscle remodeling in asthma. *Proceedings of the American Thoracic Society* 6: 683-692, 2009.

31. **Dolhnikoff M, da Silva LF, de Araujo BB, Gomes HA, Fernezlian S, Mulder A, Lindeman JH, and Mauad T**. The outer wall of small airways is a major site of remodeling in fatal asthma. *The Journal of allergy and clinical immunology* 123: 1090-1097, 1097 e1091, 2009.

32. **Du P, Lin I-K, Lu H, and Zhang X**. Extension of the beam theory for polymer bio-transducers with low aspect ratios and viscoelastic characteristics. *Journal of Micromechanics and Microengineering* 20: 095016, 2010.

33. **Ebina M, Takahashi T, Chiba T, and Motomiya M**. Cellular hypertrophy and hyperplasia of airway smooth muscles underlying bronchial asthma. A 3-D morphometric study. *The American review of respiratory disease* 148: 720-726, 1993.

34. **Elias JA, Zhu Z, Chupp G, and Homer RJ**. Airway remodeling in asthma. *The Journal of clinical investigation* 104: 1001-1006, 1999.

35. **Engler AJ, Griffin MA, Sen S, Bonnemann CG, Sweeney HL, and Discher DE**. Myotubes differentiate optimally on substrates with tissue-like stiffness: pathological implications for soft or stiff microenvironments. *J Cell Biol* 166: 877-887, 2004.

36. **Engler AJ, Sen S, Sweeney HL, and Discher DE**. Matrix elasticity directs stem cell lineage specification. *Cell* 126: 677-689, 2006.

37. **Fairbank NJ, Connolly SC, Mackinnon JD, Wehry K, Deng L, and Maksym GN**. Airway smooth muscle cell tone amplifies contractile function in the presence of chronic cyclic strain. *American journal of physiology Lung cellular and molecular physiology* 295: L479-488, 2008.

38. **Francis-Sedlak ME, Uriel S, Larson JC, Greisler HP, Venerus DC, and Brey EM**. Characterization of type I collagen gels modified by glycation. *Biomaterials* 30: 1851-1856, 2009.

39. **Fredberg JJ**. Airway obstruction in asthma: does the response to a deep inspiration matter? *Respiratory research* 2: 273-275, 2001.

40. **Fredberg JJ, Inouye DS, Mijailovich SM, and Butler JP**. Perturbed equilibrium of myosin binding in airway smooth muscle and its implications in bronchospasm. *American journal of respiratory and critical care medicine* 159: 959-967, 1999.

41. **Fu MX, Wells-Knecht KJ, Blackledge JA, Lyons TJ, Thorpe SR, and Baynes JW**. Glycation, glycoxidation, and cross-linking of collagen by glucose. Kinetics,

mechanisms, and inhibition of late stages of the Maillard reaction. *Diabetes* 43: 676-683, 1994.

42. **Gallos G, Townsend E, Yim P, Virag L, Zhang Y, Xu D, Bacchetta M, and Emala CW**. Airway epithelium is a predominant source of endogenous airway GABA and contributes to relaxation of airway smooth muscle tone. *American journal of physiology Lung cellular and molecular physiology* 304: L191-197, 2013.

43. **Girton TS, Oegema TR, and Tranquillo RT**. Exploiting glycation to stiffen and strengthen tissue equivalents for tissue engineering. *Journal of biomedical materials research* 46: 87-92, 1999.

44. **Gosens R, Stelmack GL, Dueck G, McNeill KD, Yamasaki A, Gerthoffer WT, Unruh H, Gounni AS, Zaagsma J, and Halayko AJ**. Role of caveolin-1 in p42/p44 MAP kinase activation and proliferation of human airway smooth muscle. *American journal of physiology Lung cellular and molecular physiology* 291: L523-534, 2006.

45. **Greenberg CS, Birckbichler PJ, and Rice RH**. Transglutaminases: multifunctional cross-linking enzymes that stabilize tissues. *FASEB J* 5: 3071-3077, 1991.

46. **Griffith LG, and Swartz MA**. Capturing complex 3D tissue physiology in vitro. *Nat Rev Mol Cell Biol* 7: 211-224, 2006.

47. **Grinnell F**. Fibroblast biology in three-dimensional collagen matrices. *Trends in cell biology* 13: 264-269, 2003.

48. **Guo WH, Frey MT, Burnham NA, and Wang YL**. Substrate rigidity regulates the formation and maintenance of tissues. *Biophysical journal* 90: 2213-2220, 2006.

49. **Gygi SP, Rochon Y, Franza BR, and Aebersold R**. Correlation between protein and mRNA abundance in yeast. *Mol Cell Biol* 19: 1720-1730, 1999.

50. **Hai CM, and Murphy RA**. Cross-bridge phosphorylation and regulation of latch state in smooth muscle. *Am J Physiol* 254: C99-106, 1988.

51. **Halayko AJ, Salari H, Ma X, and Stephens NL**. Markers of airway smooth muscle cell phenotype. *Am J Physiol* 270: L1040-1051, 1996.

52. **Halayko AJ, and Solway J**. Molecular mechanisms of phenotypic plasticity in smooth muscle cells. *Journal of applied physiology* 90: 358-368, 2001.

53. **Handler JS**. Overview of epithelial polarity. *Annual review of physiology* 51: 729-740, 1989.

54. **Hershenson MB, Brown M, Camoretti-Mercado B, and Solway J**. Airway smooth muscle in asthma. *Annual review of pathology* 3: 523-555, 2008.

55. **Hinson JS, Medlin MD, Lockman K, Taylor JM, and Mack CP**. Smooth muscle cell-specific transcription is regulated by nuclear localization of the myocardin-related transcription factors. *Am J Physiol Heart Circ Physiol* 292: H1170-1180, 2007.

56. **Hirst SJ, Barnes PJ, and Twort CH**. Quantifying proliferation of cultured human and rabbit airway smooth muscle cells in response to serum and platelet-derived growth factor. *Am J Respir Cell Mol Biol* 7: 574-581, 1992.

57. **Hirst SJ, Twort CH, and Lee TH**. Differential effects of extracellular matrix proteins on human airway smooth muscle cell proliferation and phenotype. *Am J Respir Cell Mol Biol* 23: 335-344, 2000.

58. **Hirst SJ, Walker TR, and Chilvers ER**. Phenotypic diversity and molecular mechanisms of airway smooth muscle proliferation in asthma. *The European respiratory journal : official journal of the European Society for Clinical Respiratory Physiology* 16: 159-177, 2000.

59. **Holgate ST**. The airway epithelium is central to the pathogenesis of asthma. *Allergol Int* 57: 1-10, 2008.

60. **Holgate ST**. Epithelium dysfunction in asthma. *The Journal of allergy and clinical immunology* 120: 1233-1244; quiz 1245-1236, 2007.

61. **Holgate ST**. The inflammation-repair cycle in asthma: the pivotal role of the airway epithelium. *Clin Exp Allergy* 28 Suppl 5: 97-103, 1998.

62. **Holgate ST, Lackie P, Wilson S, Roche W, and Davies D**. Bronchial Epithelium as a Key Regulator of Airway Allergen Sensitization and Remodeling in Asthma. *American journal of respiratory and critical care medicine* 162: S113-S117, 2000.

63. **Jakus MA, and Hall CE**. Studies of actin and myosin. *The Journal of biological chemistry* 167: 705-714, 1947.

64. **Johnson PR, Black JL, Carlin S, Ge Q, and Underwood PA**. The production of extracellular matrix proteins by human passively sensitized airway smooth-muscle

cells in culture: the effect of beclomethasone. *American journal of respiratory and critical care medicine* 162: 2145-2151, 2000.

65. **Johnson PR, Burgess JK, Underwood PA, Au W, Poniris MH, Tamm M, Ge Q, Roth M, and Black JL**. Extracellular matrix proteins modulate asthmatic airway smooth muscle cell proliferation via an autocrine mechanism. *The Journal of allergy and clinical immunology* 113: 690-696, 2004.

66. **Kamm KE, and Stull JT**. The function of myosin and myosin light chain kinase phosphorylation in smooth muscle. *Annual review of pharmacology and toxicology* 25: 593-620, 1985.

67. **Kamm KE, and Stull JT**. Myosin phosphorylation, force, and maximal shortening velocity in neurally stimulated tracheal smooth muscle. *Am J Physiol* 249: C238-247, 1985.

68. **Kaplan A**. Systems for the management of respiratory disease in primary care - an international series: Canada. *Primary care respiratory journal : journal of the General Practice Airways Group* 17: 73-78, 2008.

69. **Khan MA, Ellis R, Inman MD, Bates JH, Sanderson MJ, and Janssen LJ**. Influence of airway wall stiffness and parenchymal tethering on the dynamics of bronchoconstriction. *American journal of physiology Lung cellular and molecular physiology* 299: L98-L108, 2010.

70. **King GG, Pare PD, and Seow CY**. The mechanics of exaggerated airway narrowing in asthma: the role of smooth muscle. *Respiration physiology* 118: 1-13, 1999.

71. **Knight DA, and Holgate ST**. The airway epithelium: structural and functional properties in health and disease. *Respirology (Carlton, Vic)* 8: 432-446, 2003.

72. **Kong SK, Halayko AJ, and Stephens NL**. Increased myosin phosphorylation in sensitized canine tracheal smooth muscle. *Am J Physiol* 259: L53-56, 1990.

73. **Krishnan R, Park CY, Lin YC, Mead J, Jaspers RT, Trepat X, Lenormand G, Tambe D, Smolensky AV, Knoll AH, Butler JP, and Fredberg JJ**. Reinforcement versus fluidization in cytoskeletal mechanoresponsiveness. *PloS one* 4: e5486, 2009.

74. **Kubista M, Andrade JM, Bengtsson M, Forootan A, Jonak J, Lind K, Sindelka R, Sjoback R, Sjogreen B, Strombom L, Stahlberg A, and Zoric N**. The real-time polymerase chain reaction. *Molecular aspects of medicine* 27: 95-125, 2006.

75. **Kumar MS, and Owens GK**. Combinatorial control of smooth muscle-specific gene expression. *Arteriosclerosis, thrombosis, and vascular biology* 23: 737-747, 2003.

76. **Laitinen A, Altraja A, Kampe M, Linden M, Virtanen I, and Laitinen LA**. Tenascin is increased in airway basement membrane of asthmatics and decreased by an inhaled steroid. *American journal of respiratory and critical care medicine* 156: 951-958, 1997.

77. **Laitinen LA, Heino M, Laitinen A, Kava T, and Haahtela T**. Damage of the airway epithelium and bronchial reactivity in patients with asthma. *The American review of respiratory disease* 131: 599-606, 1985.

78. **Laitinen LA, and Laitinen A**. Inhaled corticosteroid treatment and extracellular matrix in the airways in asthma. *Int Arch Allergy Immunol* 107: 215-216, 1995.

79. **Lambert RK, and Pare PD**. Lung parenchymal shear modulus, airway wall remodeling, and bronchial hyperresponsiveness. *Journal of applied physiology* 83: 140-147, 1997.

80. **Larionov A, Krause A, and Miller W**. A standard curve based method for relative real time PCR data processing. *BMC bioinformatics* 6: 62, 2005.

81. **Lauzon AM, Tyska MJ, Rovner AS, Freyzon Y, Warshaw DM, and Trybus KM**. A 7-amino-acid insert in the heavy chain nucleotide binding loop alters the kinetics of smooth muscle myosin in the laser trap. *Journal of muscle research and cell motility* 19: 825-837, 1998.

82. **Lee KM, Tsai KY, Wang N, and Ingber DE**. Extracellular matrix and pulmonary hypertension: control of vascular smooth muscle cell contractility. *Am J Physiol* 274: H76-82, 1998.

83. **Legant WR, Pathak A, Yang MT, Deshpande VS, McMeeking RM, and Chen CS**. Microfabricated tissue gauges to measure and manipulate forces from 3D microtissues. *Proc Natl Acad Sci U S A* 106: 10097-10102, 2009.

84. **Li W, and Stephens NL**. Auxotonic loading and airway smooth muscle shortening. *Canadian journal of physiology and pharmacology* 72: 1458-1463, 1994.

85. **Long X, Bell RD, Gerthoffer WT, Zlokovic BV, and Miano JM**. Myocardin is sufficient for a smooth muscle-like contractile phenotype. *Arteriosclerosis, thrombosis, and vascular biology* 28: 1505-1510, 2008.

86. **Ma X, Cheng Z, Kong H, Wang Y, Unruh H, Stephens NL, and Laviolette M**. Changes in biophysical and biochemical properties of single bronchial smooth muscle cells from asthmatic subjects. *American journal of physiology Lung cellular and molecular physiology* 283: L1181-1189, 2002.

87. **Ma X, Wang Y, and Stephens NL**. Serum deprivation induces a unique hypercontractile phenotype of cultured smooth muscle cells. *Am J Physiol* 274: C1206-1214, 1998.

88. **Malavia NK, Raub CB, Mahon SB, Brenner M, Panettieri RA, Jr., and George SC**. Airway epithelium stimulates smooth muscle proliferation. *Am J Respir Cell Mol Biol* 41: 297-304, 2009.

89. **Marinković A, Mih JD, Liu F, and Tschumperlin DJ**. Transitions In Matrix Stiffness Uncouple Lung Fibroblast Proliferative And Morphological Responses From Cytoskeletal Tension. *Am J Respir Crit Care Med* 183: A3562, 2011.

90. **Martin C, Uhlig S, and Ullrich V**. Videomicroscopy of methacholine-induced contraction of individual airways in precision-cut lung slices. *The European respiratory journal : official journal of the European Society for Clinical Respiratory Physiology* 9: 2479-2487, 1996.

91. **Mason BN, Starchenko A, Williams RM, Bonassar LJ, and Reinhart-King CA**. Tuning three-dimensional collagen matrix stiffness independently of collagen concentration modulates endothelial cell behavior. *Acta Biomater* 9: 4635-4644, 2013.

92. **Matsumoto H, Moir LM, Oliver BG, Burgess JK, Roth M, Black JL, and McParland BE**. Comparison of gel contraction mediated by airway smooth muscle cells from patients with and without asthma. *Thorax* 62: 848-854, 2007.

93. **McParland BE, Macklem PT, and Pare PD**. Airway wall remodeling: friend or foe? *Journal of applied physiology* 95: 426-434, 2003.

94. **Mentink CJ, Hendriks M, Levels AA, and Wolffenbuttel BH**. Glucose-mediated cross-linking of collagen in rat tendon and skin. *Clinica chimica acta; international journal of clinical chemistry* 321: 69-76, 2002.

95. **Miller C, George S, and Niklason L**. Developing a tissue-engineered model of the human bronchiole. *Journal of tissue engineering and regenerative medicine* 4: 619-627, 2010.

96. **Monnier VM, and Cerami A**. Nonenzymatic browning in vivo: possible process for aging of long-lived proteins. *Science (New York, NY)* 211: 491-493, 1981.

97. **Montefort S, Roberts JA, Beasley R, Holgate ST, and Roche WR**. The site of disruption of the bronchial epithelium in asthmatic and non-asthmatic subjects. *Thorax* 47: 499-503, 1992.

98. **O'Brien LE, Zegers MM, and Mostov KE**. Opinion: Building epithelial architecture: insights from three-dimensional culture models. *Nat Rev Mol Cell Biol* 3: 531-537, 2002.

99. **Oliver WC, and Pharr GM**. An improved technique for determining hardness and elastic modulus using load and displacement sensing indentation experiments. *Journal of Materials Research* 7: 1564-1583, 1992.

100. **Parameswaran K, Willems-Widyastuti A, Alagappan VK, Radford K, Kranenburg AR, and Sharma HS**. Role of extracellular matrix and its regulators in human airway smooth muscle biology. *Cell biochemistry and biophysics* 44: 139-146, 2006.

101. **Pare PD, McParland BE, and Seow CY**. Structural basis for exaggerated airway narrowing. *Canadian journal of physiology and pharmacology* 85: 653-658, 2007.

102. **Pelham RJ, Jr., and Wang Y**. Cell locomotion and focal adhesions are regulated by substrate flexibility. *Proc Natl Acad Sci U S A* 94: 13661-13665, 1997.

103. **Pellegrini L, Tan S, and Richmond TJ**. Structure of serum response factor core bound to DNA. *Nature* 376: 490-498, 1995.

104. **Pepe C, Foley S, Shannon J, Lemiere C, Olivenstein R, Ernst P, Ludwig MS, Martin JG, and Hamid Q**. Differences in airway remodeling between subjects with severe and moderate asthma. *The Journal of allergy and clinical immunology* 116: 544-549, 2005.

105. **Pfaffl MW, Tichopad A, Prgomet C, and Neuvians TP**. Determination of stable housekeeping genes, differentially regulated target genes and sample integrity: BestKeeper--Excel-based tool using pair-wise correlations. *Biotechnology letters* 26: 509-515, 2004.

106. **Polte TR, Eichler GS, Wang N, and Ingber DE**. Extracellular matrix controls myosin light chain phosphorylation and cell contractility through modulation of cell shape and cytoskeletal prestress. *Am J Physiol Cell Physiol* 286: C518-528, 2004.

107. **Powell DW**. Barrier function of epithelia. *Am J Physiol* 241: G275-288, 1981.

108. **Ramchandani R, Shen X, Gunst SJ, and Tepper RS**. Comparison of elastic properties and contractile responses of isolated airway segments from mature and immature rabbits. *Journal of applied physiology* 95: 265-271, 2003.

109. **Ressmeyer AR, Larsson AK, Vollmer E, Dahlen SE, Uhlig S, and Martin C**. Characterisation of guinea pig precision-cut lung slices: comparison with human tissues. *The European respiratory journal : official journal of the European Society for Clinical Respiratory Physiology* 28: 603-611, 2006.

110. **Reusch P, Wagdy H, Reusch R, Wilson E, and Ives HE**. Mechanical strain increases smooth muscle and decreases nonmuscle myosin expression in rat vascular smooth muscle cells. *Circulation research* 79: 1046-1053, 1996.

111. **Roche WR, Beasley R, Williams JH, and Holgate ST**. Subepithelial fibrosis in the bronchi of asthmatics. *Lancet* 1: 520-524, 1989.

112. **Rowe SL, and Stegemann JP**. Interpenetrating collagen-fibrin composite matrices with varying protein contents and ratios. *Biomacromolecules* 7: 2942-2948, 2006.

113. **Roy R, Boskey AL, and Bonassar LJ**. Non-enzymatic glycation of chondrocyte-seeded collagen gels for cartilage tissue engineering. *J Orthop Res* 26: 1434-1439, 2008.

114. **Schwartz MA**. Integrin signaling revisited. *Trends in cell biology* 11: 466-470, 2001.

115. **Shanahan CM, Weissberg PL, and Metcalfe JC**. Isolation of gene markers of differentiated and proliferating vascular smooth muscle cells. *Circulation research* 73: 193-204, 1993.

116. **Smith-Mungo LI, and Kagan HM**. Lysyl oxidase: properties, regulation and multiple functions in biology. *Matrix biology : journal of the International Society for Matrix Biology* 16: 387-398, 1998.

117. **Smith PG, Roy C, Fisher S, Huang QQ, and Brozovich F**. Selected contribution: mechanical strain increases force production and calcium sensitivity in cultured airway smooth muscle cells. *Journal of applied physiology (Bethesda, Md : 1985)* 89: 2092-2098, 2000.

118. **Sparrow MP, Omari TI, and Mitchell HW**. The epithelial barrier and airway responsiveness. *Canadian journal of physiology and pharmacology* 73: 180-190, 1995.

119. **Stylianou A, Yova D, Alexandratou E, and Petri A**. Atomic force imaging microscopy investigation of the interaction of ultraviolet radiation with collagen thin films. 2013, p. 85940E-85940E-85915.

120. **Sung HW, Chang WH, Ma CY, and Lee MH**. Crosslinking of biological tissues using genipin and/or carbodiimide. *J Biomed Mater Res A* 64: 427-438, 2003.

121. **Tam A, Wadsworth S, Dorscheid D, Man SF, and Sin DD**. The airway epithelium: more than just a structural barrier. *Ther Adv Respir Dis* 5: 255-273, 2011.

122. **Tang D, Mehta D, and Gunst SJ**. Mechanosensitive tyrosine phosphorylation of paxillin and focal adhesion kinase in tracheal smooth muscle. *Am J Physiol* 276: C250-258, 1999.

123. **Throm Quinlan AM, Sierad LN, Capulli AK, Firstenberg LE, and Billiar KL**. Combining dynamic stretch and tunable stiffness to probe cell mechanobiology in vitro. *PloS one* 6: e23272, 2011.

124. **Tran T, Teoh CM, Tam JK, Qiao Y, Chin CY, Chong OK, Stewart AG, Harris T, Wong WS, Guan SP, Leung BP, Gerthoffer WT, Unruh H, and Halayko AJ**. Laminin drives survival signals to promote a contractile smooth muscle phenotype and airway hyperreactivity. *FASEB J* 27: 3991-4003, 2013.

125. **Trappmann B, and Chen CS**. How cells sense extracellular matrix stiffness: a material's perspective. *Current opinion in biotechnology* 24: 948-953, 2013.

126. **Ulrich P, and Cerami A**. Protein glycation, diabetes, and aging. *Recent progress in hormone research* 56: 1-21, 2001.

127. **Vogel C, Abreu Rde S, Ko D, Le SY, Shapiro BA, Burns SC, Sandhu D, Boutz DR, Marcotte EM, and Penalva LO**. Sequence signatures and mRNA concentration can explain two-thirds of protein abundance variation in a human cell line. *Molecular systems biology* 6: 400, 2010.

128. **Walker C, Gupta S, Hartley R, and Brightling CE**. Computed tomography scans in severe asthma: utility and clinical implications. *Current opinion in pulmonary medicine* 18: 42-47, 2012.

129. **Wang C**. Timoshenko Beam-Bending Solutions in Terms of Euler-Bernoulli Solutions. *Journal of Engineering Mechanics* 121: 763-765, 1995.

130. **Wang D, Chang PS, Wang Z, Sutherland L, Richardson JA, Small E, Krieg PA, and Olson EN**. Activation of cardiac gene expression by myocardin, a transcriptional cofactor for serum response factor. *Cell* 105: 851-862, 2001.

131. **Wang Z, Wang DZ, Pipes GC, and Olson EN**. Myocardin is a master regulator of smooth muscle gene expression. *Proc Natl Acad Sci U S A* 100: 7129-7134, 2003.

132. **Weadock K, Olson RM, and Silver FH**. Evaluation of collagen crosslinking techniques. *Biomater Med Devices Artif Organs* 11: 293-318, 1983.

133. **Wells RG**. The role of matrix stiffness in regulating cell behavior. *Hepatology (Baltimore, Md)* 47: 1394-1400, 2008.

134. **West AR, Connolly S, Mih JD, Billiar KL, Tschumperlin D, and Maksym GN**. Increased Extracellular Matrix Stiffness Enhances Airway Smooth Muscle Contractile Phenotype And Contractile Function. *Am J Respir Crit Care Med* 183: A4052, 2011.

135. **West AR, Zaman N, Cole DJ, Walker MJ, Legant WR, Boudou T, Chen CS, Favreau JT, Gaudette GR, Cowley EA, and Maksym GN**. Development and characterization of a 3D multicell microtissue culture model of airway smooth muscle. *American Journal of Physiology - Lung Cellular and Molecular Physiology* 304: L4-L16, 2013.

136. **Wilson JW, and Li X**. The measurement of reticular basement membrane and submucosal collagen in the asthmatic airway. *Clin Exp Allergy* 27: 363-371, 1997.

137. **Woodruff PG**. Gene expression in asthmatic airway smooth muscle. *Proceedings of the American Thoracic Society* 5: 113-118, 2008.

138. **Wright D, Sharma P, Ryu MH, Risse PA, Ngo M, Maarsingh H, Koziol-White C, Jha A, Halayko AJ, and West AR**. Models to study airway smooth muscle contraction in vivo, ex vivo and in vitro: Implications in understanding asthma. *Pulmonary pharmacology & therapeutics* 2012.

139. **Xie Z, Hakoda H, and Ito Y**. Airway epithelial cells regulate membrane potential, neurotransmission and muscle tone of the dog airway smooth muscle. *J Physiol* 449: 619-639, 1992.

140. **Young JL, and Engler AJ**. Hydrogels with time-dependent material properties enhance cardiomyocyte differentiation in vitro. *Biomaterials* 32: 1002-1009, 2011.

141. **Zhong S, and Yung LY**. Enhanced biological stability of collagen with incorporation of PAMAM dendrimer. *J Biomed Mater Res A* 91: 114-122, 2009.

142. **Zhou J, Alvarez-Elizondo MB, Botvinick E, and George SC**. Local small airway epithelial injury induces global smooth muscle contraction and airway constriction. *Journal of applied physiology (Bethesda, Md : 1985)* 112: 627-637, 2012.

143. **Zuyderduyn S, Sukkar MB, Fust A, Dhaliwal S, and Burgess JK**. Treating asthma means treating airway smooth muscle cells. *The European respiratory journal : official journal of the European Society for Clinical Respiratory Physiology* 32: 265-274, 2008.

Appendix A: Statistical Power Analysis

Post hoc statistical power calculations were performed using G*Power © (version 3.1.5) for a comparison of sample means for a one-way ANOVA. As a standard for adequacy a statistical power of 0.8 is used (80% probability that the test will detect a significant difference).

F-tests – ANOVA (Fixed effects, one-way)

Analysis: Compute required sample size

Input Parameters		**Output Parameters**	
α err prob	= 0.05	Total sample size	= 48
Effect size	= 0.6		
Power (1-βerr prob)	= 0.8		
Number of groups	= 8		

This would equal to a sample size of n≥6 per treatment group

F-tests – ANOVA (Fixed effects, one-way)

Analysis: Compute required effect size

Input Parameters		**Output Parameters**	
α err prob	= 0.05	Effect size f	= 0.94
Total sample size	= 24		
Power (1-βerr prob)	= 0.8		
Number of groups	= 8		

Appendix B: Cellular Organisation

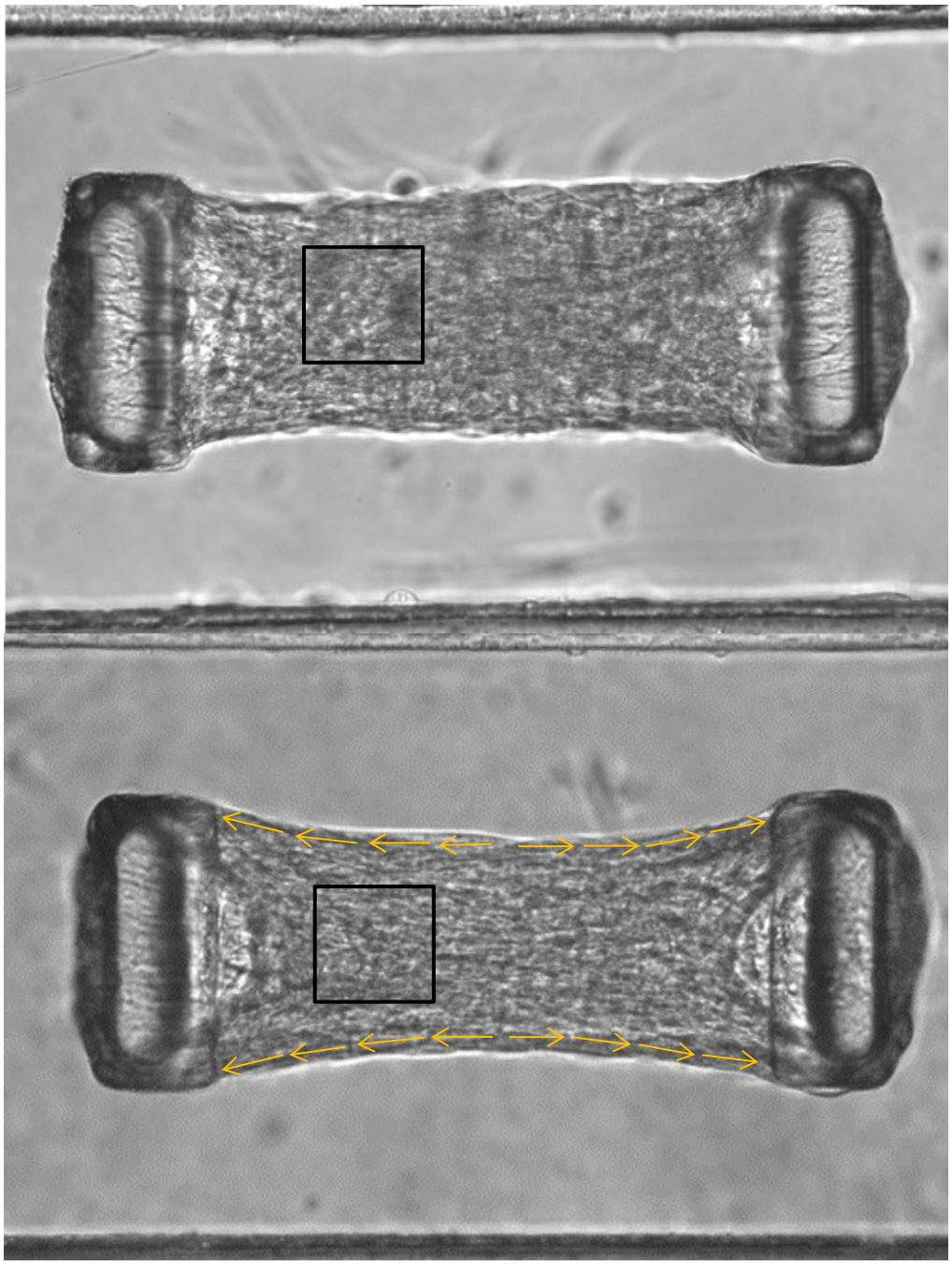

ASM cellular organisation in a soft matrix (top) and in a stiff crosslinked matrix (bottom). Black box signifies region where significant differences can be seen between cells in a soft matrix versus a stiff matrix. Cells are more aligned and along the line of greatest tension generation within a stiff crosslinked matrix (bottom). In the uncrosslinked matrix (top), the ASM cells are more disoriented and demonstrate more of a globular structure as opposed to being striated.

Appendix C: qPCR Reference Gene Selection

Crossing points for each of the 48 cDNA samples for 3 reference genes GAPDH, UBC, and YWHAZ. Candidate reference genes displayed consistency of expression between treatments. Analysis of pooled data using Bestkeeper and Normfinder software demonstrated that GAPDH was the most stably expressed candidate.

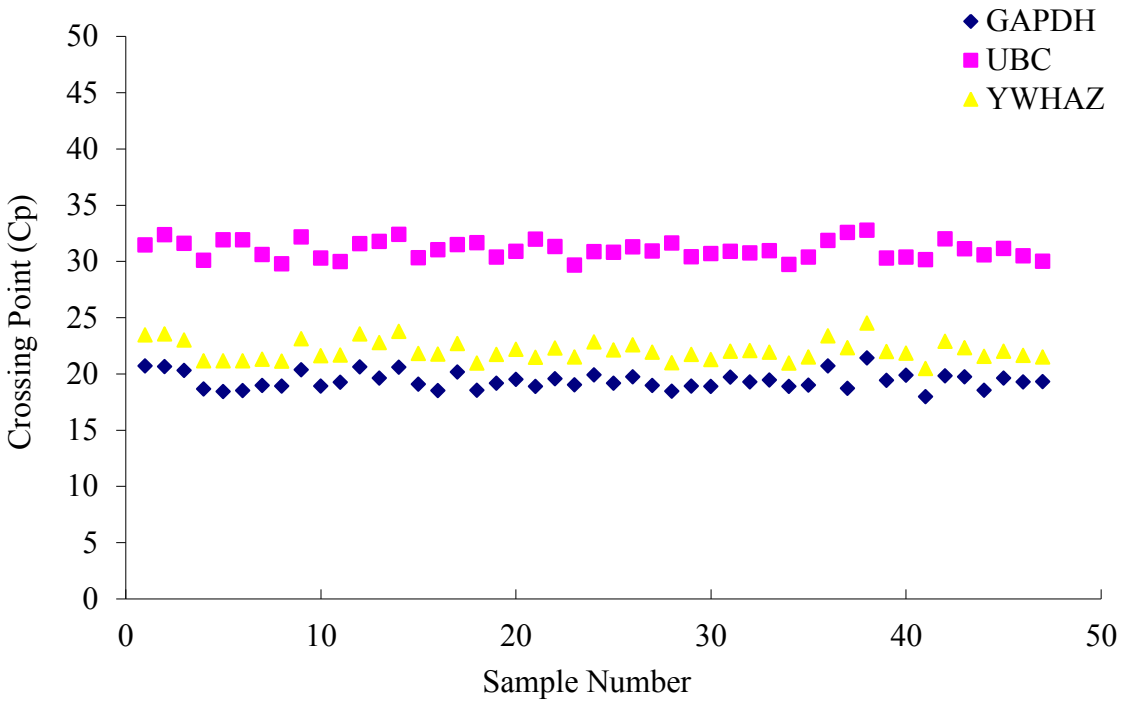

	GAPDH	UBC	YWHAZ
Mean Cp	19.39±0.09	31.03±0.11	22.04±0.12
Bestkeeper Pearson correlation coefficient	0.985	0.737	0.980
Bestkeeper p-value	0.001	0.001	0.001
NormFinder stability value	0.206	0.479	0.280